AGU PUBLICATIONS

Tectonics

RESEARCH ARTICLE
10.1002/2015TC003956

Key Point:
- Oroclinal bending occurred between Taurides and the NKM during Mesozoic

Correspondence to:
M. C. Çinku,
mualla@istanbul.edu.tr

Citation:
Çinku, M. C., Z. M. Hisarli, Y. Yılmaz, B. Ülker, N. Kaya, E. Öksüm, N. Orbay, and Z. Ü. Özbey (2016), The tectonic history of the Niğde-Kırşehir Massif and the Taurides since the Late Mesozoic: Paleomagnetic evidence for two-phase orogenic curvature in Central Anatolia, *Tectonics*, *35*, 772–811, doi:10.1002/2015TC003956.

Received 23 JUN 2015
Accepted 21 DEC 2015
Accepted article online 18 JAN 2016
Published online 30 MAR 2016

The tectonic history of the Niğde-Kırşehir Massif and the Taurides since the Late Mesozoic: Paleomagnetic evidence for two-phase orogenic curvature in Central Anatolia

Mualla Cengiz Çinku[1], Z. Mümtaz Hisarli[1], Yücel Yılmaz[2], Beyza Ülker[1], Nurcan Kaya[1], Erdinç Öksüm[3], Naci Orbay[1], and Zeynep Üçtaş Özbey[4]

[1]Faculty of Engineering, Department of Geophysical Engineering, Istanbul University, Istanbul, Turkey, [2]Kadir Has University, Istanbul, Turkey, [3]Faculty of Engineering, Department of Geophysical Engineering, Süleyman Demirel University, Isparta, Turkey, [4]Faculty of Engineering, Department of Geological Engineering, Istanbul University, Istanbul, Turkey

Abstract The Niğde-Kırşehir Massif, known also as the Central Anatolian Block, is bordered by the sutures of the Neotethys Ocean. The massif suffered several deformation phases during and after the consumption of the surrounding oceans and the postcollisional events of the continental pieces of Anatolia in latest Cretaceous to Miocene. Previous paleomagnetic studies on the Niğde-Kırşehir Massif and its surroundings displayed either insufficient data or have claimed large rotations and/or remagnetization. In order to understand the tectonic history of the Niğde-Kırşehir Massif and its adjacent blocks we have sampled 147 different sites in the age range of Upper Jurassic to Miocene from the Niğde-Kırşehir Massif throughout its W/SW and E/SE boundaries and the central-southeastern Taurides. The results display that except the limestones in central Taurides, all rocks examined carry a primary magnetization. Among these an important finding is that rotations between the massif and the central-eastern Taurides indicate an oroclinal bending with counterclockwise rotation of $R = 41.1° \pm 7.6°$ in the SE and clockwise rotation of $R = 45.9° \pm 9.3°$ in the central Taurides from Upper Cretaceous rocks with respect to the African reference direction. Paleomagnetic rotations in the SE Taurides are compatible with the vergent direction of the thrusts generated from consumption of the Intra-Tauride Ocean prior to postcollisional convergence between Taurides and the massif. In the central Taurides it has been shown that the clockwise rotation of 45.9 ± 9.3 started in Middle Eocene, because of a remagnetization in Upper Cretaceous limestones. The deformation was linked to the final closure of the southern Neotethys and the collision between the African and Eurasian plates. In the Niğde-Kırşehir Massif counterclockwise rotation up to $25.5° \pm 7.3°$ is recognized during Middle Eocene and interpreted in terms of block rotation together with the Taurides. After the Miocene a counterclockwise rotation of $16.8° \pm 3.9°$ along the Eastern Taurides shows that this area was mostly affected by the westward movement of Anatolia despite the Niğde-Kırşehir Massif and its SW/W area—the central Taurides—which is recognized as stable with counterclockwise rotation less than 10°.

1. Introduction

Anatolia represents orogenic amalgamates that began to form starting from the Late Paleozoic [*Şengör et al.*, 1984] to the late Miocene [*Şengör and Yılmaz*, 1981; *Yılmaz et al.*, 1995; *Robertson et al.*, 2004]. From north to south major components of this tectonic mosaic are the Pontides (the western part of this unit is known as the Istanbul Zone), the Sakarya Continent, the Niğde-Kırşehir Massif, the Anatolide-Tauride Platform, and the Arabian Plate (Figure 1). Some of these fragments were parts of Eurasia, e.g., Istanbul Zone [*Şengör*, 1979; *Okay et al.*, 1996], while the other continental pieces were detached from the Arabian-African Plate representing the northern part of Gondwana. As a result of the elimination of the separating oceanic realms the continental pieces collided with one another and finally accreted with Gondwana at late stage of orogenic development. Elimination of the separating oceans occurred over an extended period [*Şengör and Yılmaz*, 1981; *Ustaömer and Robertson*, 1997; *Okay and Tüysüz*, 1999; *Robertson*, 2002; *Robertson et al.*, 2004; *Okay et al.*, 2006, 2013] from the Late Triassic to Early Jurassic (the Paleo-Tethys and the Karakaya Basin) [*Şengör and Yılmaz*, 1981; *Bingöl et al.*, 1973] in the north and lasted to the latest collision along the SE Anatolian orogen in the Miocene (the Bitlis-Zagros suture Mountains) [*Yılmaz*, 1983].

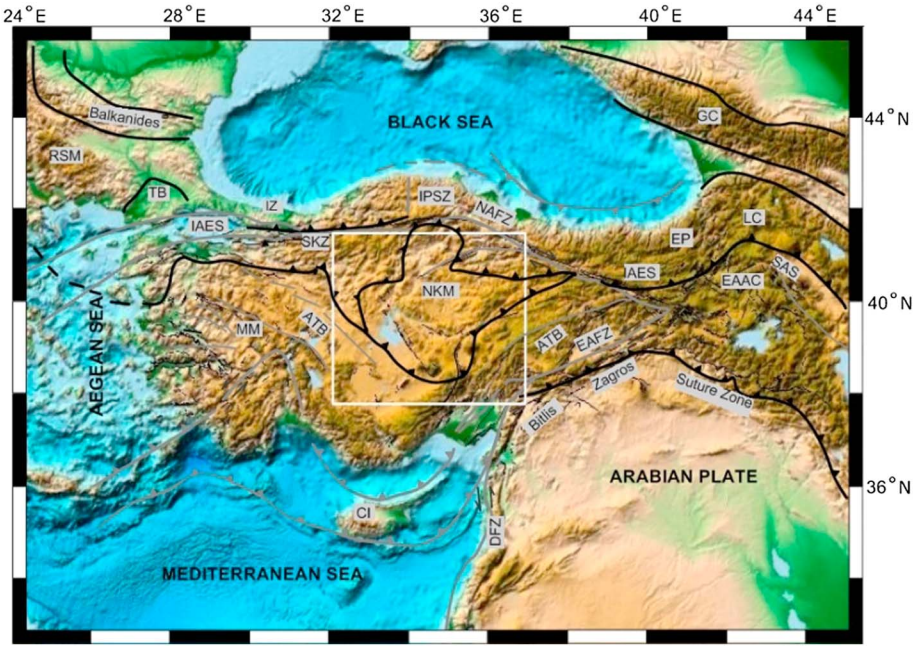

Figure 1. Main tectonic units of Anatolia and surroundings (modified after National Oceanic and Atmospheric Administration (NOAA); the white outlined box denotes the location of the studied area. ATB, Anatolide Tauride Block; CI, Cyprus Island; CP, Central Pontides; DFZ, Dead Sea Fault Zone; EAAC, Eastern Anatolian Accretionary Complex; EAFZ, Eastern Anatolian Fault Zone; EP, Eastern Pontides; GC, Great Caucasus; IAES, Izmir-Ankara-Erzincan Suture; IPSZ, Intra Pontide Suture Zone; IZ, Istanbul Zone; LC, Lesser Caucasus; MM, Menderes Massif; MP, Moesia Platform; NKM, Niğde-Kırşehir Massif; RSM, Rhodope Strandja Massif; SAS, Sevan Akera Suture; SKZ, Sakarya Zone; and TB, Thrace Basin).

The suture zone extending along the southern boundary of the Pontide separates it from the Kırşehir-Niğde Massif (Figure 1). It curves around the eastern edge of the massif and extends westward. This part of the suture is known as the Ankara-Erzincan suture. It represents the northern branch of the Neotethyan Ocean, which was eliminated by northward subduction under the Pontides [*Şengör and Yılmaz*, 1981; *Okay and Şahintürk*, 1997; *Ustaömer and Robertson*, 1997; *Rice et al*., 2006, 2009].

The southern boundary of the Niğde-Kırşehir Massif is also represented by a suture zone known as the Intra-Tauride Suture [*Şengör and Yılmaz*, 1981; *Görür et al*., 1984; *Robertson and Dixon*, 1984; *Görür and Tüysüz*, 2001; *Robertson et al*., 2009; *Parlak et al*., 2013]. The Intra-Tauride Ocean began to form as a basin rifted from the northern part of the Tauride during the Triassic [*Görür et al*., 1984; *Okay and Tüysüz*, 1999; *Robertson et al*., 2009; *Pourteau et al*., 2010], and the northerly drifted continental fragment later formed the Kırşehir Massif [*Şengör et al*., 1984; *Görür and Tüysüz*, 2001; *Whitney and Hamilton*, 2004].

During the convergence between the Pontides and the Taurides in the Late Cretaceous and Early Cenozoic, several basins developed around the southern part of the Niğde-Kırşehir Massif and the southern Taurides, interpreted as fore-arc basins [*Görür et al*., 1984], remnant oceanic basins [*Yılmaz et al*., 1997a], or postcollisional molasse basins [*Yılmaz*, 1994] formed, during the closure of the Intra-Tauride Ocean. The views may be summarized as follows: the basins began to form during the closing period of the Izmir-Ankara-Erzincan Ocean and have continued to develop in the postcollisional period. They may therefore be regarded as composite basins, basins of different tectonic origin developed one above the other.

The study area is located in a transitional zone between two contrasting tectonic environments: the eastern Anatolia deformed under N-S compressional deformation and the western Anatolian-Aegean region deformed by N-S extension. Previous paleomagnetic studies carried out around the Niğde-Kırşehir Massif have been generally sampled from Eocene and younger rocks to understand the tectonic escape regime of Anatolia [i.e., *Tatar et al*., 1995; *Piper et al*., 1996]. The block rotations were reported by *Gürsoy et al*. [1997] around the Sivas Basin, and resolution of regional block rotations has been the goal of other researchers [*Piper et al*., 1996; *Gürsoy et al*., 1998; *Kissel et al*., 2003; *Piper et al*., 2010]. In the southern part of the Niğde-Kırşehir Massif, *Kissel et al*. [1993] and *Gürsoy et al*. [1998] showed the importance of crustal deformation around the Isparta angle. In the study of

Sanver and Ponat [1981], counterclockwise rotations of 90° were obtained from Upper Cretaceous ophiolitic extrusive sequences. This result indicates that the Niğde-Kırşehir Massif underwent large rotation before reaching its present position. *Lefebvre et al*. [2013] showed different sense of rotations, obtained from Upper Cretaceous granitic rocks in the Niğde-Kırşehir Massif, which was forced to rotate between two transpressional fault zones.

To contribute to the major controversies created by the previous paleomagnetic studies, we have undertaken this paleomagnetic study aiming at larger coverage and more numerous sampling coverage. We sampled rocks from 147 different sites, which include the massif and the surrounding regions (SW and SE of the Niğde-Kırşehir Massif and the central-eastern Taurides) covering a wide age span ranging from the Upper Jurassic to Miocene. The initial geographical location and tectonic position of the central Taurides now adjacent to the Niğde-Kırşehir Massif were also investigated in this context by sampling Upper Jurassic-Lower Cretaceous platform carbonates. The Upper Cretaceous ophiolites and related sedimentary rocks in the southern (Pozantı ophiolites) and northern parts (Çiçekdağ ophiolite) of the Niğde-Kırşehir Massif and the Taurides (Mersin ophiolite) were sampled from different localities.

The tectonic position of the Ulukışla Basin located between the central Tauride and the Niğde-Ulukışla Massif was investigated by sampling Paleocene and Miocene volcanic and sedimentary rocks from the basin. We also studied relative motion history of the peripheral basins with respect to the massif. For this we sampled the basin fills and the postophiolitic cover rocks from the Kırıkkale, Haymana, Tuz Gölü, Ulukışla, and Şarkışla Basins.

2. Previous Paleomagnetic Studies

One of the pioneering studies partly related to the problems that this paper concerns was carried out by *Sarıbudak* [1989], who aimed at evaluating paleotectonic evolution of the Pontides during the Late Cretaceous-Eocene period. Later studies focused primarily on detecting the deformation that occurred related with the North Anatolian Transform Fault Zone (NAF) [*Platzman et al*., 1994; *Tatar et al*., 1995, 1996; *Piper et al*., 1996, 1997; *Gürsoy et al*., 1999; *İşseven and Tüysüz*, 2006; *Çinku and Orbay*, 2010; *Piper et al*., 2010]. In the studies more directly related with the Niğde-Kırşahir Massif, *Kaymakçı et al*. [2000, 2003] suggested that the omega shape of the Niğde-Kırşehir Massif formed as a result of the indentation of the Kırşehir Block into the Sakarya Continent. Later, *Meijers et al*. [2010] showed that this indentation occurred as an oroclinal bending on the Pontides, while *Çinku et al*. [2011, 2015] supported this conclusion with a paleomagnetic study conducted on the north-central Anatolia and stated also that the indentation was still active in the Middle Eocene.

Paleomagnetic studies carried out in the western Taurides have been mainly concentrated on the İsparta angle [*Kissel and Poisson*, 1986, 1987; *Kissel et al*., 1993, 2003; *Morris and Robertson*, 1993; *Piper et al*., 2002; *Tatar et al*., 2002; *Van Hinsbergen et al*., 2010; *Meijers et al*., 2011]. Among those, *Kissel et al*. [1993] reported clockwise rotation of 40° during the Middle Eocene from the east of the Isparta angle and a much smaller clockwise rotation during the Early Miocene to the west of the Isparta angle. *Morris and Robertson* [1993] reported remagnetization of Paleozoic to Paleocene rocks in the Beydağları area. This conclusion was not confirmed by the data produced by *Van Hinsbergen et al*. [2010]. A partial remagnetization is suggested by *Gallet et al*. [1993] from the Antalya nappes and *Meijers et al*. [2011] from Carboniferous-Paleocene limestones on Geyikdağ-Aladağ units. In areas located farther southeast, a series of paleomagnetic studies have been carried out on the Upper Cretaceous rocks, i.e., Hatay-Troodos and Baer-Bassit ophiolites, to predict the spreading center of the southern Neotethys Ocean [*Morris et al*., 1990; *Allerton and Vine*, 1991; *Hurst et al*., 1992; *Morris et al*., 1998, 2002; *Inwood et al*., 2009]. *Morris* [2003] determined a paleolatitude of 20.6°N $\pm$ 1.8° and 23.6°N $\pm$ 2.5° on the Troodos and Baear-Bassit ophiolites, respectively, which indicate that the spreading center of the Baer-Bassit segment was close to the paleolatitude of the Pontides [*Channell et al*., 1996; *Hisarlı*, 2011] in Late Cretaceous.

Paleomagnetic results from previous studies carried out around the investigation area are given in Appendix A and will be further discussed together with the results of this study.

3. Regional Geology

3.1. The Niğde-Kırşehir Massif

The Niğde-Kırşehir Massif [*Şengör and Yılmaz*, 1981] is a ~300 km × ~200 km triangular-shaped tectonic entity. The massif has been referred to under different names by different authors such as the Central Anatolian

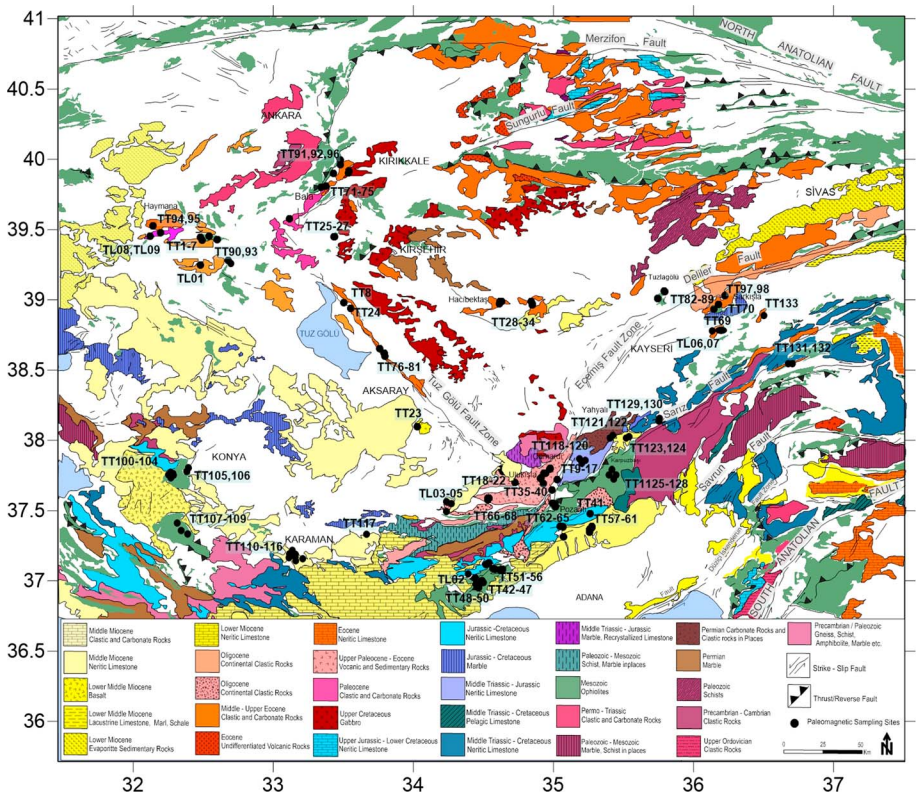

Figure 2. Geological map of the study area (after General Directorate of Mineral Research and Exploration (MTA), 1/500000 scale geological map), including the paleomagnetic sample sites.

Crystalline Complex [*Akıman et al*., 1993], the Kırşehir continent [*Şengör et al*., 1984], or the Kırşehir block [*Robertson and Dixon*, 1984]. It is bounded to the west by the Tuz Gölü fault zone [e.g., *Çemen et al*., 1999] and to the east by the Ecemiş fault zone [*Jaffey and Robertson*, 2001] (Figure 2). Its northern part is commonly represented by Mesozoic to Palaeozoic metamorphic rocks of the "Kırşehir Massif" overlain by ophiolitic rocks, which are observed along the rims of the Niğde-Kırşehir Massif. The ophiolitic rocks are interpreted as the remnants of the İzmir-Ankara-Erzincan Ocean, which was consumed as a result of its northerly subduction under the Pontide Arc during the Late Cretaceous-Eocene period [*Şengör and Yılmaz*, 1981]. A southward obduction of slabs of this ophiolite onto the Niğde-Kırşehir Massif occurred during the same period [*Yılmaz et al*., 1997b; *Nairn et al*., 2012]. This tectonic assemblage was then intruded by pulses of granitic intrusions during Late Cretaceous time [*Akıman et al*., 1993; *Boztuğ et al*., 2007]. The magmatic assemblage is variously named as the Yahsiyan formation [*Norman*, 1972] in Kırıkkale, the Çiçekdağ or Sarıkaraman formation in the Niğde-Kırşehir Massif [*Yalınız et al*., 1996; *Dönmez et al*., 2008], and the Karacaali magmatic complex [*Delibaş and Genç*, 2004].

The epi-ophiolitic cover rocks comprise Upper Cretaceous-Lower Eocene deep sea sediments and turbidites [*Tekeli et al*., 1983; *Dellaloğlu et al*., 1992; *Yılmaz et al*., 1997a, and the references therein] observed over large areas at the base of the Kırıkkale, Polatlı-Haymana, Tuz Gölü, Ulukışla, and Şarkışla Basins. The southern part of the Niğde-Kırşehir Massif is represented by the Niğde Massif regarded as a core complex [*Whitney and Dilek*, 1998]. The northern and southern parts of the Kırşehir-Niğde Metamorphic Massif display low-P metamorphism, dated Late Cretaceous (84.1 ± 0.8 Ma) [*Whitney and Hamilton*, 2004] indicating deep burial, possibly down to 20 km depths [*Whitney and Dilek*, 1997].

During the Early Eocene, the collision between the Niğde-Kırşehir Massif and the Pontides occurred. During this period severe north vergent thrusting and thick skin deformation were developed along the northern borders of the Niğde-Kırşehir Massif and in the Pontides [*Yılmaz et al*., 1997b]. However, folding and thrusting in the east and southeast affected the Tauride platform and the southern edge of the Niğde-Kırşehir Massif,

when the Pontide Arc collided with the Taurides during the Late Eocene to Early Oligocene [*Yılmaz et al*., 1997b]. In the southern areas postcollisional volcanism covered large areas during the Miocene [*Pasquare*, 1968; *Innocenti et al*., 1975; *Dirik and Göncüoglu*, 1996; *Dirik*, 2001; *Gencalioglu-Kuscu et al*., 2007].

3.2. The Central-Eastern Taurides

The Ecemiş Fault, a major left lateral strike-slip fault zone, [*Şaroğlu et al*., 1983; *Özgül*, 1984] defines the eastern boundary of the Kırşehir Massif separating it from the central Tauride. Farther south it defines the contact between the central and the eastern Taurides (Figure 1).

The Taurides are essentially a nappe stack, in which the Mesozoic and Cenozoic thrust slices were tectonically intermixed. In the study area, at the base of the nappes are schists and Permo-Triassic limestone followed upward by Jurassic-Cretaceous recrystallized limestone. Collectively, they form the Bozkır unit regarded as the relative autochton of the central Tauride with respect to the overlying tectonic slices. It is tectonically overlain by the Bozkır unit Triassic-Jurassic limestone, pelagic limestone, and overlying ophiolitic rocks. The nappe above this is known as the Geyikdağ unit. It consists of shelf carbonates of Jurassic, Lower, and Upper Cretaceous ages [*Özgül*, 1984]. All of the nappes were thrust from north to south [*Özgül*, 1984, 1997].

4. Paleomagnetic Sampling

We collected volcanic and sedimentary rocks at 147 different sites under the Kırıkkale, Haymana, Tuz Gölü, Ulukışla, Mersin, Pozantı-Çamardı, Kırşehir, and Konya-Karaman subareas (Figures 2 and 3). The Upper Jurassic-Lower Cretaceous sediments were sampled at 13 sites, and the Upper Cretaceous sedimentary and volcanic rocks were sampled at 50 and 14 sites, respectively. Palaeocene sedimentary rocks were mostly sampled around the Ulukışla and Tuz Gölü-Haymana basins at 18 different sites, and the lavas were sampled at 8 sites. Middle Eocene sedimentary rocks were sampled at 23 sites, whereas Oligocene and Middle Miocene rocks were sampled at 5 and 15 sites, respectively. In addition, a conglomerate test conducted on pebbles of the Upper Cretaceous Haymana formation was applied to test the age of magnetization. Main geological characters of the subareas are summarized below.

4.1. The Haymana Basin

The Haymana basin is located in the southwest of Ankara. The Tuz Gölü basin defines its southern boundary. To the north it is surrounded by the İzmir-Ankara-Erzincan accretionary complex (İAEAC) [*Görür et al*., 1984]. The basement rocks of the Haymana basin are composed of Upper Jurassic-Lower Cretaceous neritic limestone and ophiolitic rocks of the İAEAC [*Ünalan et al*., 1976; *Görür et al*., 1984; *Norman*, 1972; *Koçyigit et al*., 1988; *Koçyigit*, 1991]. For paleomagnetic study a volcanoclastic layer of the ordered ophiolite succession was sampled in addition to the cover rocks from SE of Bala (TT26 and TT27) (Figures 2 and 3a).

A limestone unit known as the Asmaboğazı Formation covers the ophiolite after its tectonic emplacement. It is followed upward by a sandstone-marl alternation of Upper Cretaceous age (the Haymana Formation) that is relatively extensive in the region. It is followed by a sandstone unit of Paleocene age that is known as the Dizilitaşlar Formation, which in turn passes laterally to the Kartal Formation consisting of sandstone-mudstone alternation. The Upper Cretaceous-Lower Eocene successions are unconformably overlain by the Middle Eocene sandstone and sandstone units (The the Yoncalı and Çayraz Formations, respectively) and the Middle Miocene cover rocks.

4.2. The Kırıkkale Basin

The basement in the Kırıkkale region consists of three main tectono-stratigraphic units [*Nairn*, 2010]. These are the İAEAC, basalt, and andesite lavas located in the center of the basin together with intercalated sedimentary rocks and younger granitic rocks. The İAEAC is also named previously as the Irmak formation [*Norman*, 1972], Çiçekdağ formation [*Yalınız et al*., 1996], or the Hisarköy formation [*Akyürek et al*., 1984] in different studies. The ophiolitic rocks are covered successively by pelagic limestone followed upward unconformably by conglomerates and sandstone [*Norman*, 1972; *Nairn et al*., 2012].

In the study area lavas and sandstones of the volcanic complex are sampled at the northeast of Kırıkkale (TT74, TT75, and TT135), whereas sandstone and chert are taken from the Çiçekdağ ophiolite (TT71, TT91, and TT92) (Figures 2 and 3b).

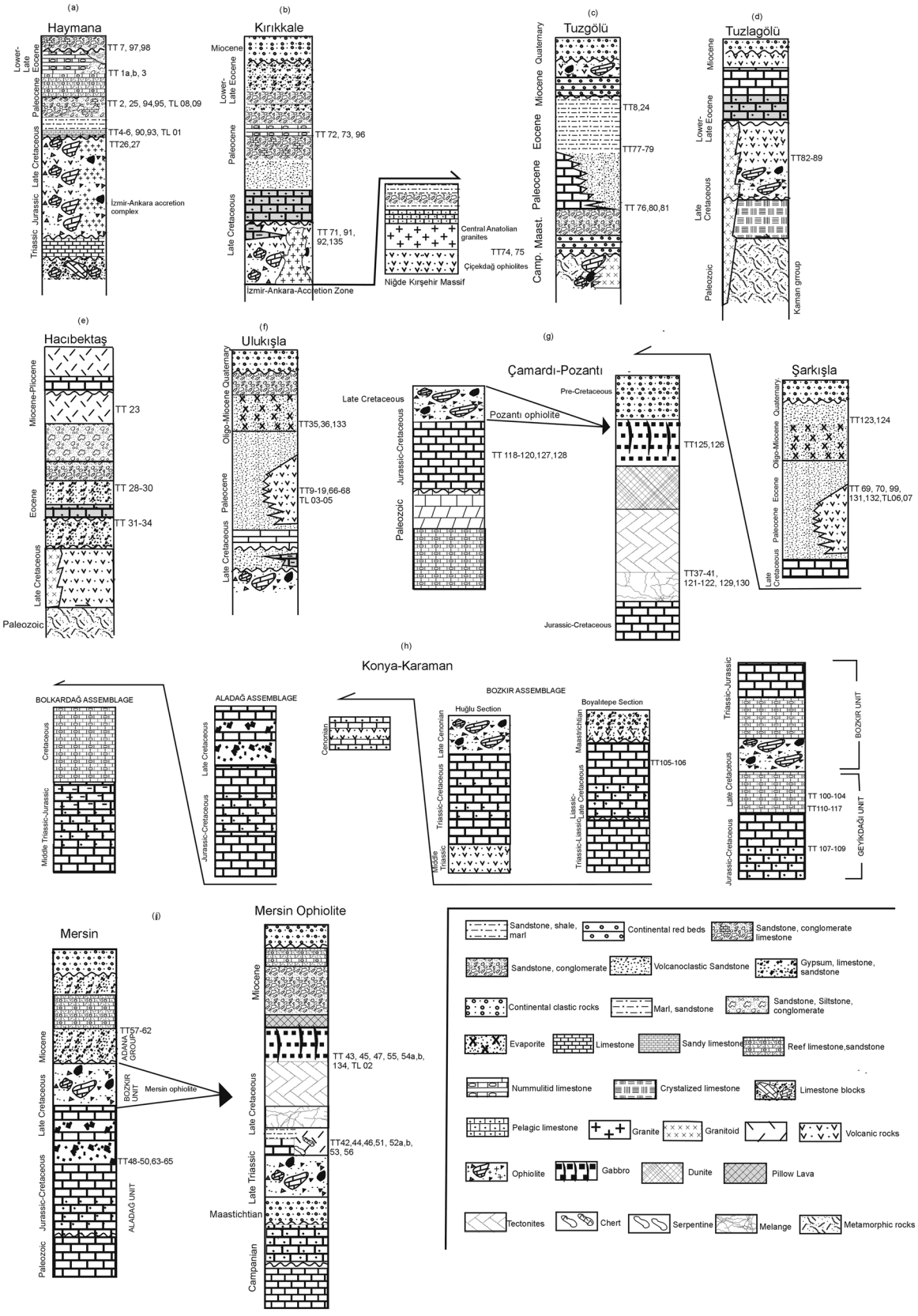

Figure 3. Stratigraphic column section showing the sampling sites after (a, b) Nairn (2010) and the 1/100000 scale geological map of MTA; (c) *Görür et al.* [1998]; (d, e, g, h) 1/100000 scale geological map of MTA (f) *Clark and Robertson* [2005]; and (i) *Parlak et al.* [2013].

The top of the ophiolites comprises Upper Cretaceous-Lower Cenozoic sediments and turbidites which grade upward into limestone, sandstone (the Dizilitaş formation), and conglomerate-limestone (the Karagüney and Çayraz formations) deposited as younger basin fills. Following a phase of uplift continental red beds (red sandstone and conglomerate) transiting locally to lacustrine marl and limestone were deposited in the basin during Oligocene time [*Norman*, 1972, 1973a, 1973b]. They suffered a severe deformation during late Oligocene, which formed tight folding, faulting, and thrusting. To differentiate this deformation stage from the earlier deformations, related possibly with the ophiolite obduction event, paleomagnetic sampling was conducted on the postophiolitic rocks (TT72, TT73, and TT96; Figure 3b).

4.3. Tuz Gölü Basin

Both the Tuz Gölü and Haymana basins are interpreted as synchronous fore-arc basins developed after total demise of the northern branch of the Neotethyan Ocean [*Arıkan*, 1975; *Görür et al*., 1984; *Koçyigit et al*., 1988; *Koçyigit*, 1991; *Görür et al*., 1998]. The Tuz Gölü basin is located adjacent to the Niğde-Kırşehir Massif across the Tuz Gölü fault zone.

The oldest basin fill is composed of conglomerate of Upper Cretaceous age (the Kartal formation). This formation passes vertically to sandstone and shale unit of the Asmaboğazı formation [*Rigo de Righi and Cortesini*, 1959]. It is followed by an overlying limestone (the Dizilitaşlar formation) of Maastrichtian age [*Norman*, 1972]. The younger basin fill consists of sandstone of Middle Eocene (the Yoncalı formation) and Oligo-Miocene evaporites.

Around the Tuz Gölü Basin, sandstones of Paleocene age (the Dizilitaşlar formation) were sampled near Çardak (TT76, TT80, and TT81), while sandstones of Middle Eocene Yoncalı formation were sampled in sites TT77–TT79 (Figures 2 and 3c). Near Şereflikoçhisar Oligocene sandstones and mudstones (the İncik formation of *Birgili et al*. [1975]) were sampled in TT8 and TT24 sites (Figure 3c).

4.4. Ulukışla Basin

The Ulukışla formation around Niğde-Çamardı-Ulukışla consists mainly of volcanoclastic rocks, lavas, pyroclastic rocks, and intercalated sandstone and shale. The age of the Ulukışla formation was determined as Paleocene-Middle Eocene by *Demirtaşlı et al*. [1975] and *Clark and Robertson* [2005]. The paleomagnetic sampling was conducted on sandstones (TT9–TT17) in the south of Çamardı, basaltic rocks (TT18, TT19, and TL05) in the south of Postallı, and lavas in the sites of TT66–TT68, TL03, and TL04 of Ulukışla (Figures 2 and 3d). The Aktoprak formation overlies the Ulukışla formation. The tuff (*Beekman* [1966]-Melendizdağ tuffs) and mudstone (*Atabey and Ayhan* [1986]-Gökbe formation) of the Melendiz group [*Pasquare*, 1968] form the top of the unit. Along the road between Çamardı-Yelatan and Aşçıbekirli located within the branches of the Ecemiş fault sites TT35–TT36 were sampled from the Oligocene mudstones of the Aktoprak formation in this region while the overlying tuffs were sampled at sites TT20–TT22 (Figure 3d).

4.5. The Çamardı-Pozantı Region

The Pozantı ophiolitic rocks tectonically overlie the Triassic-Lower Cretaceous limestone [*Tekeli et al*., 1983; *Çataklı*, 1983; *Parlak et al*., 2000, 2002]. It is separated from the Mersin ophiolites located farther west by the left lateral Ecemiş fault. The Pozantı ophiolitic complex is composed of a dismembered ophiolitic assemblage represented from bottom to top from harzburgite-dunite tectonites followed upward by ultramafic to mafic cumulates, isotropic gabbro, dike, and pillow lava [*Çataklı*, 1983; *Parlak et al*., 2000, 2002]. Previous radiometric age dating from the metamorphic sole of the ophiolite identified a cooling age of 92–90 Ma [*Dilek et al*., 1999; *Çelik et al*., 2006].

An Upper Jurassic-Lower Cretaceous limestone unit were sampled around Çamardı in sites TT118–120, TT127, and TT128. Its equivalent units (the Divrikdağı/Demirkazık Formations) were also sampled around Kayseri-Kapuzbaşı (TT48–TT50, TT63–TT65, and TT127–TT128 sites) (Figures 2 and 3d).

Cumulate Gabbros of the Pozantı-Karsantı ophiolite was sampled at TT125–TT126 sites, near Kayseri-Kapuzbaşı. Upper Maastrichtian shallow marine carbonates overly the ophiolitic rocks. In turn, they are unconformable overlain by Oligocene shallow marine and lagoon sediments [*Ünlügenç et al*., 1993] sampled near Pozantı (TT37–TT41), Yahyalı (TT121–TT122), and Bakırdağı (TT129 and TT130; Figure 3d).

To the NE ophiolitic rocks are unconformably overlain by clastic sedimentary rocks of Eocene and Quaternary ages [*Görür et al*., 1998]. Middle Eocene sandstone and siltstone were sampled at different localities (TT69, TT70, TT99, TT131, TT132, TL08, and TL09; Figures 2 and 3d) from the Şarkışla Basin. The cover rocks around the study

area consist of Miocene to Quaternary sedimentary and volcanic rocks, which cover the older units with a distinct angular unconformity. We sampled siltstone and sandstone at sites TT123 and TT124 (Figure 3d). The volcanic units were previously sampled from a wide region [*Gürsoy et al*., 1997; *Platzman et al*., 1998; *Gürsoy et al*., 2011] and were not resampled again in this study.

4.6. Tuzlagölü and Hacıbektaş Areas

The ophiolites that crop out in the northeastern and northwestern part of the Niğde-Kırşehir Massif (the Sarıkaraman and Çiçekdağ ophiolites) [*Yalınız et al*., 1996] were sampled from lavas, pelagic limestone and siltstone-fine-grained sandstone in Haymana (TT26 and TT27) and Kırıkkale (TT74 and TT75) regions, whereas sandstone (TT82, TT86, TT87, and TT89), lava (TT83), mudstone (TT84), pelagic limestone (TT85), and chert (TT88) were sampled in Kayseri-Tuzlagölü (Figures 2 and 3e).

Eocene sandstones which belong to the Altıpınar formation and the Kızılöz formation were sampled around Kırşehir-Hacıbektaş at TT28–TT34 sites (Figure 3e).

The Central Anatolian volcanic rocks are exposed extensively around Aksaray. Although these volcanics were sampled in earlier studies, we also sampled lavas from Upper Miocene Keçikalesi volcanics (TT23) (Figure 3e) for a further examination.

4.7. Konya-Karaman

In the central and eastern Taurides located to the south of the Kırşehir-Niğde Massif, the Bozkır, Bolkardağ, Aladağ, and Geyikdağı nappes were differentiated from north to south [*Özgül*, 1976] which show wide lithological variations. Around Konya-Karaman, Jurassic-Lower Cretaceous shelf sediments (Hacıalabaz limestone) [*Demirkol*, 1981; *Hakyemez et al*., 1992] pass upward into Upper Cretaceous neritic carbonates (Saytepe formation) to form the Geyikdağı nappe. In the study area the Geyikdağı nappe is tectonically overlain by ophiolitic rocks of the Bozkır nappe [*Göğer and Kıral*, 1969]. Tectonic slices of the Bozkır nappe comprise the Maastrichtian Hatip ophiolitic mélange at the bottom. Cherty-clayey carbonates and radiolarites belong to deep shelf edges of Upper Cretaceous Boyalıtepe groups. Middle and Triassic-Jurassic aged massive neritic carbonates of Gencek groups are at the top. Clastics and volcanic rocks are the cover rocks formed during Late Miocene-Early Pliocene transgression.

We sampled the Upper Jurassic-Lower Cretaceous aged Hacıalabaz limestones from the Konya region (sites TT105 and TT106) and Upper Cretaceous pelagic limestones from the Geyikdağı nappe (TT100–TT104 and TT107–TT117; Figures 2 and 3f).

4.8. Mersin Ophiolite

The outcrops of the Mersin ophiolite located in the southernmost part of the study area are regarded as a part of the Bozkır unit [*Özgül*, 1976]. The sinistral Ecemiş fault defines the eastern border of the ophiolite. Along the southern and western parts Miocene sedimentary rocks were deposited above the ophiolite. In the north against the Bolkardağ metamorphics the contact is a normal fault, which resulted by the exhumation of the metamorphic rocks [*Juteau*, 1980; *Parlak*, 1996]. The ophiolitic mélange constitutes, in addition of the different members of the ophiolites, mainly serpentinite, gabbro and basalt, Permian to Upper Cretaceous sandstone, shale, mudstone, and limestone. The melange unit is overlain tectonically by metamorphic rocks [*Parlak and Delaloye*, 1996]. An ^{40}Ar-^{39}Ar dating cooling age of 96–91 Ma were obtained from the metamorphic rocks [*Parlak and Delaloye*, 1999; *Dilek et al*., 1999].

Volcanic rocks of the Çamlıyayla-Arslanköy area were sampled from lavas (TT43, TT46, and TT134), diabase (TT45 and TT55), and pillow lavas (TT54a, TT54b, and TL02). The sedimentary rocks, chert (TT42, 44, 53), sandstone (TT51), limestone (TT52a and TT52b), and claystone (TT56) were also sampled at different localities from the top of the Mersin ophiolite (Figures 2 and 3g). The cover sedimentary rocks were sampled from Middle Miocene marl-claystone and limestone of the Gildirli formation [*Schmidt*, 1961] which is a part of the Adana group (TT57–TT62; Figure 3g).

5. Laboratory Procedures

5.1. Paleomagnetic and Rock Magnetism

Cores were cut into standard 2.2 cm long cylindrical specimens. A motorized portable core drill was used to collect core samples. Sample orientation was determined using both magnetic and sun compasses. All

measurements were carried out at the paleomagnetic laboratory of Karls Eberhardt Universtity in Tübingen and the Yılmaz İspir paleomagnetic laboratory at İstanbul University. The directions and intensities of the natural remanent magnetization (NRM) were measured with a 2G Enterprises 755R three-axis DC-SQUID cryogenic magnetometer and a JR6 spinner magnetometer. Thermal demagnetization was conducted using an ASC TD48, MTD-80, and MMTD70 furnace in progressive steps between room temperature and 680°C, and alternating field (AF) demagnetization was performed with either a LDA-3A or a 2G-Enterprises degausser attached to the magnetometer between 0 and 100 mT. The vector components were defined by principal component analysis [*Kirschvink*, 1980] and the average ChRM for the sites calculated using the Fisher statistical analysis [*Fisher*, 1953]. The NRMs of the volcanic samples typically range between 100 and 3020 mA/m, whereas those of the sedimentary rocks are between 0.01 and 40 mA/m. The 1862 samples from 147 different sites have been demagnetized both with AF and TH in sister samples, showing negligible differences in the results. However, AF was more effective in cleaning 80% of the samples, suggesting magnetite as the main magnetic carrier.

Detailed rock magnetic experiments, including thermomagnetic measurements, acquisition of isothermal remanent magnetization (IRM), and thermal demagnetization of three-axis composite IRM [*Lowrie*, 1990] were conducted on typical lithologies. Thermomagnetic experiments were measured on representative samples by heating in air at room temperature, using an MS2 device and an AGICO KLY-2 Kappabridge fitted with an oven. The stepwise acquisition of IRM was made with an ASC pulse magnetizer (Model IM-10-30) up to 1 T along the sample *z* axis (hard component). Afterward, 0.4 T (medium component) was applied to the sample *y* axis and 0.12 T (soft component) to the sample *x* axis [*Lowrie*, 1990]. Subsequently, samples were thermally demagnetized to identify the magnetic carriers based on their coercivity and unblocking behavior.

5.2. Rock Magnetic Results

The thermomagnetic results of different lithology including volcanic and sedimentary rocks show a strong decrease in susceptibility between 500 and 600°C typical of Ti-poor magnetite in a variety of sample (Figures 4a1, 4c1, and 4e1). The susceptibility upon cooling is lowered in all the volcanic samples, suggesting some degree of oxidation (Figures 4a1 and 4b1), while in most of the sedimentary rocks the cooling curves show higher susceptibility values after heating, indicating the growth of new minerals after heating (Figures 4c1–4f1). IRM curves show rapid acquisition of magnetization to about 200 and 300 mT in general, suggesting the existence of a soft coercivity component (Figures 4a2, 4c2, and 4e2). Thermal demagnetization of the cross-component IRM shows that the low-coercivity component is gradually unblocked until 600°C (Figures 4a3, 4c3, and 4e3). The second strongest component of the IRM is the medium component, in almost all the samples, which is demagnetized at 400°C or 600°C presents the existence of titanomagnetite (Figures 4a3–4f3).

In some basalt samples (TT43, i.e., Figure 4a1), Curie temperatures below 600°C, and a drop between 350 and 400°C may indicate the transformation of magnetite into maghemite or titanomagnetite. IRM curves show rapid acquisition of magnetization to about 200 and 300 mT in general, suggesting the existence of a soft coercivity component (Figure 4a2). Thermal demagnetization of the cross-component IRM shows that the low-coercivity component is gradually unblocked until 600°C (4a3). From a group of gabbro samples (TT125, i.e., Figure 4b1), Curie temperatures above 600°C show evidence of titanohematite. For these samples a saturation at 1 T could not be reached, and the three-component demagnetization curves indicate that the high-coercivity component is demagnetized above 600°C (Figures 4b2 and 4b3).

In most of the sandstone samples, the Curie point is defined below 600°C, with minor amount of alteration (Figure 4c1) and a rapid increase in the IRM curves at approximately 300 mT (Figure 4c2). In these samples the demagnetization curves of three-component IRM show that this low-coercivity component is unblocked until 600°C, which is obvious in the thermomagnetic curves (Figures 7a3 and 7c3). In another group of sedimentary rocks, the Curie point is defined at about 650°C, with noticeably amount of alteration suggesting the existence of (titano) hematite (Figure 4d1). The IRM acquisition curve shows that the saturation could not be reached at maximum field (Figure 4d2). It is shown that both the soft and high-coercivity components are dominant and unblocked gradually at 650°C (Figure 4d3).

The thermomagnetic results of the limestone samples show two different types of behavior which exhibit one magnetic phase. One group is characterized by Curie temperatures between 550 and 580°C, showing some degree of alteration (Figure 4e1). In the other group of limestone samples Curie temperatures above 600°C show evidence of titanohematite (Figure 4f1). The IRM acquisition curve shows two different types

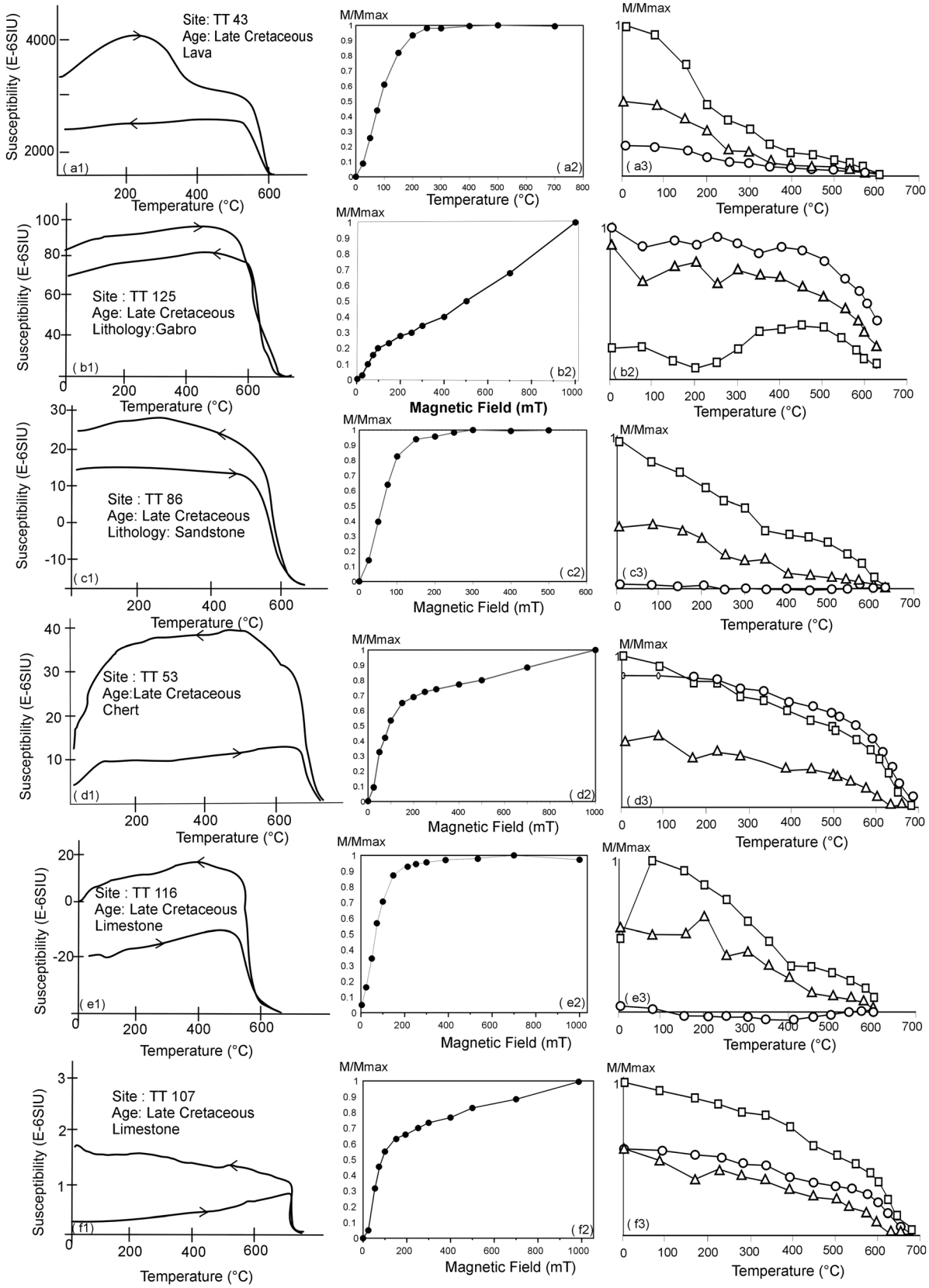

Figure 4. (a1–f1) Typical thermomagnetic curves for representative samples. (a2–f2) Normalized IRM acquisition curves. (a3–f3) Thermal demagnetization with three-axis IRM in fields of 1 T along the sample *z* axis (circles), 0.4 T along the sample *y* axis (triangle), and 0.12 T along the sample *x* axis (square).

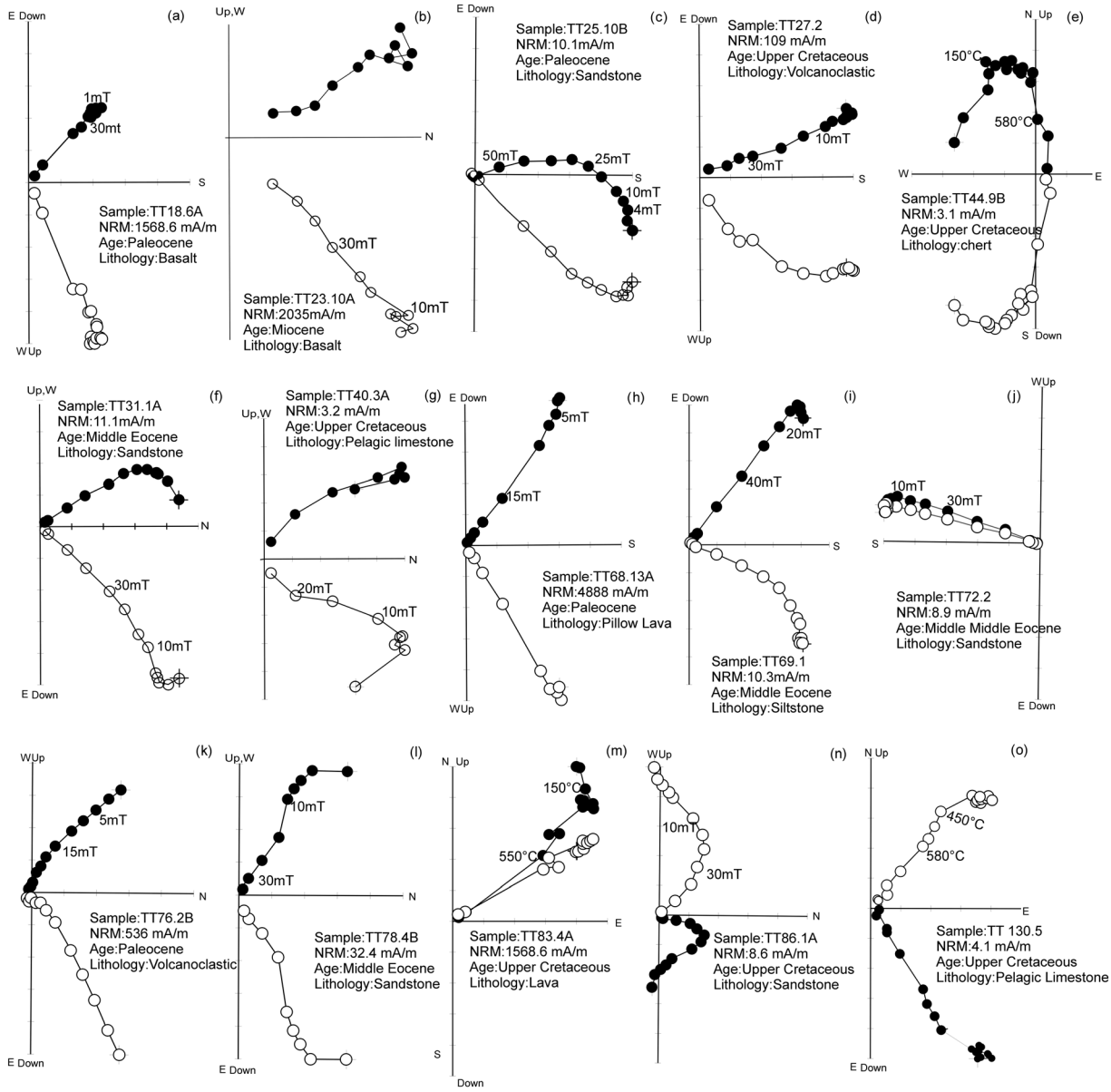

Figure 5. NRM intensities and orthogonal vectors of representative samples during stepwise thermal and alternating field demagnetization (in degrees Celsius and miliTesla (mT)). The solid symbols correspond to projections onto the horizontal plane, while the open symbols are projections onto the vertical plane.

of behavior which is recognized with a soft and hard component (Figures 4e2 and 4f2). The unblocking temperatures of the triaxial IRM were identified by 600°C for low and medium components (Figure 4e3) or 650°C in all three components (Figure 4f3).

5.3. Paleomagnetic Analysis

NRM components were isolated both with AF and thermal demagnetization. The ChRM vectors of lavas, sandstones, and claystones which indicate low-coercivity (temperature) components are isolated with AF (thermal) cleaning at alternating fields up to 40 mT (unblocking temperature below 600°C) (Figures 5a–5d and 5f–5n), while the limestones and chert samples with high unblocking temperatures were demagnetized thermally with maximum unblocking temperatures above 600°C (Figures 5e and 5o). Two NRM components are generally recognized during demagnetization. The low unblocking temperatures or low-coercivity components recording probably a minor viscous origin with random distribution are removed between 50°C and 300°C or 5–10 mT, respectively (Figures 5a, 5b, 5h, and 5k). The directions of this secondary component is scattered, while the present field direction, which was unblocked at 150–200°C, was only obtained in site TT1b (*D*/

AGU Tectonics

10.1002/2015TC003956

Table 1. Paleomagnetic Results for the Late Jurassic-Lower Cretaceous and Middle Miocene Formations of This Study and Previous Paleomagnetic Results[a]

Site	Lithology	Latitude(°N)	Longitude(°E)	Strike/Dip	*N/n*	D_g	I_g	D_s	I_s	ΔD_X	ΔI_X	α_{95}	*k*	A_{95}	A_{95min}	A_{95max}
						Late Jurassic/Lower Cretaceous										
						Mersin (TTJ-G1)										
TT48	Limestone	37.12689	34.54117	153/32	12/12	347.8	19.3	334.8	24.0	5.9	9.9	7.6	47.3	5.7	4.3	16.3
TT49	Limestone	37.11833	34.52754	322/27	14/13	107.4	−28.5	124.6	−40.7	10.8	13.4	9.5	24.2	9.9	4.3	16.3
TT50[c]	Limestone	37.11377	34.51807	210/51	12/11	29.7	40.5	176.2	−23.9	-	-	6.9	44.8	-	-	-
TT63[b]	Limestone	37.38321	35.06666	256/34	10/10	248.6	32.7	247.9	26.1	-	-	23.7	6.4	-	-	-
TT64	Limestone	37.38856	35.06153	190/32	15/15	156.4	−45.7	139.41	−23.7	7.7	12.7	9.2	28.8	7.5	4.1	14.9
TT65	Limestone	37.38841	35.04662	288/25	8/7	293.7	44.4	314.8	37.2	8.3	11.0	7.9	73.6	7.7	5.5	24.1
		Mean Sites TT48, TT49, TT64, and TT65				317.0	37.6					33.5	8.5			
								319.2	31.9			15.9	34.4			
						Çamardı (TTJ-G2)										
TT118[b]	Limestone	37.76909	35.09224	280/27	10/7	134.3	46.4	102.3	55.4	-	-	12.6	29.1	-	-	-
TT119	Limestone	37.75750	35.09552	280/27	10/10	302.7	30.4	313.5	17.4	9.0	16.0	11.9	22.3	8.8	4.8	19.2
TT120	Limestone	37.75761	35.09602	280/27	9/9	298.6	40.0	315.1	27.5	6.2	10.3	7.6	146.1	6.0	5.0	20.5
TT127[d]	Limestone	37.78884	35.43665	210/17	9/9	10.6	46.0	356.7	38.3	-	-	15.4	12.1			
TT128	Limestone	37.82495	35.45068	130/30	10/8	326.6	20.0	313.9	25.5	13.9	22.6	15.1	22.4	13.4	5.2	22.1
		Mean Sites TT119, TT120, and TT128				310.2	30.7					25.7	24.0			
								314.1	23.5			8.2	227.4			
						Konya										
TT105[b]	Limestone	37.76496	32.36335	13/40	-	-	-	-	-	-	-	-	-	-	-	-
TT106	Limestone	37.76571	32.36418	320/37	10/8	37.2	58.5	38.4	21.5	4.3	7.5	6.0	161.7	5.1	5.2	22.1
						Late Cretaceous										
						Haymana (TTC-G1)										
TT 4	Marl	39.26788	32.28775	193/22	8/8	322.5	36.2	315.8	18.3	7.6	13.6	7.5	55.7	7.4	5.2	22.1
TT 5	Sandstone	39.25437	32.29646	190/40	15/15	357.7	64.0	313.5	38.9	6.1	8.0	5.4	51.3	5.7	4.1	14.9
TT 6[b]	Sandstone	39.25079	32.35907	118/52		-	-	-	-	-	-	-	-	-	-	-
TT90	Sandstone	39.27403	32.31086	234/32	10/8	103.0	−83.1	137.9	−53.0	9.6	8.1	8.6	62.0	7.9	5.2	22.1
TT93	Sandstone	39.26788	32.28775	193/22	10/10	341.5	55.7	322.5	41.0	6.2	12.3	6.4	53.2	5.6	4.8	19.2
TT26[b]	Volcano-clastic	39.44822	33.43436	66/84	10/7	204.8	8.9	49.4	39.2	-	-	20.4	11.3	-	-	-
TT27	Volcano-clastic	39.44888	33.43702	94/38	10/9	338.6	12.9	327.8	45.8	11.4	12.3	9.7	28.9	10.1	5.0	20.5
		Mean Sites TT4, TT5, TT90, TT93, and TT27				335.5	51.6					28.6	8.1			
								318.8	39.5			12.9	36.1			
						Conglomerate Test Site										
TL01	Sandstone	39.44247	32.52009	-	10/10	-	-	-	-	-	-	-	-	-	-	-
						Kırıkkale (TTC-G2)										
TT71	Chert	39.47963	33.20532	355/45	10/9	335.9	29.7	5.4	33.5	3.7	5.5	8.7	78.5	5.5	4.8	19.2
TT74	Sandstone	39.54057	33.32268	16/47	15/14	339.1	53.9	52.6	54.1	8.5	7.0	12.5	34.3	7.0	4.2	15.6
TT75[c]	Lava	39.54007	33.32209	16/47	15/12	173.6	−34.5	210.8	−38	-	-	14.1	26.3	-	-	-
TT91	Sandstone	39.57054	33.27347	6/88	10/8	144.4	−32.1	224.9	−35.5	6.3	9.1	6.3	31.4	6.0	5.2	22.1
TT92	Sandstone	39.58499	33.27785	193/63	10/10	226.8	−23.2	184.2	−39.4	5.2	6.8	8.4	42.7	4.9	4.8	19.2
TT135[b]	Lava	39.57114	33.26447	15/50	-	-	-	-	-			-	-	-	-	-
		Mean Sites TT71, TT74, TT91, and TT92				352.1	38.5					29.2	7.8			
								26.2	41.7			17.7	15.0			
						Tuzla Gölü (TTC-G3)										
TT82[b]	Sandstone	39.06146	35.79205	240/10	10/8	307.4	33.8	309.5	24.4	-	-	27.5	8.6	-	-	-
TT83[b]	Lava	39.06146	35.79205	240/10	10/8	33.8	27.5	9.9	29.8	-	-	22.8	5.5	-	-	-
TT84	Mudstone	39.05563	37.79548	240/10	17/13	163.8	−42.4	162.1	−32.7	7.7	12.3	13.5	10.4	7.4	4.8	19.2
TT85	P.Limestone	39.05563	37.79548	54/37	10/6	334.2	0.2	336.8	36.5	13.5	18.6	13.5	25.6	12.6	5.9	26.5
TT86	Sandstone	39.05563	37.79548	287/32	10/7	263.3	47.1	301.0	50.0	9.6	8.7	14.5	28.9	8.1	5.5	24.1

AGU Tectonics

10.1002/2015TC003956

Table 1. (continued)

Site	Lithology	Latitude(°N)	Longitude(°E)	Strike/Dip	*N*/*n*	D_g	I_g	D_s	I_s	ΔD_X	ΔI_X	α_{95}	*k*	A_{95}	A_{95min}	A_{95max}
TT87	Sandstone	39.05563	37.79548	240/10	10/8	350.0	39.4	347.8	29.9	9.8	14.8	8.9	39.8	9.3	5.2	22.1
TT88	Chert	39.00773	35.74366	6/52	10/7	154.6	−29.3	191.1	−36.6	5.9	8.1	11.5	29.5	5.5	5.5	24.1
TT89	Sandstone	39.00748	35.74475	0/52	10/7	146.2	−26.3	183.2	−41.8	6.9	8.1	10.5	41.01	6.3	5.5	24.1
		Mean Sites TT84–TT89				148.7	−33.6					25.2	8.0			
								165.5	−40.7			16.5	17.4			
					Çamardı (TTC-G4)											
TT37	P. Limestone	37.53933	37.97983	185/10	10/10	322.0	34.5	317.8	27.4	14.2	16.8	8.0	37.7	12.8	4.8	19.2
TT38	P. Limestone	37.53811	34.98404	85/10	10/10	166.9	−26.7	166.0	−36.6	7.5	10.5	10.3	22.8	7.1	5.0	20.5
TT39[b]	P. Limestone	37.53901	34.99049	83/22	14/11	3.1	44.2	10.7	65.6	-	-	11.2	18.3	-	-	-
TT40	P. Limestone	37.52.571	35.01604	20/18	15/10	320.5	12.4	324.0	27.7	10.4	16.9	10.0	24.6	10.1	4.8	19.2
TT41	P. Limestone	37.47818	35.26336	131/48	14/14	162.0	−22.8	133.2	−37.8	8.4	10.6	7.1	41.9	7.7	4.3	16.3
TT125[c]	Cumulate Gabbro	37.78443	35.38416	254/32	12/8	326.6	61.3	334.5	30.1	-	-	15.4	24.1	-	-	-
TT126[b]	Cumulate Gabbro	37.77013	35.39173	198/44	10/8	41.8	12.7	26.3	25.6	-	-	20.2	21.6	-	-	-
TT129	P. Limestone	38.18768	35.92443	253/32	14/11	328.1	63.8	335.3	32.4	14.4	17.5	12.1	13.7	13.1	4.6	18.1
TT130	P. Limestone	38.18881	35.92132	253/32	10/10	330.2	68.4	337.2	36.7	7.2	10.1	9.9	47.1	6.8	4.8	19.2
TT122[b]	P. Limestone	38.03682	35.44870	112/37	12/8	299.4	32.0	276.6	29.3	-	-	14.5	119.5	-	-	-
TT121[b]	P. Limestone	38.02925	35.42566	15/63	14/9	353.2	44.3	52.0	33.6	-	-	10.4	15.7	-	-	-
		Mean Sites TT37, TT38, TT40, TT41, TT129, and TT130				332.2	38.4					21.1	11.0			
								317.4	33.5			15.1	50.9			
					Mersin/Sedimentary Rocks (TTC-G5)											
TT42[b]	Chert	36.98709	34.49905	95/52	-	-	-	-	-	-	-	-	-	-	-	-
TT44	Chert	37.01874	34.44000	142/80	21/15	341.1	45.0	277.5	20.5	4.5	7.9	3.2	82.1	4.4	4.1	14.9
TT51	Sandstone	37.08549	34.57032	133/17	16/12	349.9	27.8	340.6	37.0	6.7	10.9	6.7	38.7	6.5	4.3	16.3
TT52[c]	Limestone	37.08402	34.58140	355/20	15/15	106.9	−17.2	110.9	−35.5	8.4	10.8	6.3	48.4	7.8	4.8	19.2
TT52[d,b]	Limestone	37.08402	34.58140	355/20	10/6	167.1	−47.6	193.9	−47.4			26.8	18.8	-	-	-
TT53	Chert	37.08406	34.63416	52/65	14/14	305.3	−30.1	304.8	32.6	2.9	4.4	5.5	52.5	5.8	4.2	15.6
TT56	Sandstone	37.07784	34.62303	360/38	10/7	312.4	10.4	325.1	36.1	3.2	4.4	4.7	95.7	6.0	5.5	24.1
		Mean Sites TT44, TT51, TT52a, TT53, and TT56				326.4	42.1					67.8	2.2			
								306.4	34.5			21.9	13.4			
					Mersin/Volcanic Rocks (TTC-G6)											
TT43	Lava	36.99777	34.49.905	182/40	22/22	8.2	50.1	327.4	39.2	9.1	12.0	3.1	143.4	8.4	5.9	26.5
TT45	Diabase	36.97.425	34.44721	136/22	16/15	332.2	35.8	315.3	38.8	3.7	4.9	3.7	110.2	4.4	4.1	14.9
TT46	Lava	36.95891	34.45695	177/52	14/7	1.7	65.3	297.0	36.3	6.4	8.8	5.3	132.2	6.0	5.5	24.1
TT47[b]	Serpentine	36.95013	34.46515	177/52	23/10	272.4	87.6	262.5	35.6	-	-	24.1	10.5	-	-	-
TT54[c,b]	Pillow Lava	37.08089	34.63012	360/38	15/14	186.9	−46.1	216.5	−31.1	-	-	25.6	12.9	-	-	-
TT54[d]	Pillow Lava	37.08089	34.63012	360/45	14/12	145.1	0.4	153.4	−23.6	3.0	5.0	5.9	61.6	4.9	4.2	15.6
TL02	Pillow Lava	37.09889	34.64657	350/30	20/17	295.2	−2.4	298.3	22.3	2.1	3.2	4.1	134.2	4.6	3.9	13.8
TT55[b]	Diabase	37.07784	34.62303	360/38	10/7	315.7	−3.1	320.8	22.8	-	-	14.4	18.5	10.6	5.5	24.1
TT134[b]	Lava	37.01434	34.55294	170/45	-	-	-	-	-	-	-	-	-	-	-	-
		Mean Sites TT43, TT45, TT4654b, TTL02, and TT55				336.2	56.0					87.7	1.7			
								314.7	31.6			15.9	24.5			
					Konya-Karaman (TTC-G7)											
TT100	P. Limestone	37.76443	32.28920	50/67	10/9	31.2	2.0	44.3	18.1	8.8	10.0	6.4	66.9	7.9	5.2	22.1
TT101	P. Limestone	37.76453	32.28924	335/41	10/7	6.6	52.5	30.7	22.9	6.5	12.2	8.4	84.7	6.4	5.5	24.1
TT102[b]	P. Limestone	37.76463	32.28927	310/31	14/12	42.5	54.2	42.3	25.1	-	-	20.5	9.2	-	-	-
TT103	P. Limestone	37.76413	32.28930	310/25	7/7	74.1	41.8	66.4	20.1	11.2	13.3	7.9	73.5	10.2	5.5	24.1
TT104	P. Limestone	37.76496	32.27552	310/25	7/7	56.5	42.8	52.7	18.6	7.1	8.3	14.6	17.4	6.4	5.5	24.1
TT107	P. Limestone	37.34078	32.35261	77/20	10/10	3.0	4.2	4.4	23.4	13.8	21.3	5.6	84.1	13.3	4.8	19.2
TT108	P. Limestone	37.34411	32.35045	77/20	8/8	8.0	17.7	12.1	36.2	9.9	13.0	6.4	34.1	9.2	5.2	22.1

AGU Tectonics

10.1002/2015TC003956

Table 1. (continued)

Site	Lithology	Latitude(°N)	Longitude(°E)	Strike/Dip	*N/n*	D_g	I_g	D_s	I_s	ΔD_X	ΔI_X	α_{95}	*k*	A_{95}	A_{95min}	A_{95max}
TT109	P. Limestone	37.36422	32.38279	20/22	14/10	68.1	46.5	80.2	29.4	5.6	9.6	15.3	20.2	5.5	4.8	19.2
TT110	P. Limestone	36.99848	33.03415	52/56	10/9	10.2	25.0	53.6	47.5	7.1	12.4	6.4	66.9	7.0	5.0	20.5
TT111	P. Limestone	37.00653	33.04443	184/28	8/8	43.4	1.1	39.5	18.4	5.8	10.0	14.3	15.6	5.7	5.2	22.1
TT112[b]	P. Limestone	37.01277	33.05331	85/25	10/10	317.3	29.9	302.8	47.9	-	-	10.6	21.6	-	-	-
TT113	P. Limestone	37.01278	33.05360	35/25	10/7	179.3	−30.9	196.2	−42.4	5.6	9.9	14.6	18.0	5.5	5.5	24.1
TT114	P. Limestone	37.04240	33.08057	233/38	10/7	41.0	41.3	17.2	25.1	15.2	27.9	12.3	25.2	15.0	5.5	24.1
TT115	P. Limestone	36.99718	33.12404	294/37	10/10	108.7	62.7	62.7	43.2	6.9	10.5	14.7	11.7	6.6	5.0	20.5
TT116[b]	P. Limestone	37.02902	33.08059	264/24	-	-	-	-	-	-	-	-	-	-	-	-
TT117	P. Limestone	37.18109	33.74371	284/54	10/9	133.7	66.3	43.2	44.4	6.9	10.9	8.0	41.9	6.6	5.0	20.5
Mean Sites TT100, TT101, TT103, TT104, TT107–TT111, TT114, TT115, and TT117						34.9	38.6					19.9	5.3			
								40.3	29.7			11.5	13.1			
Paleocene																
Haymana (TTP-G1)																
TT2[b]	Sandstone	39.27226	32.07305	295/22	14/13	356.6	57.7	6.3	37.5	-	-	4.2	98.5	-	-	-
TT25	Sandstone	39.56317	33.12260	194/60	24/21	52.1	50.8	150.3	−46.5	7.7	8.2	6.1	28.2	6.8	3.6	12.0
TT94	Sandstone	39.28677	32.11646	153/26	10/10	197.7	−19.0	187.1	−35.7	8.9	12.3	11.2	26.7	8.4	4.8	19.2
TT95	Sandstone	39.28761	32.12915	265/23	10/10	163.0	−53.1	166.7	−30.4	5.9	8.9	6.5	42.4	5.6	4.8	19.2
TL08	Sandstone	39.55310	33.11200	206/35	24/20	24.2	55.2	345.2	41.2	5.9	7.2	4.7	92.6	5.4	3.6	12.4
TL09	Sandstone	39.28500	32.08121	199/45	30/25	35.5	45.7	350.4	40.3	5.6	6.9	3.8	105.4	6.5	3.8	13.3
Mean Sites TT25, 94, 95, TL08, and TL09						23.0	47.0					21.7	13.3			
								348.5	39.5			11.2	47.9			
Tuz Gölü (TTP-G2)																
TT76	Volcanoclastc	38.59774	33.79875	143/22	10/9	337.9	33.8	322.3	36.6	11.7	15.2	9.6	28.5	10.8	5.0	20.5
TT80	Mudstone	38.39093	33.45675	225/24	8/8	129.3	−53.5	131.1	−29.6	15.0	23.6	13.3	18.2	14.4	5.2	22.1
TT81	Sandstone	38.39093	33.45675	225/24	10/10	331.4	50.4	326.7	27.0	11.5	19.7	12.0	17.2	11.2	4.8	19.2
Mean Sites TT76, TT80, and TT81						327.7	46.6					22.6	30.7			
								320.0	31.2			13.0	90.9			
Ulukışla Basin Sedimentary Rocks (TTP-G3)																
TT 9[b]	Sandstone	37.47.872	34.58.525	258/62		-	-	-	-	-	-	-	-	-	-	-
TT 10[b]	Sandstone	37.47.611	34.58.509	260/62	17/17	4.6	54.3	318	19.5			27.1	6.2	-	-	-
TT 11	Sandstone	37.45.956	34.56.645	8/40	9/9	131.9	0.4	139.1	−31.9	13.1	17.9	12.6	17.6	12.3	5.0	20.5
TT 12	Sandstone	37.45.955	34.56.322	140/36	14/14	16.5	13.3	4.2	41.5	7.2	8.7	8.2	245	6.6	4.2	15.6
TT 13	Sandstone	37.45.904	34.56.036	224/24	17/17	38.4	53.2	11.6	45	7.7	8.6	6.2	39	6.9	3.8	13.3
TT 14	Sandstone	37.43.999	34.54.802	300/36	14/13	335.3	58.9	0.5	31.1	8.4	12.6	8.7	25.9	8.0	4.3	16.3
TT 15	Sandstone	37.44.018	34.54.797	18/24	8/6	347.2	32.3	4.2	41.6	13.5	16.2	11.5	34.9	12.3	5.9	26.5
TT 16	Sandstone	37.43.670	34.54.420	288/20	19/19	2.7	53.1	7	33.6	5.7	8.2	5.6	37.1	5.4	3.7	12.8
TT 17[b]	Sandstone	37.41.612	34.55.667	334/42		-	-	-	-			-	-			
Mean Sites TT11–TT16						173.2	−38.8					30.7	5.7			
								177.5	−38.8			13.9	24.2			
Ulukışla Basin Volcanic Rocks (TTP-G4)																
TT 18	Basalt	37.41918	34.43501	202/20	13/13	159.5	−73.6	134.3	−56.7	8.1	6.2	5.8	52.3	6.5	3.0	13.3
TT 19[b]	Basalt	37.41918	34.43501	202/20	7/7	224.5	−39.9	206.5	−44.6	-	-	7.4	36.4	-	-	-
TT66[b]	Pillow Lava	37.57793	34.53052	307/16	8/8	125.7	−39.1	138.4	−37.7	-	-	14.7	15.15	-	-	-
TT67[b]	Pillow Lava	37.59047	34.53072	307/16	10/8	325.1	41.5	156.7	−35.0	-	-	11.8	21.8	-	-	-
TT68	Pillow Lava	37.58905	34.53796	307/16	12/9	111.4	−32.4	122.0	−35.3	5.3	7.5	6.1	56.4	5.0	4.8	19.2
TL03	Pillow Lava	37.59439	34.54237	45/47	15/15	330.9	−8.5	334.7	36.5	3.3	5.0	6.2	63.2	4.4	4.1	14.9
TL04	Pillow Lava	37.59025	34.54076	45/47	25/22	309.2	−9.8	307.8	37.0	2.4	3.4	4.3	112.4	4.2	3.5	11.7
TL05	Basalt	37.05240	34.17650	295/15	10/8	105.4	−30.4	114.5	−31.7	2.4	3.2	3.9	104.2	6.0	5.2	22.1

AGU Tectonics

10.1002/2015TC003956

Table 1. (continued)

Site	Lithology	Latitude(°N)	Longitude(°E)	Strike/Dip	N/n	D_g	I_g	D_s	I_s	ΔD_X	ΔI_X	α_{95}	k	A_{95}	A_{95min}	A_{95max}
Mean Sites TT18, TT68, and L03–L05						305.8	24.2					41.9	4.3			
								308.2	40.7			15.9	24.2			
Middle Eocene																
Haymana																
TT1[c]	Sandstone	39.31734	32.08431	111/34	9/6	354.8	40.6	346.6	51.5	18.0	15.5	11.4	45.9	14.9	5.9	26.5
TT1[d]	Sandstone	39.31734	32.08431	111/34				356.6	56.7	-	-	4.9	354.8	-	-	-
TT3	Siltstone	39.14728	32.28910	242/50	9/6	336.4	54.3	334.6	4.4	9.2	18.1	14.1	43.4	9.2	5.9	26.5
Tuz Gölü (TTE-G1)																
TT77	Limestone	38.62221	33.79332	268/46	9/9	245.6	27.1	274.3	34.0	8.8	12.5	10.9	38.6	8.3	5.0	20.5
TT78	Sandstone	38.62221	33.79332	143/52	9/6	7.1	44.4	297.4	55.3	8.2	6.5	5.8	133.6	6.6	5.9	26.5
TT79	Sandstone	38.62221	33.79332	151/59	9/6	15.1	63.8	268.4	46.5	7.1	7.5	10.4	42.4	6.3	5.9	26.5
Mean Sites TT77–TT79						321.6	64.5					96.2	2.8			
								278.6	45.9			22.6	30.7			
Kırşehir /Hacıbektaş (TTE-G2)																
TT28	Claystone	38.97166	34.61616	100/80	18/18	344.7	−28.4	338.3	44.5	5.2	5.8	4.4	62.1	4.6	3.7	12.8
TT29	Limestone	38.98843	34.61720	299/78	15/13	57.6	−54.1	186.7	−42.3	14.2	17.0	11.3	14.37	12.9	4.3	16.3
TT30	Limestone	38.98583	34.63195	100/84	9/7	330.4	−50.7	343.8	23.9	8.9	15.3	10.8	32.2	8.7	5.5	24.1
TT31	Sandstone	38.97031	34.85011	268/3	13/13	345.7	28.7	346.0	25.7	8.0	13.3	8.2	26.8	7.8	4.3	16.3
TT32	Sandstone	38.95538	34.84196	354/74	10/7	116.4	25.3	122.0	−38.1	12.9	17.1	12.6	24.1	12.0	5.5	24.1
TT33	Sandstone	38.96447	34.84978	240/28	9/9	11.9	44.5	0.9	21.7	12.2	21.5	12.6	17.7	12.0	5.0	20.5
TT34	Sandstone	38.96447	34.84978	30/22	8/8	333.4	23.7	342.1	41.2	14.7	19.9	14.1	16.6	13.7	5.2	22.1
						343.4	−10.9					45.9	2.7			
								343.6	35.4			14.7	17.8			
Kırıkkale (TTE-G3)																
TT72	Sandstone	39.48457	33.22619	355/45	10/9	321.4	45.1	4.7	53.4	6.1	5.5	9.8	32.5	5.1	5.0	20.5
TT73	Claystone	39.48457	33.22619	235/35	15/13	39.1	61.6	1.8	40.3	7.9	10.0	7.3	36.6	7.3	4.3	16.3
TT96	Sandstone	39.54010	33.25899	331/22	10/10	341.6	55.7	7.2	46.6	9.3	10.4	9.3	25.4	8.3	4.8	19.2
Mean Sites TT72, TT73, and TT96						347.7	58.3					36.8	12.3			
								7.9	46.1			11.2	123.3			
Şarkışla (TTE-G4)																
TT69	Siltstone	38.93214	36.14378	193/20	12/12	31.2	34.8	196.3	−38.6	6.5	8.5	9.8	20.7	6.0	4.4	17.1
TT70	Siltstone	39.06103	36.30883	210/23	20/20	22.4	62.3	348.9	52.3	9.2	10.4	13.0	25.2	8.2	3.6	12.4
TT99[b]	Siltstone	39.06103	36.30883	210/23	15/15	-	-	-	-	-	-	-	-	-	-	-
TT131	Sandstone	38.47345	36.54902	84/68	10/7	169.1	26.1	168.2	−41.8	9.3	11.4	14.8	16.2	8.5	5.5	24.1
TT132[b]	Sandstone	38.47433	36.55166	60/44	-	-	-	-	-	-	-	-	-	-	-	-
TL06	Sandstone	38.57132	36.35104	200/15	30/26	355.3	60.2	336.6	51.4	7.1	5.9	8.6	45.2	5.8	3.3	10.5
TL07	Sandstone	38.54030	36.54017	155/15	24/20	345.1	52.0	326.9	50.2	5.8	6.7	11.2	38.4	5.2	3.6	12.4
Mean Sites TT69, TT70, TT131, TL06, and TL07						356.4	45.0					38.8	4.8			
								341.4	49.0			8.4	83.3			
Oligocene																
Tuz Gölü																
TT 8	Sandstone	38.58784	33.30173	110/18	8/6	345.8	48.3	340.3	63.6	26.2	17.2	10	43	19.6	5.9	26.5
TT24[b]	Mudstone	38.56203	33.33171	28/32		-	-	-	-	-	-	-	-	-	-	-
Ulukışla																
TT35	Mudstone	37.72036	35.02756	194/28	9	0.5	54	332.8	40.5	9.0	11.3	8.5	37.3	8.2	5.0	20.5
Pınarbaşı																
TT133[b]	Mudstone	38.78338	36.44816	224/14	12/9	333.1	42.8	326.9	48.3	-	-	22.7	11.1	-	-	-
TT36	Mudstone	37.64647	34.99027	212/34	11/11	320.4	59.0	312.4	25.9	5.9	9.8	5.7	65.4	5.7	4.6	18.1

AGU Tectonics

10.1002/2015TC003956

Table 1. (continued)

Site	Lithology	Latitude(°N)	Longitude(°E)	Strike/Dip	*N/n*	D_g	I_g	D_s	I_s	ΔD_X	ΔI_X	α_{95}	k	A_{95}	A_{95min}	A_{95max}
							Miocene									
							Haymana (TTM-G1)									
TT 7	Sandstone	39.16685	32.40796	258/62	8/6	205.7	71.0	332.4	42.2	7.7	9.3	6.4	109.3	7.0	5.9	26.5
TT 97	Sandstone	39.08603	36.31503	258/62	10/10	152.2	62.4	0.4	54.1	4.8	4.1	5.2	123.2	5.0	4.8	19.2
TT 98	Sandstone	39.07503	36.31271	258/62	10/10	341.6	−55.7	160.3	−62.3	5.4	3.4	4.8	131.0	7.8	4.8	19.2
		Mean Sites TT7, TT97, and TT98				175.5	61.6					21.2	35.0			
								343.6	53.5			20.8	36.3			
							Niğde (TTM-G2)									
TT 20	tuff	37.41918	34.43501	252/30	34/34	244.8	−70.2	195.5	−52.5	5.5	4.6	3.7	45.6	4.5	2.9	8.9
TT 21	tuff	37.46647	34.38343	252/30	13/13	255.7	−63.4	208.6	−52.1	3.4	3.0	2.3	335.4	4.9	4.3	16.3
TT 22	tuff	37.46647	34.38343	252/30	8/8	254	−72.3	195	−56.2	6.6	5.2	4.2	179.1	5.3	5.2	22.1
TT 23	Basalt	37.46701	34.37920	horizontal	8/8	349.4	46	349.4	46	10.4	11.0	7.8	51.3	9.1	5.2	22.1
		Mean Sites TT20–TT23				221.5	−68.7					26.9	12.7			
								191.4	−52.6			12.9	52.0			
							Yahyalı-Niğde									
TT 123	Siltstone	38.02848	35.50195	horizontal	16/16	8.0	58.9	-	-	4.5	3.1	5.5	45.7	4.4	4.0	14.3
TT 124	Mudstone	38.03421	35.50253	horizontal	10/9	317.0	41.5	-	-	13.3	16.2	12.0	19.4	12.1	5.0	20.5
							Mersin (TTM-G3)									
TT 57	Sandstone	37.36697	35.25990	67/22	18/14	6.6	34.3	19.6	52.3	11.7	11.1	10.9	17.9	10.0	4.3	16.3
TT 58	Marl	37.37244	35.26647	334/10	10/8	345	46.7	354.8	44.0	7.1	12.2	9.8	17.9	6.9	5.0	20.5
TT 59	Sandstone	37.37807	35.27280	35/12	14/11	347.9	49.0	360.0	57.0	10.0	7.3	8.8	27.7	7.8	4.6	18.1
TT 60	Claystone	37.38512	35.27619	50/28	17/17	342.5	34.0	357.5	58.6	6.9	5.4	9.8	14.6	5.6	3.9	13.8
TT 61	Sandstone	37.34491	35.25715	90/11	23/23	359.9	38.3	359.9	49.2	6.7	6.6	5.1	36.8	5.8	3.4	11.4
TT 62[b]	Sandstone	37.31316	35.07203	55/10	16/16	50.8	36.5	58.2	36.6	-	-	8.9	18.1	-	-	-
		Mean Sites TT57–TT61				352.8	40.8					10.1	58.0			
								2.1	52.5			7.9	94.8			

[a]Site numbers, lithology, geographic location (latitude and longitude), and bedding attitudes are given first. *N* denotes number of sites, and n the number of sites used for site mean calculation. Declination $D_{g(s)}$ and inclination $I_{g(s)}$ describe themean directions in geographic (before tilt correction) and stratigraphic (after tilt correction) coordinates, respectively. α_{95} is the 95% confidence circle and k is the precision parameter [*Fisher*, 1953], ΔD_X and ΔI_X are the declination and inclination errors calculated after *Deenen et al.* [2011].

[b]Correspond to sites where no mean direction could be obtained, because of unstable demagnetization behaviour and mean directions with large α_{95}.

[c]Shows single sites of volcanic rocks which are not included into the mean direction of sedimentary rocks.

[d]Denotes sites with anomalous declination from the rest of their group means (see main text) (P. limestone corresponds to Pelagic limestone).

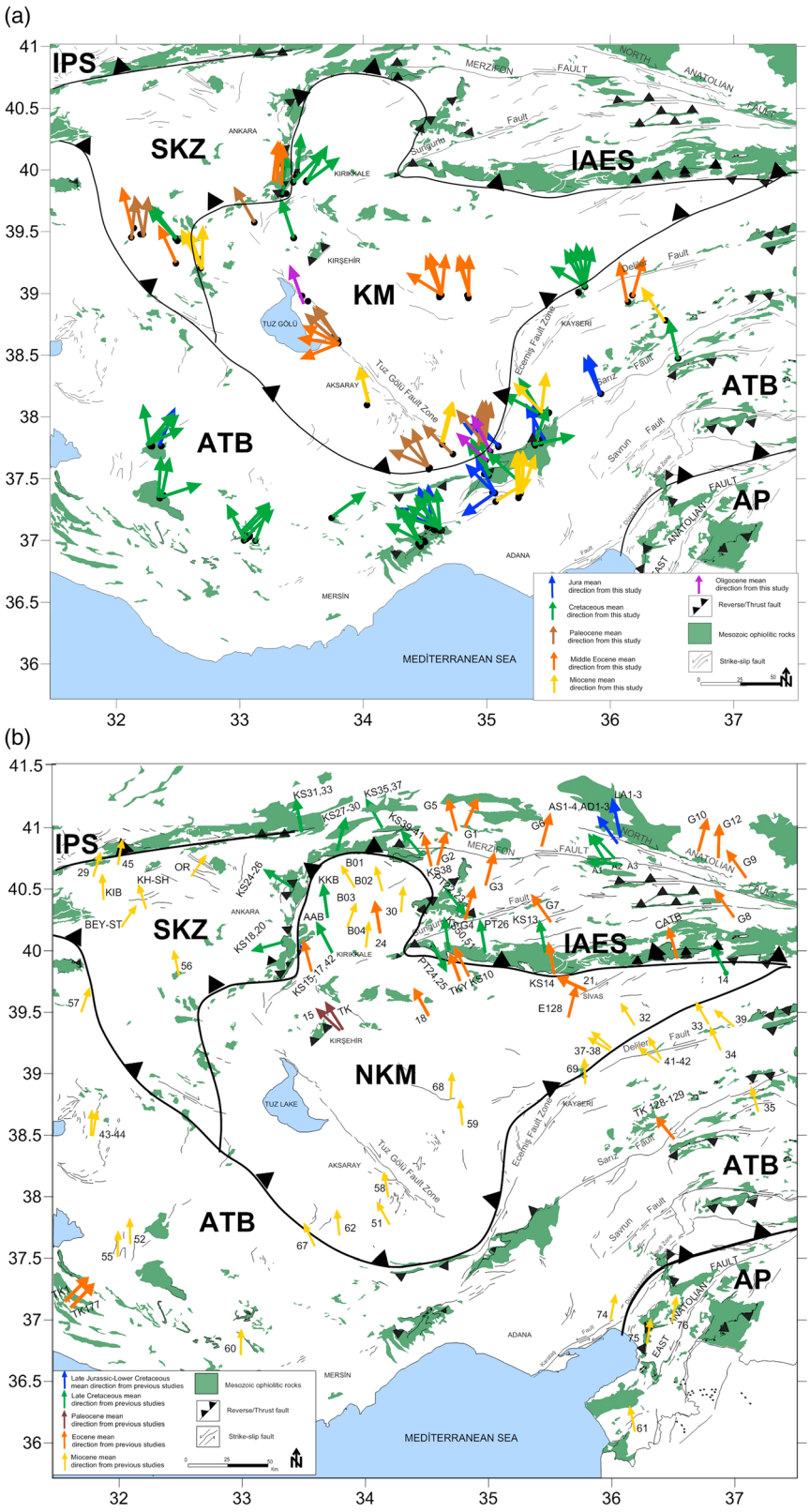

Figure 6. Paleomagnetic declination vectors (a) from this study and (b) from previous studies according to different ages (blue arrows indicate Late Jurassic rotations, green arrows refer to Late Cretaceous rotations, and orange and yellow arrows indicate Middle Eocene and Middle Miocene rotations, respectively. IAES, Izmir Ankara Erzincan suture; IPS, Intra Pontide Suture; SKZ, Sakarya zone; NKM, Niğde-Kırşehir Massif; ATB, Anatolide-Tauride Block; and AP, Arabian platform).

$I = 359.6°/61.6°$). After removal of the weak overprint, a ChRM direction was calculated from the vector that decays linearly to the origin (Figures 5b, 5c, 5e–5g, 5i, 5j, and 5l–5o).

The site-mean directions before and after tectonic correction for individual sites according to their age and locality are given in Table 1. The mean directions of individual sites are relatively well grouped with α_{95} values between 2.3° and 15.4°. Out of 147 sites, 34 sites were discarded because of a confidence circle greater than 20° (TT19, TT26, TT47, TT52b, TT54a, TT63, TT82, TT83, TT102, and TT133), unreliable behavior in the Zijderveld diagram [*Zijderveld*, 1967] (TT6, TT9, TT24, TT42, TT99, TT105, TT116, 132, and TT135), and too much dispersion from the group mean direction (TT1b, TT10, TT39, TT66, TT112, TT118, TT121, and TT126) (Table 1). Sites TT75 and TT125 which consist of volcanic rock are not included into the mean direction of sedimentary rocks. Sites TT50 and TT127 showed difference in declination from the rest of the group in TTJ-G1 and TTJ-G2, respectively (Table 1). In addition to this filtering, we apply the criteria of *Deenen et al*. [2011] who used k values >50 for volcanic rocks. Therefore, sites TT55, TT66, and TT67 were discarded from the group mean direction (Table 1, TTC-G5). All ChRM directions are calculated by fitting a line to four or more consecutive demagnetization steps and show Medium Destructive Field (MAD) values equal to or less than 5°.

5.4. Paleomagnetic Mean Directions

In Figures 6a and 6b, the paleomagnetic directions from this study and those from earlier studies are given on separate tectonic maps. The Late Jurassic-Lower Cretaceous vectors indicate counterclockwise rotation in SE Taurides in almost all sites, while one single site in the central Taurides (TT106) shows clockwise rotation. Previous Late Cretaceous paleomagnetic vectors from the ophiolites and the overlying sedimentary rocks indicate a concordance with the curvature of the Izmir-Ankara-Erzincan Suture (IAES) [*Çinku et al*., 2015]. However, in this present study, clockwise rotations up to 52° are obtained inside the Niğde-Kırşehir Massif in the Kırıkkale area, and counterclockwise rotations are found in the Polatlı-Haymana Basin which could be linked to local deformation (Table 1). In the SE Taurides, counterclockwise rotations are obtained between Mersin and Kayseri, while clockwise rotations are shown in the central Taurides (Table 1).

The mean directions from Palaeocene sites in the east of the Ulukışla Basin show declination in clockwise sense, while counterclockwise rotations occur farther west of the basin. The counterclockwise rotation in Tuz Gölü continues through Kırıkkale, although small clockwise rotations are obtained in the Haymana Basin. The Middle Eocene results clearly show counterclockwise rotations in both the SE Taurides and the Niğde-Kırşehir Massif. In the Tuz Gölü area, large counterclockwise rotations ranging from 63° to 112° are observed, while no significant rotations are shown in northern Kırıkkale. When considering the Middle Miocene results, as a general picture, clockwise rotations are obtained in the southern Niğde-Kırşehir Massif and counterclockwise rotations are apparent in the north (Figures 6a and 6b). Moreover, no significant rotations are shown in the SE Taurides, whereas in local areas large rotations are found in the borders of small faults.

5.4.1. The Haymana Basin

Two different group mean directions have been calculated around the Haymana basin in Latest Cretaceous. The Late Cretaceous mean site direction is calculated as $D = 318.8°$ and $I = 39.5°$ ($k = 36.1$, $a_{95} = 12.9°$) in stratigraphic coordinates (Figure 7a1). In the *McElhinny* [1964] fold test the mean direction passes the fold test at 95% confidence level with $k_s/k_g = 4.5$ (critical values at 95% limit: 3.44 and 99% limit: 6.03). In the *McFadden* [1990] test the precision parameter reached a maximum at 97% unfolding (Figure 7a4). For Paleocene rocks a ChRM direction of $D = 348.5°$ and $I = 39.5°$ ($k = 47.9$, $a_{95} = 11.2°$) is obtained in stratigraphic coordinates (Figure 7a2). The ratio of tilt corrected and in situ precision parameter is $k_s/k_g = 3.6$ (critical values at 95% limit: 3.44 and 99% limit: 6.03) after *McElhinny* [1964], and a k_{max} is achieved at 93% tilt correction (Figure 7a4). In addition, three sites from Middle Miocene sandstones obtained from the same strata indicate a ChRM direction of $D = 343.6°$ and $I = 53.5°$ ($k = 35.0$, $a_{95} = 21.2$; Figure 7a3). Out of three Middle Eocene sites, one reliable site showed small counterclockwise rotation, while the others showed either very small inclination or a secondary component with a nearly present field direction (Table 1).

In order to determine the timing and stability of the remanence we could perform only one conglomerate test in cobbles from the Late Cretaceous sandstones of the Haymana formation. During the conglomerate tests, high medium destructive fields (MDF > 30 mT) were isolated in the Zijderveld diagrams (Figure 7a5). The mean direction of the cobble specimens scattered, as seen in the stereonet (Figure 7a5) showing random distribution with $\alpha_{95} = 52.6°$ and $R < R_0$ according to the Watson test [*Watson*, 1956], indicates that they pass the conglomerate test and is therefore considered a primary remanence.

5.4.2. The Kırıkkale Basin

Data groups have been assigned according to the age of different sites in Kırıkkale. The Late Cretaceous group mean direction is obtained with two normal polarity and two reversed polarity sites, yielding a mean ChRM direction of $D = 26.2°$ and $I = 41.7°$ ($k = 15.0$, $a_{95} = 17.7°$) in stratigraphic coordinates (Figure 7b1). In the *McFadden* [1990] fold test, the precision parameter reaches a maximum at 71% of unfolding, indicating a prefoding magnetization (Figure 7b3). The Middle Eocene mean direction of three normal-polarity sites is well defined with a mean ChRM direction of $D = 7.9°$ and $I = 46.1°$ ($k = 123.3$, $a_{95} = 11.2°$) in stratigraphic coordinates (Figure 7b2). The precision parameter (k) increases ($k_s/k_g = 10.1$; critical values at 95% limit: 6.39 and 99% limit: 16.00) after tilt correction, which indicates a positive fold test [*McElhinny*, 1964] at the 95% confidence limit. In the McFadden fold test [*McFadden*, 1990], k_{max} reached at 77% unfolding (Figure 7b3).

5.4.3. The Tuz Gölü Basin

The ChRM site mean directions obtained from three Paleocene sites yielding a ChRM mean direction of $D = 320.0°$ and $I = 31.2°$ ($k = 90.9$, $a_{95} = 13.0°$) in stratigraphic coordinates Figure 7c1. The precision parameter appears at 77% unfolding after applying the *McFadden* [1990] fold test (Figure 7c3). The Middle Eocene sites from three reliable normal polarity sites show a mean direction of $D = 278.6°$ and $I = 45.9°$ ($k = 30.7$, $a_{95} = 22.6°$) in stratigraphic coordinates (Figure 7c2). For this group mean direction the fold test of *McElhinny* [1964] yields a ratio of $k_s/k_g = 11.2$ (critical values at 95% limit: 6.39 and 99% limit: 16.00) which is significant at 95% level. In the *McFadden* [1990] fold test, however, a maximum precision parameter is reached at 121% of unfolding, suggesting a complex structural fold (Figure 7c3).

One reliable site (TT8) was obtained from Oligocene sandstones showing a more northerly direction (Table 1). This site was, however, not considered in further interpretation.

5.4.4. The Ulukışla Basin

Group mean directions from Paleocene Ulukışla formation was calculated separately for lavas and sedimentary rocks. We then obtained a mean direction from four normal polarity and one reversed polarity sites of the sedimentary rocks, which is $D = 177.5°$ and $I = -38.8°$ ($k = 24.2$, $a_{95} = 13.9°$) in stratigraphic coordinates (Figure 7d1). The volcanic rocks showed three reversed polarity and one normal polarity sites and a mean direction of $D = 308.2°$ and $I = 40.7°$ ($k = 24.2$, $a_{95} = 15.9°$) in stratigraphic coordinates (Figure 7d2). In the *McElhinny* [1964] fold test, the k ratio of tilt corrected and in situ precision parameters are 4.2 (critical values at 95% limit: 2.97 and 99% limit: 4.85) and 5.7 (critical values at 95% limit: 3.44 and 99% limit: 6.03) for sedimentary and volcanic rocks, respectively. Both the sedimentary and volcanic rocks pass the *McFadden* [1990] test at 115% and 122% unfolding (Figure 7d4).

In the same area close to the Ecemiş fault, one single site from Oligocene mudstones showed a mean direction of $D = 332.8°$ and $I = 40.5°$ ($k = 37.3$, $a_{95} = 8.5°$) in stratigraphic coordinates (Table 1, site TT35). The overlying Middle Miocene sedimentary rocks showed a mean direction of $D = 191.4°$ and $I = -52.6°$ ($k = 56.0$, $a_{95} = 12.9°$) in stratigraphic coordinates (Figure 7d3). Both the *McElhinny* [1964] and *McFadden* [1990] test was inconclusive for these sites, because of only one single tilt correction applied for three sites and a horizontal layered site.

5.4.5. The Çamardı-Pozantı-Şarkışla Region

When considering the mean direction on stereonets, two different groups could be separated. The Late Jurassic mean direction from three normal polarity sites is $D = 314.1°$ and $I = 23.5°$ ($k = 227.4$, $a_{95} = 8.2°$) after tilt correction (Figure 7e1). The k ratio of tilt corrected and in situ precision parameters was estimated to be 9.5 (critical values at 95% limit: 6.39 and 99% limit: 16.00), and the maximum precision parameter was reached at 92% unfolding (Figure 7e4).

The Late Cretaceous ChRM site-mean direction obtained from six normal and two reversed polarity sites yielding a ChRM mean direction of $D = 328.8°$ and $I = 33.7°$ ($k = 50.9$, $a_{95} = 9.5°$) in stratigraphic coordinates (Figure 7e2). To constrain the age of magnetization, the fold test of *McElhinny* [1964] showed a k ratio of $k_s/k_g = 4.6$ (critical values at 95% limit: 2.97 and 99% limit: 4.85) which is significant at 95% level. The *McFadden* [1990] fold test demonstrates that the precision parameter reached a maximum at 88% of unfolding (Figure 7e4).

Further northeast around Şarkışla, Middle Eocene sites obtained from three normal and two reversed polarity sites yield a mean direction of $D = 341.4°$ and $I = 49.0°$ ($k = 83.3$, $a_{95} = 8.4°$; Figure 7e3). When concerning the fold test of *McElhinny* [1964] a ratio of precision $k_s/k_g = 17.2$ (critical values at 95% limit: 3.44 and 99% limit: 6.03) is calculated at 99% confidence level. In the *McFadden* [1990] test the Middle Eocene sites exhibit a prefolding after 108% of unfolding (Figure 7e4).

5.4.6. The Tuzlagölü-Hacıbektaş Area

The ChRM mean direction of the Late Cretaceous sites from three normal and reversed polarity sites is $D = 165.5°$ and $I = -40.7°$ ($k = 17.4$, $a_{95} = 16.5°$; Figure 7f1). A prefolding was considered for this group mean direction after a positive fold test [*McFadden*, 1990] at 86% unfolding (Figure 7f3).

The site mean direction from Middle Eocene sites in Hacıbektaş indicates five normal and two reversed polarity sites which is $D = 343.6°$ and $I = 35.4°$ ($k = 17.8$, $a_{95} = 14.7°$; Figure 7f2) after tilt correction. In the *McElhinny* [1964] fold test, the k ratio of tilt corrected and in situ precision parameters is 6.6 (critical values at 95% limit: 2.69 and 99% limit: 4.16) A positive fold test is obtained after *McFadden* [1990], with a maximum unfolding at 105% (Figure 7f3).

Close to the Ecemiş and Sarız faults (Figure 2) single reliable site from Oligocene mudstones (TT35, TT36, and TT133) and two sites from Miocene sandstones (TT123 and TT124) showed declinations in NW direction (Table 1). These sites, however, were not enough for calculating a mean direction.

5.4.7. The Mersin Region

The ChRM direction obtained from Late Jurassic-Lower Cretaceous sedimentary rocks of three normal and two reversed polarity sites is $D = 326.9°$ and $I = 31.2°$ ($k = 34.4$, $a_{95} = 15.9°$) after tilt correction (Figure 7g1). A significant improvement of the statistical parameters is obtained after tilt correction; however, the fold test of *McFadden* [1990] shows that the maximum precision parameter is obtained at 120% unfolding (Figure 7g5). Late Cretaceous sites are grouped into volcanic and sedimentary rocks to better see the affect of shallowing in sedimentary rocks. We obtained a mean direction of $D = 303.9°$ and $I = 36.9°$ ($k = 33.0$, $a_{95} = 6.3°$), from five normal polarity sites of Late Cretaceous sedimentary rocks after tilt correction (Figure 7g2). The mean direction of five normal polarity sites obtained from lavas is $D = 320.7$ and $I = 32.7°$ ($k = 27.8$, $a_{95} = 14.8°$) after tilt correction (Figure 7g3). The mean direction obtained from both the sedimentary and volcanic rocks exhibits a prefolding with maximum untilting at 83% and 103%, respectively (Figure 7g5). The *McElhinny* [1964] fold test which was conclusive only for lavas shows that the precision parameter (k) increases ($k_s/k_g = 6.2$; critical values at 99% limit: 2.97 and 99% limit: 4.85) after tilt correction. In the same area Middle Miocene sedimentary rocks show a mean direction of $D = 2.1°$ and $I = 52.5°$ ($k = 94.8$, $a_{95} = 7.9°$) after tilt correction with a maximum unfolding achieved at 67% after *McFadden* [1990] (Figure 7g5).

5.4.8. The Konya-Karaman Region

The ChRM direction obtained from limestones almost showing normal polarity at 12 reliable sites is $D = 40.0°$ and $I = 31.8°$ ($k = 13.1$, $a_{95} = 11.9°$) after tilt correction (Figure 7h1). The fold test of *McElhinny* [1964] showed a k ratio of $k_s/k_g = 3.6$ (critical values at 95% limit: 3.44 and 99% limit: 6.03) which is significant at 95% level. The *McFadden* [1990] fold test demonstrates a prefolding where the precision parameter reached a maximum at 93% of unfolding (Figure 7h2).

5.5. Paleosecular Variation and Timing of Magnetization Acquisition

For meaningful tectonic interpretation of the paleomagnetic results it is necessary to demonstrate (a) the adequate sampling of paleosecular variation (PSV) and (b) the age of magnetization.

The criteria for paleosecular variation of the geomagnetic field developed by *Deenen et al*. [2011] depend on the investigation of the statistical values of paleomagnetic data sets given by the A_{95} cone of confidence envelopes of the VGP populations and on the number of samples (N). If the A_{95} value calculated for a mean VGP is between the lower (A_{95min}) and upper (A_{95max}) limits predicted from the geomagnetic field models, then we can conclude that the scatter observed in the VGP population is consistent with and averages of PSV. If A_{95} values are below or above the limits, then PSV should be considered unreliable [*Deenen et al*., 2011].

In this approach, the paleomagnetic directions are transformed into VGPs to calculate the Fisher mean VGP for each site. The *Vandamme* [1994] cutoff criteria as well as the fixed 45° angular cutoff are used to check the reliability of A_{95} values at the site level with the A_{95min} and A_{95max} of the *Deenen et al*. [2011] criteria. All reliable sites yield A_{95} values that lie within the reliability envelope (Table 1). Therefore, we consider that PSV is adequately averaged in our data set.

In addition, both the lavas and the sedimentary rocks have been sampled at independent and widely spaced sites and are distributed within the geological formations over time intervals long enough to average out the geomagnetic secular variation.

Table 2. Late Jurassic to Middle Miocene Mean Site Directions Obtained From This Study and Previous Paleomagnetic Results in the SE/E, SW/W, and Inside Areas of the Niğde-Kırşehir Massif[a]

Group/Site	Site λ, ϕ (N°, E°)	D/I	α_{95}	λ_{obs}, ϕ_{obs} (N°, E°)	α_{95}	$R \pm \Delta R$ Africa	Paleolatitude (λ °N)
			***Late Jurassic-Lower Cretaceous* (~150 Ma)**				
TTJ-G1	37.25/35.00	319.2/31.9	15.9	49.1/287.4	13.4	−32.2 ± 11.0	$\lambda = 16.2°N^{+5.2°}_{-4.6°}$[b]
TTJ-G2	37.76/35.50	314.1/23.5	8.2	42.1/286.1	6.4	−37.2 ± 6.1	$\lambda = 14.5°N^{+6.5°}_{-5.7°}$[b]
Mean G1 and G2	**37.5/35.00**	**316.9/28.3**	**8.6**	**45.9/286.3**	**8.6**	**−35.1 ± 8.2**	$\boldsymbol{\lambda = 15.5°N^{+3.5°}_{-3.3°}}$[b]
			***Late Cretaceous* (~80 Ma)**				
TTC-G1	39.25/32.30	318.8/39.5	12.9	49.2/288.9	12.0	−35.2 ± 11.0	$\lambda = 22.4°N^{+5.2°}_{-4.6°}$[c]
TTC-G2	39.55/33.32	26.2/41.7	17.7	63.1/150.4	16.9	32.1 ± 14.7	$\lambda = 24.8°N^{+5.2°}_{-4.6°}$[b]
TTC-G3	39.05/35.79	165.5/-40.7	16.5	70.0/258.0	15.6	−8.9 ± 13.6	$\lambda = 21.5°N^{+5.2°}_{-4.6°}$[b]
TTC-G4	37.53/37.97	317.4/33.5	15.1	48.2/292.7	13.0	−37.1 ± 14.9	$\lambda = 17.7°N^{+2.5°}_{-2.4°}$[b]
TTC-G5	37.08/34.58	306.4/34.5	21.9	40.0/298.7	19.0	−48.0 ± 15.7	$\lambda = 17.7°N^{+4.8°}_{-4.3°}$[b]
TTC-G6	37.00/34.45	314.7/33.0	15.9	45.6/290.5	13.4	−40.1 ± 11.4	$\lambda = 17.9°N^{+5.2°}_{-4.6°}$[b]
Mean G4–G6	**37.00/35.00**	**314.3/33.5**	**8.0**	**45.8/292.3**	**6.8**	**−41.1 ± 7.6**	$\boldsymbol{\lambda = 17.5°N^{+1.9°}_{-1.9°}}$[b]
TTC-G7	37.50/32.50	40.3/29.7	11.5	48.5/142.7	9.9	45.9 ± 9.3	$\lambda = 18.5°N^{+1.8°}_{-1.7°}$[b]
			***Paleocene* (~60 Ma)**				
TTP-G1	39.50/32.12	348.5/39.5	11.2	71.5/231.8	10.4	−10.2 ± 7.9	$\lambda = 22.4°N^{+9.0°}_{-7.3°}$[b]
TTP-G2	38.40/33.70	320.0/31.2	13.0	48.6/281.1	10.9	−39.54 ± 9.9	$\lambda = 16.8°N^{+5.1°}_{-4.6°}$[b]
TTP-G3	37.45/34.55	177.5/-38.8	13.9	74.3/223.1	12.8	−2.1 ± 10.4	$\lambda = 21.1°N^{+3.8°}_{-3.5°}$[b]
TTP-G4	37.50/34.45	308.2/40.7	15.9	50.5/298.5	15.0	−51.5 ± 13.1	$\lambda = 19.4°N^{+1.9°}_{-1.8°}$[b]
			***Middle Eocene* (~40 Ma)**				
TTE-G1	38.62/33.79	278.6/45.9	22.6	25.1/320.1	23.1	−85.5 ± 19.3	-
TTE-G2	39.48/33.22	343.6/35.4	14.7	65.6/253.2	12.9	−20.6 ± 10.5	$\lambda = 18.9°N^{+5.5°}_{-4.8°}$[b]
TTE-G3	38.47/36.55	7.9/46.1	11.2	77.1/183.3	11.5	3.9 ± 10.0	$\lambda = 28.2°N^{+9.7°}_{-7.8°}$[b]
TTE-G4	39.31/36.08	341.4/49.0	11.2	71.7/285.4	10.9	−24.3 ± 9.8	$\lambda = 27.8°N^{+4.3°}_{-3.9°}$[b]
EG5	39.00/34.00	158.6/-29.7	8.7	60.3/259.0	8.0	−25.5 ± 7.3	$\lambda = 19.4°N^{+1.9°}_{-1.8°}$[b]
EG6	37.00/32.00	219.6/-30.1	13.2	49.3/142.0	10.9	40.2 ± 8.7	$\lambda = 16.9°N^{+8.2°}_{-6.9°}$[b]
			***Middle Miocene* (~10 Ma)**				
TTM-G1	39.10/32.40	343.6/53.5	20.8	75.9/290.4	24.2	−20.5 ± 21.5	-
TTM-G2	37.46/34.38	191.4/-52.6	12.9	79.4/153.0	14.8	7.6 ± 13.4	$\lambda = 33.2°N^{+14.4°}_{-10.6°}$[c]
TTM-G3	37.37/35.27	355.3/53.2	10.8	84.7/263.1	12.5	−8.7 ± 11.2	$\lambda = 33.7°N^{+12.0°}_{-9.2°}$[c]
MG4	37.00/31.00	353.3/53.6	5.1	83.8/275.3	5.9	−8.3 ± 5.5	$\lambda = 34.1°N^{+5.2°}_{-4.6°}$[c]
MG5	38.00/36.00	346.9/52.6	3.4	77.3/282.7	3.9	−16.8 ± 3.9	$\lambda = 33.8°N^{+3.6°}_{-3.3°}$[c]
MG6	39.00/34.00	174.4/-50.5	4.1	81.0/246.2	4.1	−9.0 ± 3.7	$\lambda = 31.2°N^{+2.9°}_{-2.7°}$[c]

[a] N = number of sites used for mean site calculation. Declination $D_{g(s)}$ and inclination $I_{g(s)}$ describe the mean directions in geographic (before tilt correction) and stratigraphic (after tilt correction) coordinates, respectively. α_{95} is the 95% confidence circle, and k is the precision parameter [*Fisher*, 1953].

[b] Paleolatitudes determined after inclination only-data [*Enkin and Watson*, 1996].

[c] Fisher analysis (1953).

Reference poles of Africa are used after *Besse and Courtillot* [2002] for Late Jurassic-Lower Cretaceous (150 Ma: $\lambda = 67.0$, $\phi = 26.6$; $\alpha_{95} = 6.85$); Late Cretaceous (80 Ma: $\lambda = 84.7$, $\phi = 275.8$; $\alpha_{95} = 6.0$); Paleocene (60 Ma: $\lambda = 84.7$, $\phi = 217.6$; $\alpha_{95} = 2.8$); Middle Eocene (40 Ma: $\lambda = 84.3$, $\phi = 172.4$; $\alpha_{95} = 3.3$); and Middle Miocene (10 Ma: $\lambda = 86.0$, $\phi = 160.8$; $\alpha_{95} = 2.0$).

See Appendix A:

EG5: KS10,11,14-17,38,42 [*Çinku et al.*, 2015], TK117 [*Kissel et al.*, 2003], E128-131, E72-73, E75 [*Gürsoy et al.*, 1997].

EG6: TK176-180,TK196,TK197 [*Kissel et al.*, 1993].

MG4: K1,K2 [*Platzman et al.*, 1998]. TK192-194 [*Kissel et al.*, 1993]. Harami,Karaman-Karacadağ-Hasandağ 3-5,7,8,10,12-16,18,19-24,26,28-38,41-45 [*Gürsoy et al.*, 1998].

MG5: 3-8,11,12,14-8,21-25,29,32-43,46-48,51,53,55-59,61-62,64-67,69,72,7375-79,83-84,86,88-92 [*Gürsoy et al.*, 2011]. M12,M13, M19,M20, M76,M78,M101, M103-105,M227,M228 [*Gürsoy et al.*, 1997]. S8-11 [*Platzman et al.*, 1998].

MG6: N6 [*Platzman et al.*, 1998]. 1-3,5-11, 12-15, 17, 20, 22-28, 31-33 [*Piper et al.*, 2002]. BO01-04, SU01-02, TU01 [*Lucifora et al.*, 2013]. UR, KUC [*Kaymakçı et al.*, 2003].

Inclination-only calculation: (*N*:number of samples).

MeanTTJ-G1,G2: Geographic:Inc:34.2 ± 7.8, $k = 25.7$ Stratigraphic: Inc:27.7±5.7, $k = 48.7$.

MeanTTC-G1(N:6) after *Fisher* [1953], see Table 1.

MeanTTC-G2:(N:5) Geographic:Inc:37.8±10.1, $k = 24.8$ Stratigraphic: Inc:40.6 ± 8.5, $k = 35.0$.

MeanTTC-G3: (N.6) Geographic:Inc:31.9+33.8-16.9, $k = 8.4$ Stratigraphic: Inc:38.2 ± 6.3, $k = 52.2$.

MeanTTC-G4-6: (N:17) Geographic:Inc:37.8 ± 10.1, $k = 24.8$ Stratigraphic: Inc:40.6±8.5, $k = 35.0$.

MeanTTC-G7: (N:14) Geographic:Inc:34.7 + 16.9-11.4, $k = 4.9$ Stratigraphic: Inc:28.8 ± 7.5, $k = 16.0$.

MeanTTP-G1: (N:5) Geographic:Inc:46.0 + 14.6-10.9, $k = 9.6$ Stratigraphic: Inc:39.0 ± 6.3, $k = 63.6$.

MeanTTP-G2: (N:3) Geographic:Inc:46.1 + 34.6-16.9, $k = 11.1$ Stratigraphic: Inc:31.1±7.7, $k = 70.7$.

MeanTTP-G3: (N:6) Geographic:Inc:38.9 + 41.9-23.5, $k = 3.2$ Stratigraphic: Inc:37.6 ± 5.3, $k = 75.9$.

MeanTTP-G4: (N:4) Geographic:Inc:46.1 + 34.6-16.9, $k = 11.1$ Stratigraphic: Inc:31.1±7.7, $k = 70.7$.

Table 2. Notes (continued)

MeanTTE-G2: (N:7) Geographic:Inc:37.6 ± 10.8, $k = 15.3$, Stratigraphic: Inc:34.4 ± 7.8, $k = 29.4$.
MeanTTE-G3: (N:3) Geographic:Inc:54.5 + 10.2-8.8, $k = 18.3$, Stratigraphic: Inc:47.0 ± 10.3, $k = 39.8$.
MeanTTE-G4: (N:6) Geographic:Inc:51.9+14.4-10.1, $k = 8.4$, Stratigraphic: Inc:46.5 ± 5.0, $k = 84.0$.
MeanTTE-G5: (N:8) Geographic:Inc:51.1 + 12.7-9.7, $k = 20.5$, Stratigraphic: Inc:28.5 ± 5.3, $k = 55.6$.
MeanTTE-G6: (N:) Geographic:Inc:34.1 + 7.6-12.8, $k = 6.2$, Stratigraphic: Inc:25.4 ± 10.6, $k = 15.9$.
MeanTTM-G2 (N:4), TTM-G3(N:5), MG4(N:40), MG5(N:81), MG6(N:38) after *Fisher* [1953], see Table 1.

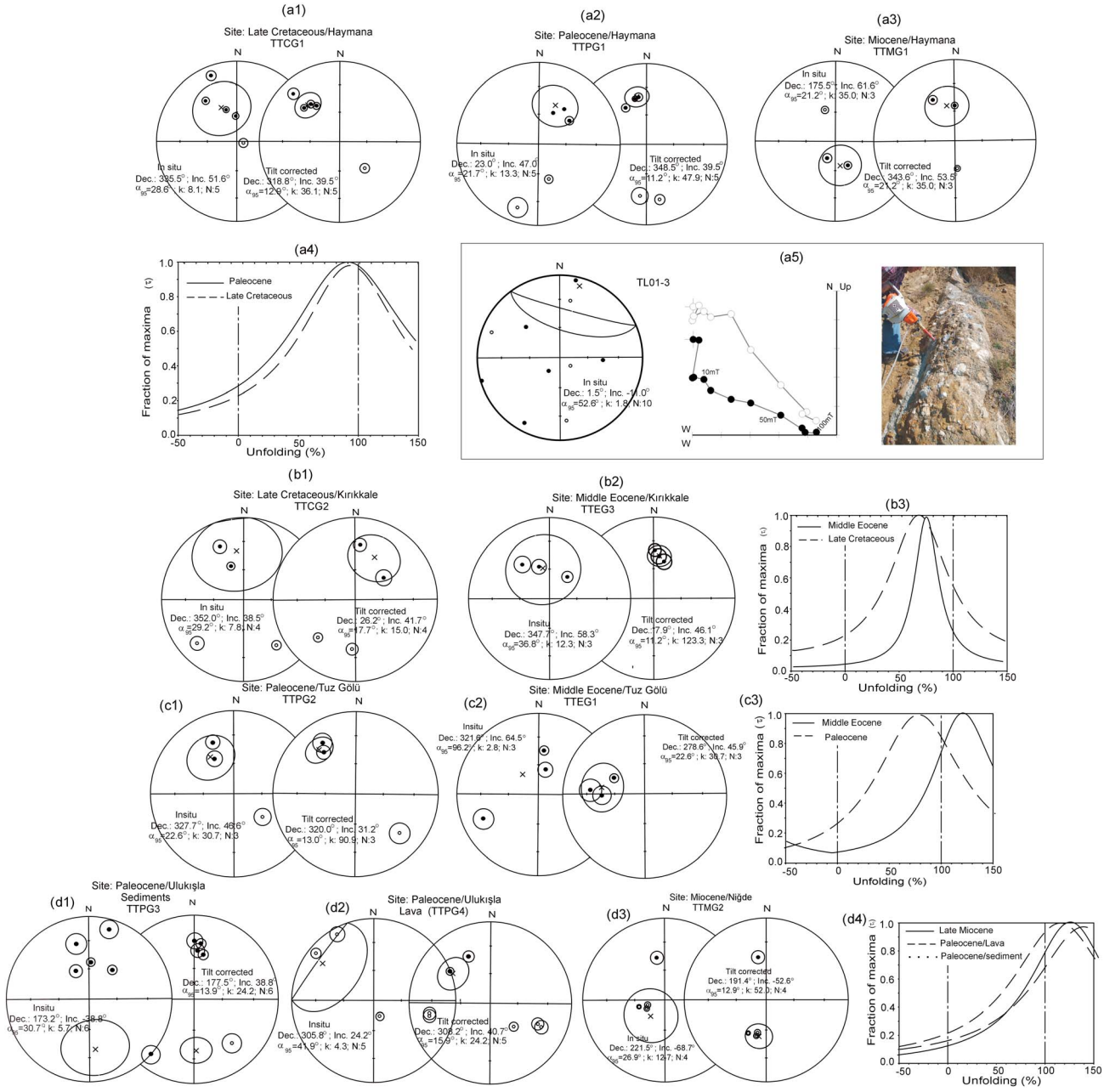

Figure 7. Paleomagnetic mean site directions before and after tilt correction together with the fold test of *McFadden* [1990] from this study in different time intervals (a1–a4) Haymana; (b1–b3) Kırıkkale; (c1–c3) Tuz Gölü; (d1–d4) Ulukışla-Niğde; (e1–e3) Çamardı-Pozantı; (f1–f4) Tuzlagölü-Hacıbektaş-Şarkışla; (g1–g5) Mersin; (h1–h2) Konya-Karaman (Solid (open) symbols on lower (upper) hemisphere of equal area stereographic projection). (a5) Conglomerate test showing mean direction in the stereonet with statistical parameters and the AF treatment in Zijderveld diagram [*Zijderveld*, 1967] together with a field photo in Haymana.

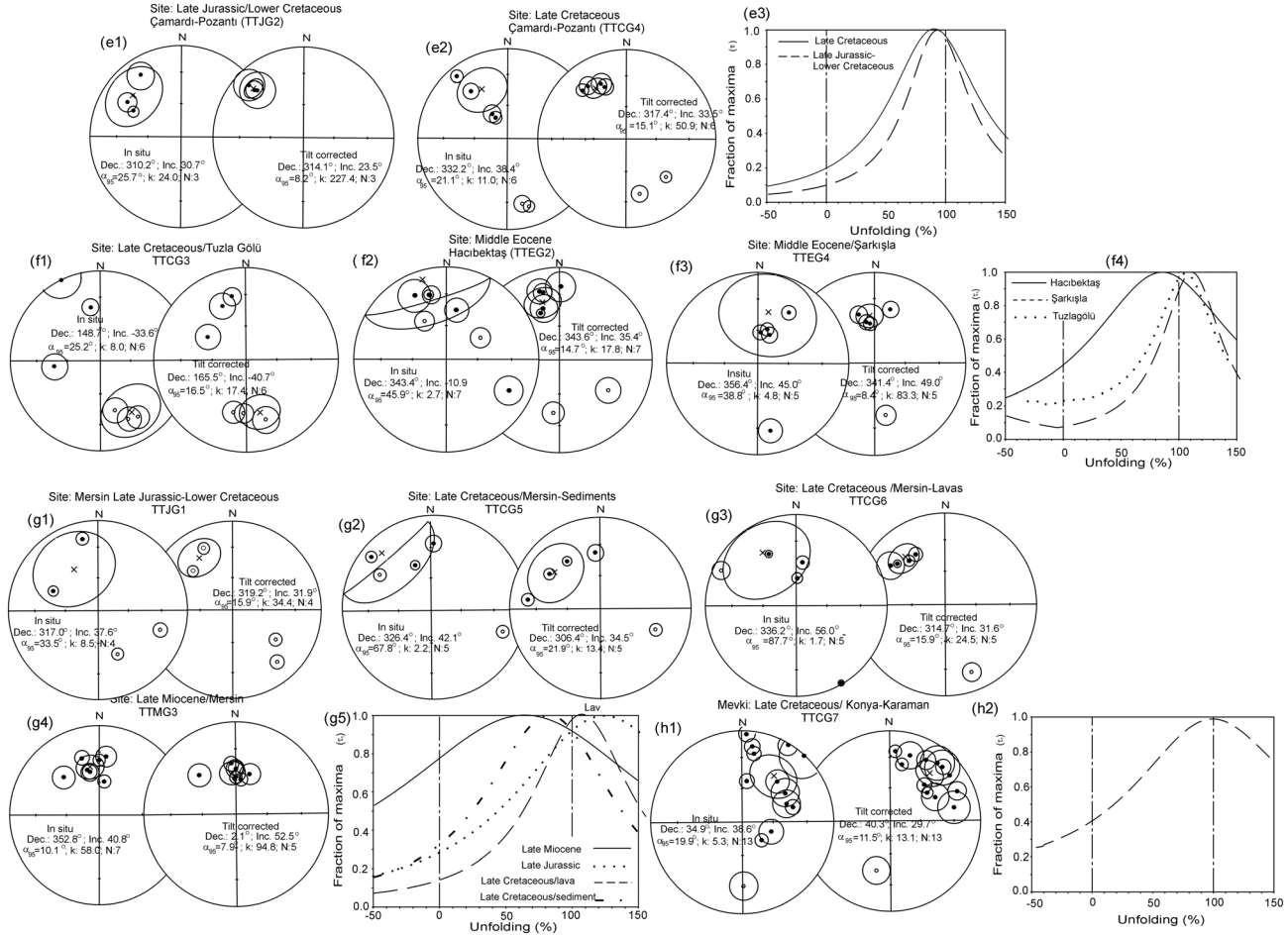

Figure 7. (continued)

During this study, the age of magnetization has been constrained by the application of several statistical fold tests depending on the clustering of the paleomagnetic directions (see text above and *Watson and Enkin* [1993]) (see Table 2). It has been shown that almost all groups indicate a prefolding age.

It has been reported that besides the incremental fold tests additional rock magnetic interpretations are necessary especially if the remagnetization has occurred before folding. The measurement of hysteresis loops makes the identification of remagnetized and nonremagnetized trends. However, for weakly magnetic samples, this approach is invalid. Therefore, an end-member approach which depends on analyses of the IRM acquisition curves is considered [e.g., *Weltje*, 1997; *Heslop and Dillon*, 2007; *Gong et al*., 2009a, 2009b]. Several case studies that demonstrate this approach can be successful for recognizing remagnetization in both sedimentary and volcanic rocks [*Gong et al*., 2009a, 2009b; *Van Hinsbergen et al*., 2010; *Meijers et al*., 2011]. It has been previously reported of a remagnetization in the central Taurides [*Morris and Robertson*, 1993], while *Meijers et al*. [2011] confirm a widespread remagnetization from the end-member modeling approach. For this reason we use the end-member modeling for Upper Cretaceous limestone in the central Taurides as well as the SE Taurides.

The basic approach of the end-member modeling depends on determination of the model from the data with an inverse mathematical method. The number of invariants are termed as the end-members calculated by iterative minimization of the data variability. The end-member calculation was made in MATLAB (after D. Heslop).

At first, specimens were preheated until 150°C and AF demagnetized at 300 mT to minimize the influence of magnetic interaction. The IRM was acquired in 28 to 31 steps up to 700 and 800 mT. The IRM component analysis was done according to *Kruiver et al*. [2001].

We use IRM acquisition curves from 48 limestones in the SE and central Taurides for the end-member model. Three end-members are used that describe the lithological groupings. One end-member represents the high-

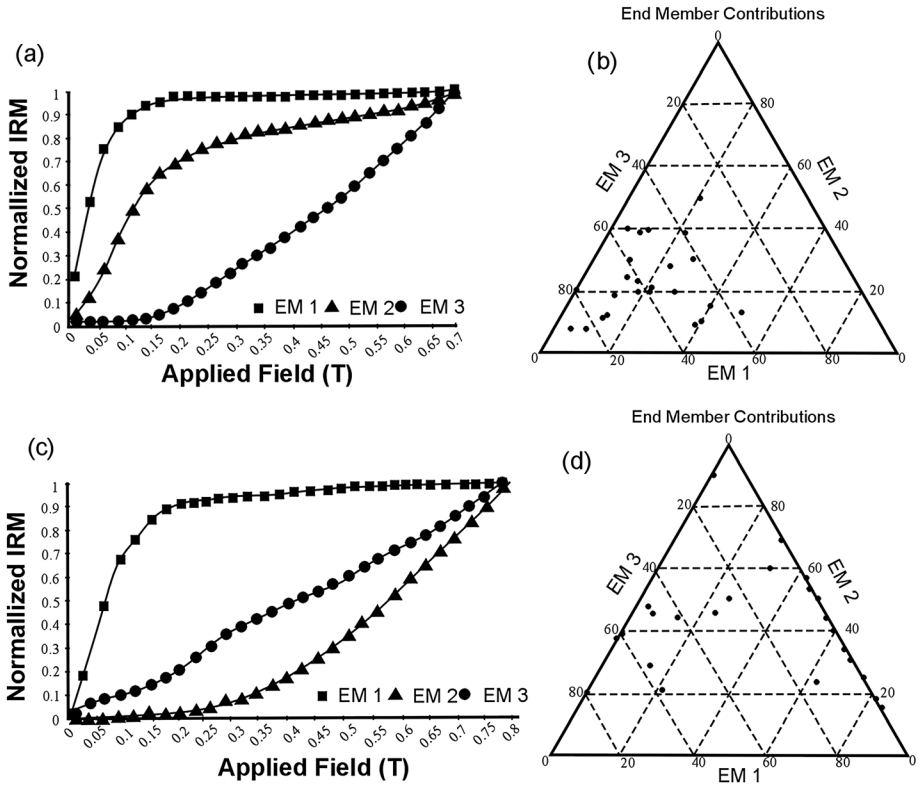

Figure 8. End-member models for the IRM acquisition curves from the limestone groups that were preheated at 150°C. (a) Calculated end-members for the limestones in central Taurides in the three end-member model. (c) End-members for the limestones in SE Taurides in the three end-member model. (b, d) Ternary plot with the EM partitioning for each sample. Limestones in the SE Taurides are between EM1 and EM3, while limestones in the central Taurides are characterized between EM3 and EM2.

coercivity contribution, whereas the low-coercivity part can be described by either one end-member. The shape of the three end-members (EM1, EM2, and EM3) is shown in Figures 8a and 8c. We interpret EM3 as caused by hematite showing a large amount of the high-coercivity component. EM1 is interpreted as due to magnetite. The saturation Isothermal Remanent Magnetization of EM1 is ~500 mT for limestones in central Taurides, while EM2 and EM3 are not saturated at fields of 700 mT. The saturation of EM1 in high fields is not common for magnetite. In the ternary plot the majority of the samples can be seen as mixtures of EM3 and EM2 (Figure 8d). On the other hand, limestone samples from the SE Taurides show that the EM1 reaches saturation at ~ 200 mT, while EM2 and EM3 define a lower slope than the limestones in SW Taurides. When considering the samples in the ternary diagram, the limestones in SE Taurides have a high percentage of end-member 1, which is clearly distinguishable (Figure 8b). Because of the difference in the saturation field and the EM1 behavior for limestones we interpret the first as to be remagnetized despite the fact that the limestones in the SE Taurides are nonremagnetized.

Hence, we concluded that the magnetization acquisition corresponds to a period between the consumption of the branches of the Neotethys Ocean and the collision between the Anatolian blocks and Eurasia from the Late Jurassic-Lower Cretaceous to Middle Miocene. Despite evidence of a prefolding in the Niğde-Kırşehir Massif and SE Taurides, the limestone in central Taurides shows a remagnetization.

6. Discussion

6.1. Tectonic Rotations Combined With Previous Paleomagnetic Results

The individual rotations experienced by the deformation of the Niğde-Kırşehir Massif and the central-SE Taurides are considered in the light of the new paleomagnetic data set reported here. These results are combined with previous paleomagnetic studies given in Table 2. Criteria for data selection are considered that depend on (a) $\alpha_{95} < 15°$, (b) consistent inclination values, (c) accordance with averaged site means, and (d) mean sites including a minimum number of five samples. In a further step we compare the group

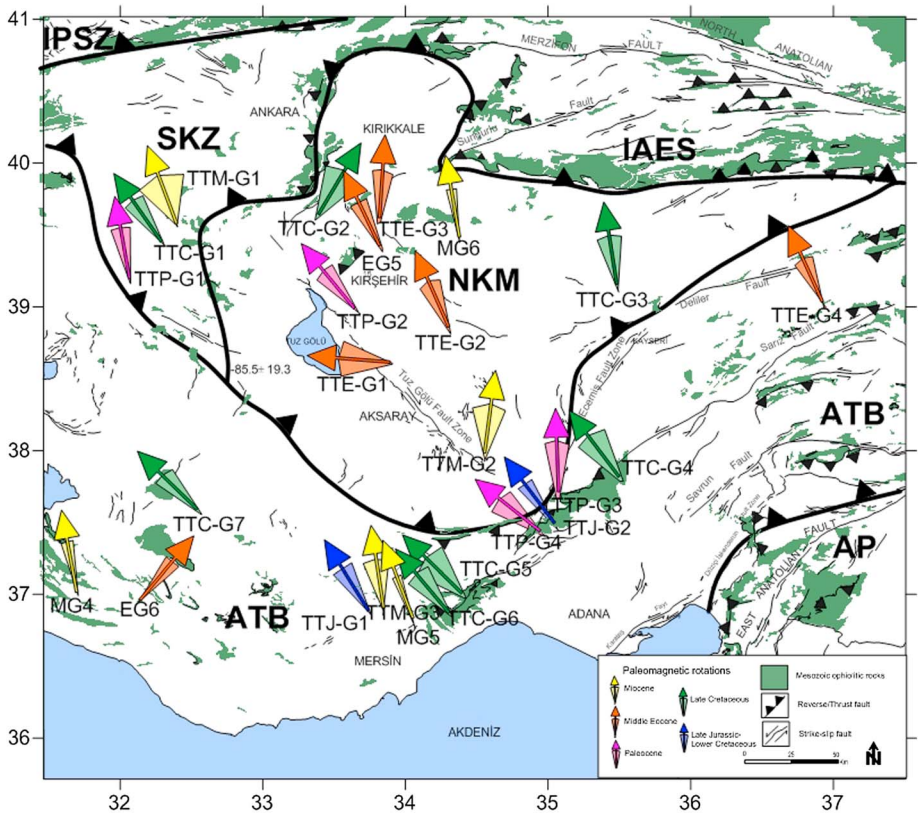

Figure 9. Paleomagnetic rotations (*R*) together with their error envelopes are combined together from this study and previous studies (see Table 2 and Appendix A) according to Late Jurassic-Lower to Middle Miocene ages in different subareas (For abbreviations, see Figures 1 and 8).

mean directions with the expected direction at Miocene to Late Jurassic-Lower Cretaceous for the African plate at a reference point in the study area to determine relative motion between the studied area and the African plate after *Besse and Courtillot* [2002]. The integrated mean poles for Africa at different time spans are given in Table 2.

When considering the Upper Jurassic-Lower Cretaceous results in SE Taurides a counterclockwise rotation of $R = 35.1 \pm 8.2°$ is obtained (Table 2 and Figure 9). Note that besides of the good quality results in sites TT50 and TT127 they were not considered in the overall mean direction because they show dispersion with the rest of the sites. In the central Taurides, however, only one single site with clockwise rotation of 38° was obtained (Table 1).

We calculate a counterclockwise rotation of $R = 41.1° \pm 7.6°$ in SE Taurides from Upper Cretaceous sedimentary rocks (Table 2; Mean G4-G6). On the other hand, a clockwise rotation of $R = 45.9° \pm 9.3°$ is obtained in the central Taurides (TTC-G7; Table 2 and Figure 9) for the same age. However, when considering the end-member approach for the studied limestones in the central Taurides, a remagnetization is assumed. When considering the tectonic rotations in the Middle Eocene in this area, a similar clockwise rotation of $R = 40.2° \pm 8.7°$ (EG6) is obtained after *Kissel et al.* [2003]. We therefore conclude that the clockwise rotation obtained from Upper Cretaceous limestones in central Taurides started during the Middle Eocene.

In the Niğde-Kırşehir Massif, no rocks older than Late Cretaceous have been collected. This is simply because all of the older rocks underwent Barrovian metamorphism during the Late Cretaceous [*Whitney and Dilek*, 1998]. The Upper Cretaceous ophiolites known as the Çiçekdağ ophiolites, which are emplaced onto the NW and NE areas of the Niğde-Kırşehir Massif, show clockwise rotation of 26.2° in the Kırıkkale Basin and counterclockwise rotation of 14.5° in the Tuzlagölü area (TTC-G2, TTC-G3; Table 1 and Figure 9). The counterclockwise rotation in Tuzlagölü is consistent with the sense of rotation obtained from the SE Taurides, however, the clockwise rotations in Kırıkkale Basin are incompatible with this rotation pattern. This connection may be associated with local deformation that occurred during the ophiolite emplacement.

When considering the amount of rotation between the Late Cretaceous and Middle Eocene in the northwestern boundary of the Niğde-Kırşehir Massif (TTC-G2, TTE-G3), clockwise rotation of $R = 32.1° \pm 14.7°$ and $R = 8.9° \pm 3.6°$ is calculated, respectively (Figure 9). The divergence in rotation between this time interval shows that a significant amount of rotation occurred during the collision between the Niğde-Kırşehir Massif and the Pontides in Latest Cretaceous times. This is also observed farther east of the Niğde-Kırşehir Massif (TTC-G1, TTP-G1) with counterclockwise rotations of $R = 35.2° \pm 11.0°$ and $R = 10.2° \pm 7.9°$ in Late Cretaceous and Paleocene, respectively (Figure 9).

Along the Tuz Gölü fault zone starting from Tuz Gölü in northwest extending to Ulukışla to the southeast, counterclockwise rotation of $R = 39.5° \pm 9.9°$ (TTP-G2) and $R = 51.5° \pm 13.1°$ (TTP-G4) is obtained in the Paleocene. The amount of rotation decreases significantly to $R = 2.1° \pm 10.4°$ (TTP-G3) in the eastern part of this fault zone. It should be noted that in Tuz Gölü counterclockwise rotation of $R = 85.5° \pm 19.3°$ is obtained in the Middle Eocene (Figure 9). This rotation apparently occurred with respect to the fault in the approximate position of the Tuz Gölü fault while the initial form of the fault zone is thought to be a major normal fault with small strikeslip component. *Lefebvre et al*. [2013] suggest that the different sense of rotations in the Niğde-Kırşehir Massif is provided by regional faulting as a result of the compression of the Pontides and the Niğde-Kırşehir Massif. In the same manner, *Lucifora et al*. [2013] also suggest that strike-slip fault activity was effective on block rotations in the Çankırı Basin during the Miocene.

When considering the Middle Eocene rotations in the Niğde-Kırşehir Massif which are far away from the fault zones, counterclockwise rotation of $R = 20.6° \pm 10.5°$ (TTE-G2) and $R = 25.5° \pm 7.3°$ (EG5) (Figure 9) is interpreted with a coherent block rotation, besides the rotation pattern associated with local fault deformation.

In the north of the SE Taurides counterclockwise rotation of $R = 24.3° \pm 9.8°$ is obtained from this study (TTE-G4; Table 2 and Figure 9). In Middle Miocene no significant rotations are obtained in the Niğde-Kırşehir Massif (TTM-G4 and MG6) and the central Taurides (TTM-G3 and MG4), while a counterclockwise rotation of $R = 16.8° \pm 3.9°$ is obtained in the SE Taurides (MG5) (Figure 9).

6.2. Paleomagnetic Direction Versus Folding Direction

The possibility of oroclinal bending is attested by plotting the paleomagnetic declinations as a function of strike deviation obtained from structural maps (Figure 2, MTA 1/100000 geological maps). The theoretical regression line displays a slope of 45°, which is expected for an originally oroclinal bend. The linear regression analysis between the strikes and the declinations of the tilt corrected sites yields a correlation coefficient of $R^2 = 0.77$. Declinations from Upper Cretaceous rocks SE of the strike axis show a counterclockwise pattern, while the declinations from those to the SW show a clockwise sense of rotation (Figure 10).

6.3. Paleolatitude

Inclination flattening analysis of the primary remanent magnetization vector in sedimentary rocks shows generally lower values than expected. This bias is known as the shallow bias of inclination angle in sedimentary rocks. [*Jackson et al*., 1991, *Tan et al*., 2003, *Bilardello and Kodama*, 2009a, 2009b and *Kodama*, 2009]. We applied the method proposed by *Tan and Kodama* [2003] using anisotropy of anhysteretic remanent magnetization data for the correction of the inclination shallowing. An inclination increase of 10° is then obtained when considering the flattening factor (*f*) ranging from 0.7 and 0.6 for limestones and sandstones, respectively. By using these values for Late Jurassic-Lower Cretaceous and Late Cretaceous, a higher paleolatitude is obtained compared with the paleolatitudes obtained from volcanic rocks in the Pontides given in previous studies [*Sarıbudak*, 1989; *Channell et al*., 1996; *Çinku et al*., 2010]. In addition, when comparing Upper Cretaceous and Paleocene volcanic and sedimentary rocks in sites TTC-G5, TTC-G6 and TTP-G3, TTP-G4, respectively, it could be seen that no significant inclination variations are obtained. We therefore conclude that we are justified in not considering the inclination shallowing factor.

To obtain a reliable paleolatitude for each mean group, we use the *Fisher* [1953] statistical analysis; however, in the mean most groups the large dispersion in rotations makes it essential to predominantly use the inclination-only test of *Enkin and Watson* [1996]. In Table 2, paleolatitudes for individual groups are given according to Fisher analysis and inclination-only data.

It is shown that the Upper Jurassic-Lower Cretaceous mean paleolatitude from central Taurides is separated from the African margin with a paleolatitude of $= 15.5°N^{+3.5°}_{-3.3°}$ (Table 2, Mean G1, G2; Figure 11). A more northern paleolatitude of 29.5°N is obtained after *Channell et al*. [1996] and *Çinku* [2011] for the Pontides, which

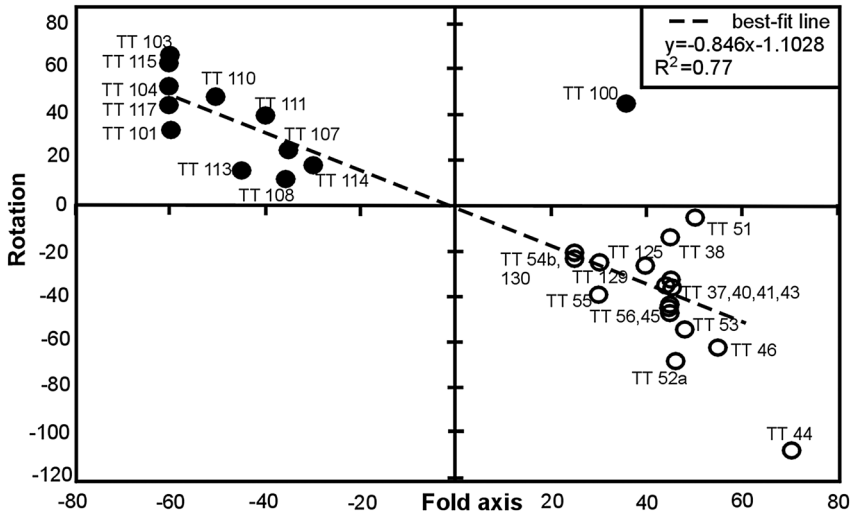

Figure 10. Site mean declinations versus strike of beds in Late Cretaceous strata.

implies a ~14° (1540 km) gap between the Pontides and the central Taurides. In the same area, a paleolatitude of $= 18.5°N^{+1.8°}_{-1.7°}$ is calculated from 17 Late Cretaceous sites (Table 2, TTC-G7). This group, however, is considered to be remagnetized probably during Middle Eocene. The difference between these two ages suggests no important crustal shortening. The Late Cretaceous paleolatitude obtained in the SE Taurides does not differ from the central Taurides, indicating a paleolatitude of $= 17.5°N^{+1.9°}_{-1.9°}$ (Figure 11 and Table 2, Mean G4-G6).

A systematic decrease in Late Cretaceous paleolatitudes is obtained from the north to the south of the Niğde-Kırşehir Massif on the order of $= 24.8°N^{+5.2°}_{-4.6°}$ (Table 2, TTC-G2) to $= 17.9°N^{+5.2°}_{-4.6°}$ (Table 2, TTC-G6) when considering the separate sites from this study (Figure 11).

The paleolatitude obtained from the ophiolite arc-type rocks in Kırıkkale (TTC-G2) indicates a closer position to the Eurasian margin with a paleolatitude of 24.8°N than the ophiolitic rocks in the Tuzlagölü with

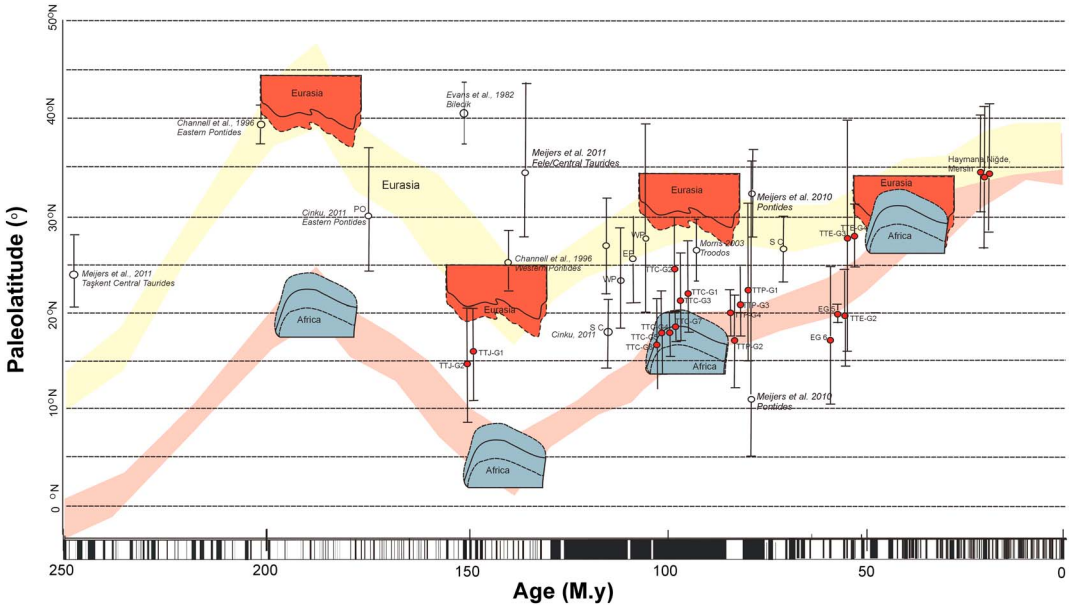

Figure 11. Age versus reference palaeolatitude curve with error envelopes derived from the Apparent Polar Wander Path (APWP) paths of Eurasia and Gondwana for a locality near Kırşehir (44°N, 32°E) after *Torsvik et al.* [2012]. Previous paleomagnetic data are taken from *Evans et al.* [1982], *Channell et al.* [1996], *Çinku* [2011], *Meijers et al.* [2010, 2011], and *Morris* [2003] with error bars. Paleomagnetic results from this study are given for each site group and mean group (A: Niğde-Kırşehir Massif, B: SE/E area of the Niğde-Kırşehir Massif, C: SW/W area of the Niğde-Kırşehir Massif, red circles correspond to mean groups on different areas).

a paleolatitude of 21.5°N (TTC-G3) and those from the Mersin-Çamardı (TTC-4-TTC-G6) showing a paleolatitude of approximately 17.7°N (Table 2 and Figure 11). The difference in paleolatitude among these ophiolites clearly indicates ophiolite emplacement in two distinct areas. It is reported that the ophiolites in the northern Niğde-Kırşehir Massif are the result of the slab rollback of the İzmir-Ankara-Erzincan oceanic slab in a later phase after the ophiolite emplacement along the borders between the Niğde-Kırşehir Massif and the Pontides [*Nairn*, 2010]. The paleolatitudinal difference between the ophiolites in the north of the Pontides and Niğde- Kırşehir Massif could, therefore, support this model. In addition, the ophiolites emplaced in Mersin and Çamardı display similar paleolatitudes, supporting evidence of a similar subduction zone, namely, the Intra-Tauride Ocean.

The Late Cretaceous paleolatitudes from the Central and SE Taurides clearly show this zone far away from the African margin (Figure 11). Previous paleomagnetic studies present paleolatitudes for the different blocks in Anatolia. A paleolatitude from the Mersin ophiolites is obtained as $\lambda = 6.6°$N from the study of *Ömer et al*. [2013], which places the ophiolites in a far too southern paleolatitude. From the studies of several researchers, the western Pontides were in a paleolatitude of 28.2°N to 23.5°N [*Channell et al*., 1996; *Çinku et al*., 2015] and the Eastern Pontides at $\lambda = 26.6°$N [*Channell et al*., 1996; *Hisarlı*, 2011].

In the Paleocene, we obtain a paleolatitude of ≈ 21°N for the south of the Niğde-Kırşehir Massif (Table 2, TTP-G3, TTPG4; Figure 11), indicating its northward movement from the Taurides. Farther north, however, the results from Tuz Gölü are interpreted with local fault motion therefore showing low paleolatitude, while in group TTP-G1 the paleolatitude of $= 22.4°\text{N}^{+9.0°}_{-7.3°}$ in accordance with the position of Pontides.

In the Middle Eocene, a mean paleolatitude of $= 18.9°\text{N}^{+5.5°}_{-4.8°}$, $= 19.4°\text{N}^{+1.9°}_{-1.8°}$, and $= 28.2°\text{N}^{+9.7°}_{-7.8°}$ (Figure 11 and Table 2; TTE-G2, EG5, and TTE-G3) is calculated both from this study and previous studies [*Kissel et al*., 2003; *Gürsoy et al*., 1997; *Çinku et al*., 2013] for the Niğde-Kırşehir Massif. The results for the SE Taurides and central Taurides are calculated as $= 27.8°\text{N}^{+4.3°}_{-3.9°}$ and $= 16.9°\text{N}^{+8.2°}_{-6.9°}$, respectively (Table 2, TTE-G4, EG6; Figure 11).

In the Middle Miocene, a paleolatitude of $\lambda = 31.2°N^{+2.9°}_{-2.7°}$ is obtained for the Niğde-Kırşehir Massif (Table 2, MG6; Figure 11) and $\lambda = 33.8°N^{+3.6°}_{-3.3°}$ and $\lambda = 34.1°N^{+5.2°}_{-4.6°}$ for the SE and central Taurides, respectively (Table 2, MG5 and MG4; Figure 10). Although these values are close to the African margin, they are consistent with results obtained from the Pontides [*Channell et al*., 1996; *Çinku*, 2004; *Hisarlı*, 2011].

6.4. Kinematic Model

All of the mean paleomagnetic group directions in several subareas and in different ages are restored to their original position by subtracting the younger rotations from the older ones. In the SE Taurides, a small clockwise rotation of 6° is obtained for the Late Jurassic-Late Cretaceous period by subtracting the Late Jurassic-Lower Cretaceous rotation from the Late Cretaceous counterclockwise rotation (TTJ-G1 and G2/TTC-G4-6). Likewise, counterclockwise rotation of 17° (TTC-G4-G5/TTE-G4) and 7° (TTE-G4/MG5) is obtained during the Late Cretaceous-Middle Eocene and Middle Eocene-Middle Miocene, respectively. In a period between Middle Miocene to present, however, counterclockwise rotation of 17° is calculated for the SE Taurides (Table 2, MG5).

In the Niğde-Kırşehir Massif, evidence of fault bounded block rotations is found in Paleocene rocks. Then counterclockwise rotation of 14° (TTE-G2 and EG5/MG6) is obtained during the Middle Eocene-Middle Miocene (Table 2). From the Late Miocene to the present, no significant rotation is observed within the Niğde-Kırşehir Massif. It may be stated that the Massif has behaved as a coherent body since that period.

In the central Taurides, the Late Cretaceous results obtained during this study and the data of the Middle Eocene rocks from farther west of the study area obtained by *Kissel et al*. [2003] both show clockwise rotation of 40°–45° (Table 2, TTC-G7 and EG6). This suggests that no significant rotation occurred between the Late Cretaceous and the Middle Eocene period. They both indicate collectively that the time of clockwise rotation in the central Taurides occurred during the Middle Eocene and becomes smaller till the Middle Miocene, when considering that the area is remagnetized in Late Cretaceous. The small amount of rotation in the Middle Miocene (Table 2, MG4) suggests that this area was rather stable.

Late Cretaceous paleomagnetic results from this study clearly indicate two different types of rotation in the Taurides. The counterclockwise rotations in the SE Taurides change direction NW of Mersin. Along Karaman-Konya, the Late Cretaceous rotations are found to be in a clockwise sense (Figure 9). This contrasting sense of rotation in the Late Cretaceous may be taken as evidence of oroclinal bending. The bending point appears to be located to the north of Mersin.

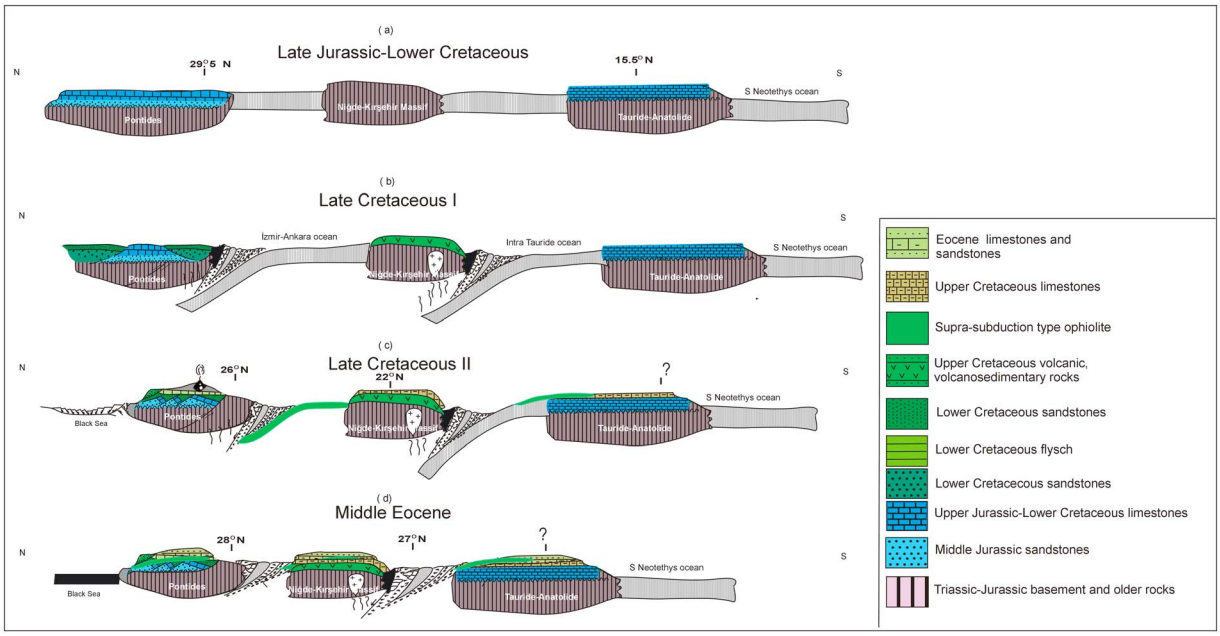

Figure 12. (a–d) Tectonic evolution of the Niğde-Kırşehir Massif and adjacent blocks during the Late Jurassic to the present (NKM, Niğde-Kırşehir Massif; IA, Isparta angle; and C, Cyprus).

The branches of the northern Neotethys Ocean existed between the Pontides, Taurides, and the Niğde-Kırşehir Massif during the Late Jurassic-Lower Cretaceous (Figure 12a). The data we obtained lead us to propose a model for the closure of the Intra-Tauride Ocean and the collision between the Taurides and the Niğde-Kırşehir Massif in the SE/E which occurred during the Late Cretaceous-Eocene period with counterclockwise rotation of 17° (Figure 12b). Part of the collision related deformation may have been accommodated along the Ecemiş fault zone. The Niğde-Kırşehir Massif also rotated as a block; however, internal deformation during the Middle Eocene is also predicted from our data.

In the central Taurides, a clockwise rotation of 48.5° is obtained from the Middle Eocene to Middle Miocene (EG6/MG4). This implies that the convergence between the Taurides and the Niğde-Kırşehir Massif continued in a later period even if it is reported in a earlier time. The following deformation phases may have played role in this process: (a) the development of the Isparta angle, (b) the final closure phase of the southern Neotethys Ocean which resulted the present Bitlis-Zağros Mountain, and (c) the collision between the African and Eurasian plates (Figure 12c). In the north, the compressional deformation between the Niğde-Kırşehir Massif and the Pontides started in the Late Cretaceous [*Şengör and Yılmaz*, 1981] and the subsequent collision occurred during the Early Eocene, as elaborated by *Yılmaz et al.* [1997b] During the Late Cretaceous to Middle Eocene, the paleomagnetic results clearly indicate that the ophiolitic rocks wrapped around the Niğde-Kırşehir Massif conforming to its outer frame [*Çinku et al.*, 2015]. In the same area, results from Middle Eocene rocks indicate that compression between the Pontides and the Niğde-Kırşehir Massif continued strongly during this period, as elaborated by geological data by *Yılmaz et al.* [1997b] and supported further by paleomagnetic data by *Çinku et al.* [2011].

From the Middle Miocene to the present, no significant rotations are observed in the central Taurides and the Niğde-Kırşehir Massif, while counterclockwise rotations of 17° are obtained in the SE Taurides, indicating that the Neotectonic deformation possibly occurred under the influence of the westward extrusion of the Anatolian plate (Figure 12d). Various local effects inside the Niğde-Kırşehir Massif and its surrounding areas, which are well established in this study, appear to be due to fault bounded block rotations, i.e., the large counterclockwise rotations in the Tuz Gölü area at this stage may be attributed to the dextral motion of the Tuz Gölü fault.

6.5. Paleogeographic Evolution

The paleogeographic position of the Pontides in the Late Jurassic-Lower Cretaceous is known from the previous paleomagnetic study of *Çinku* [2011], which revealed a paleolatitude of 29.5°N. The paleomagnetic results obtained during this study placed the Tauride carbonate platform firmly to 15.5°N (Figure 13a). The

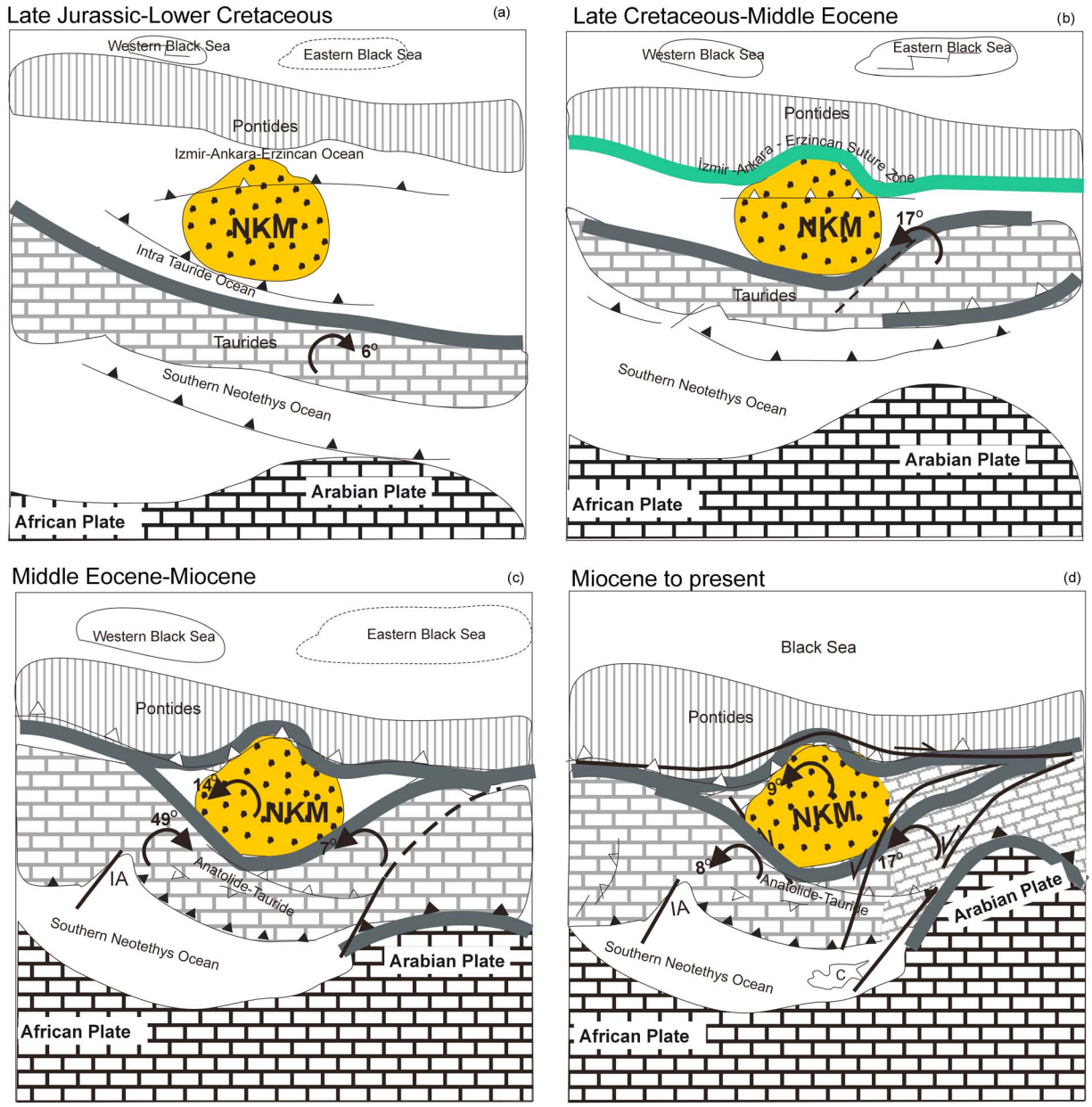

Figure 13. (a–e) Proposed paleogeographic evolution of the Niğde-Kırşehir Massif, Pontides, and Taurides from Late Jurassic to present.

amount of latitudinal difference between the Pontides and the Taurides corresponds approximately to a distance of about 1400 km, which is wide enough to separate the Niğde- Kırşehir Massif from the Taurides Ocean. In the Late Cretaceous, continuing closure of the ocean between the Niğde-Kırşehir Massif, the Pontides, and the Taurides places the Pontides to 26°N [*Sarıbudak*, 1989; *Channell et al*., 1996; *Çinku*, 2004; *Hisarlı*, 2011; *Meijers et al*., 2010], the Niğde-Kırşehir Massif at 22°N, and the Taurides at a paleolatitude of 17.5°N. The difference between these paleolatitudes supports further for survival of a remnant basin that separates the surrounding continents for the remnant basins in the area. In the later phases, ophiolitic rocks emplaced onto the continental blocks (Figures 13b and 13c). The paleolatitudes in the Middle Eocene are obtained as 28°N [*Piper et al*., 1996; *Çinku et al*., 2011; *Hisarlı et al*., 2011] for the Pontides and 27°N (TTE-G3) for the Niğde-Kırşehir Massif defining the closure of these blocks in the north (Figure 13d). However, we must also consider that in sites TTE-G2 and EG5 a paleolatitude of ~19° is obtained for the Niğde-Kırşehir Massif. A low paleolatitude is also obtained for the central Taurides (17°N (EG6)), while in the northernmost part of the SE Taurides a paleolatitude of ~28° is obtained.

Table A1. Paleomagnetic Results From Previous Studies (For Abbreviations, See Table 1)

Site	Formation/Lithology/Region	Latitude(°)N, Longitude (°)E	N	D_s	I_s	α_{95}	k	Reference
		Late Jurassic-Lower Cretaceous						
AS1-4 and AD1-3	Ferhatkaya/Limestone	40.3, 35.5	46	324.3	43.3	9.5	94.7	*Çinku* [2011]
LA1-3	Kelkit/Sandstone	40.5, 36.0	19	168.2	−47.3	5.9	46.1	
		Late Cretaceous						
KS13	Sandstone	39.4, 35.3	13	178.1	−70.2	10.5	16.5	*Çinku et al.* [2015]
KS18	Sandstone	39.5, 33.2	7	2.2	−18.6	17.3	7.9	
KS20	Sandstone	39.5, 33.2	9	305.9	−31.6	32.8	4.4	
KS27	Sandstone	40.4, 33.4	10	21.5	32.5	12.8	15.1	
KS28	Sandstone	40.4, 33.4	5	39.3	61.1	12.3	20.3	
KS29	Sandstone	40.4, 33.4	6	2.3	66.1	10.3	81.2	
KS30	Sandstone	40.4, 33.4	7	334.1	24.2	13.4	21.3	
KS31	Sandstone	41.0, 33.4	7	191.8	−48.1	5.4	124.6	
KS33	Sandstone	41.0, 33.4	7	336.3	32.1	13.5	209.3	
KS35	Volcanic rocks	40.5, 34.0	8	147.7	−47.5	10.0	31.8	
KS37	Volcanic rocks	40.5, 34.1	7	353.3	47.1	8.9	38.5	
KS39	Volcanic rocks	40.4, 34.2	8	329.8	41.2	8.7	41.2	
KS40	Sandstone	40.4, 34.2	8	336.1	32.3	10.0	59.4	
KS41	Sandstone	40.4, 34.2	7	307.7	49.2	10.8	32.3	
PT22	Lava	40.2, 34.3	17	167.8	43.2	4.2	33.7	
PT23	Chert	40.2, 34.3	6	130.8	55.8	4.3	53.2	
PT24	Lava	40.0, 34.3	8	161.4	61.5	7.8	45.4	
PT25	Chert	40.0, 34.3	6	106.5	32.0	8.5	63.1	
PT26	Sandstone	39.5, 34.5	8	347.9	41.1	7.8	25.5	
KS50	Lava	39.5, 34.3	7	11.0	7.5	8.4	27.9	
KS51	Chert	39.5, 34.3	16	356.8	11.9	7.3	22.3	
KS24	Lava	40.3, 33.2	5	326.6	40.1	10.3	27.7	
KS25	Pelagic limestone	40.3, 33.2	7	134.2	−36.6	12.1	27.2	
KS26	Pelagic limestone	40.3, 33.2	11	117.2	−36.7	6.1	57.1	
KKB	Granite	39.35, 33.89	26	350.7	57.9	2.3	14.8	*Lefebvre et al.* [2013]
AAB	Granite	38.69, 34.10	29	331.6	51.9	2.6	12.7	
14	Sivas/Lava	39.8, 36.9	8	155.3	−56.0	14.1	16.4	*Gürsoy et al.* [1997]
		Paleocene						
15	Kaman/Lava	39.2, 33.9	10	148.0	−61.0	8.7	31.8	*Sanver and Ponat* [1981]
TK	Kaman/Lava	39.2, 33.9	3	313	48	16.0	62.0	*Kissel et al.* [2003]
		Middle Eocene						
TK176	Akseki/Limestone	37°30, 31°80	9	223.0	−15.0	9.5	28.0	*Kissel et al.* [1993]
TK177	Akseki/Limestone	37°30, 31°80	9	231.0	−28.0	11.9	30.0	
TK178	Akseki/Limestone	37°30, 31°80	8	212.0	−21.0	13.6	30.0	
TK179	Akseki/Limestone	37°30, 31°80	7	233.0	−17.0	7.7	10.0	
TK180	Akseki/Limestone	37°30, 31°80	10	213.0	−30.0	9.6	15.0	
KS10	Lava	39°50, 34°50	10	151.3	−34.4	7.7	35.1	*Çinku et al.* [2013]
KS11	Sandstone	39°48, 34°46	22	149.2	−32.3	3.7	72.6	
KS14	Sandstone	39°50, 35°30	12	153.2	−31.2	8.6	32.4	
KS15–KS17, and KS42	Sandstone	39°50, 33°20	48	340.0	25.0	6.9	9.9	*Çinku et al.* [2013]
KS38	Sandstone	40°40, 34°30	7	170.4	−34.8	12.2	25.2	
TK117	Volcanic	39°09, 34°06		178.0	−53.0	3.0	189.0	*Kissel et al.* [2003]
E128	Volcanic sediment	39°83, 36°45	4	15.0	39.0	11.1	70.0	*Gürsoy et al.* [1997]
E129	Andesitic tuff	39°83, 36°45	5	277.3	69.0	6.2	154.3	
E130	Andesitic tuff	39°83, 36°45	5	350.1	53.1	7.8	96.1	
E131	Basaltic tuff	39°83, 36°45	6	160.5	−53.1	4.4	234.2	
E72	Basaltic andesite	39°78, 36°74	7	139.0	−67.9	6.5	86.9	
E73	Basaltic andesite	39°72, 36°72	3	35.2	68.4	23.3	29.1	
E75	Volcanic sediment	39°73, 36°72	4	136.9	−56.8	11.8	61.7	
G1	Volcanic rocks	41.2, 33.5	8	356.0	39.0	11.0	26.2	*Piper et al.* [1996] (32, 34, 35); *Çinku et al.* [2011] (KY1, KY2, KY3, IG1, and IG2)
G2	Volcanic rocks	40.5, 33.6	12	41.0	29.7	7.5	29.2	*Çinku et al.* [2011] (OS1, OS3, OS4, OG1, OG2, DO1, and DO2); *İşseven and Tüysüz* [2006] (OSM4–OSM7, OSM12–OSM14);
G3	Volcanic rocks	40.41, 34.59	6	20.8	54.5	13.2	26.8	*İşseven and Tüysüz* [2006] (OSM8 and COM1–COM5)

Table A1. (continued)

Site	Formation/Lithology/Region	Latitude(°)N, Longitude (°)E	N	D_s	I_s	α_{95}	k	Reference
G4	Volcanic rocks	40.17, 34.42	4	38.1	44.3	14.3	42.3	*İşseven and Tüysüz* [2006] (SU1–SU4)
G5	Volcanic rocks	40.52, 34.55	18	344.4	46.1	9.6	14.8	*İşseven and Tüysüz* [2006] (KAM1–KAM3, OSM1, OSM10, OSM11, GHK1, GHK2, GHK3, GHK5, and GHK6); *Çinku et al.* [2011] (OS5, OS7, HO1, GH1, GH2, SY1, and SY2)
G6	Volcanic rocks	40.54, 35.37	8	17.0	39.7	20.0	8.6	*İşseven and Tüysüz* [2006] (MER1, MER4, MER5, MER7, MER9; *Piper et al.* [1996] (24); *Çinku et al.* [2011] (HV1 and HV2)
G7	Volcanic rocks	40.21,35.39	13	13	−50.5	12.7	11.6	*İşseven and Tüysüz* [2006] (ORT1 and ORT4); *Piper et al.* [1996] (11–14 and 18–22)
G8	Volcanic rocks	40.22,36.54	10	146.5	−48.3	7.0	48.8	*Piper et al.* [1996] (50–56; 61); *Platzman et al.* [1994] (TV1 and TV2)
G9	Volcanic rocks	40.4, 37.0	15	150.5	−41.9	9.6	16.7	*Platzman et al.* [1994] (TV6, TV8, TV13, TV14, and TV16); *Piper et al.* [1996] (33–42)
G10	Volcanic rocks	40.4, 36.6	9	9.9	48.6	15.2	12.5	*Piper et al.* [1996] (1–10, except 8)
G12	Volcanic rocks	40.5, 36.6	4	171.5	−67.4	9.5	168.5	*Platzman et al.* [1994] (TV9, TV10, TV14, and TV15)
18	Kırşehir/Lava	34.5, 39.5	6	152.9	−47.7	18.9	13.5	*Sanver and Ponat* [1981]
21	Akdagmadeni/Lava	35.8, 39.7	3	113.9	−43.5	5.2	563.1	*Tatar et al.* [1996]
TKY	Yozgat/volcanics and sediments	39.5, 34.4	7	167.0	−13	22.3	8.0	*Kissel et al.* [2003]
24	Çankırı Basin/evaporites	34.1, 40.2	6	168.6	−30.7	17.4	15.8	*Kaymakçı et al.* [2003]
CATB	Central Anatolia/volcanic rocks	36.5, 39.8	5	169.7	−47.6	19.9	15.7	*Gürsoy et al.* [1997]
TKS	Sarız/Limestone	36.5, 38.5	3	140.3	−38.0	10.0	153	*Kissel et al.* [2003]
TKI	Isparta/Limestone	31.6, 37.2	7	224.0	−23.7	11.9	26.7	*Kissel et al.* [1993]
		Oligocene-Miocene-Pliocene-Quaternary						
K1	Volcanic	37°41, 32°02	8	174.0	−30.0	8.0	48.4	*Platzman et al.* [1998]
K2	Volcanic	37°39, 31°58	4	358.0	57.0	6.3	212.0	
TK192	Deposits	37°20, 31°03	11	5.0	50.0	4.6	97.0	*Kissel et al.* [1993]
TK193	Deposits	37°20, 31°02	8	350.0	56.0	3.4	268.0	
TK194	Deposits	37°20, 31°01	6	1.0	54.0	2.8	369.0	
3	Andesite	37°36, 33°19	7	188.2	−53.3	3.2	347.9	*Gürsoy et al.* [1998]
4	Andesite	37°37, 33°18	6	6.6	43.0	12.9	28.0	
5	Andesite	37°40, 33°13	6	174.7	−48.1	8.7	60.3	
7	Andesite	37°38, 33°15	7	172.8	−49.1	4.4	186.7	
8	Andesite	37°39, 33°16	6	174.8	−39.8	4.1	261.7	
10	Basalt	37°43, 33°19	7	166.3	−67.9	5.1	140.2	
12	Basalt	37°44, 33°09	7	348.1	33.0	4.0	225.7	
13	Basalt	37°43, 33°10	7	29.2	63.2	2.8	458.9	
14	Andesite	37°43, 33°12	3	191.4	−65.0	21.1	35.2	
15	Basalt	37°46, 33°17	7	143.8	−38.8	3.3	329.5	
16	Basalt	37°46, 33°20	6	147.6	−40.4	5.3	161.5	
18	Basalt	37°49, 33°26	6	290.3	82.7	7.3	84.9	*Gürsoy et al.* [1998]
19	Basalt	37°61, 33°58	6	337.0	30.7	10.4	42.4	
21	Basalt	37°70, 33°57	7	337.9	40.4	7.8	50.3	
22	Basalt	37°71, 33°58	5	318.6	53.5	5.7	182.9	
23	Basalt	37°66, 33°60	5	358.0	55.2	3.4	483.0	
24	Basalt	37°64, 33°65	7	334.9	28.4	4.7	163.5	
26	Andesite	37°76, 33°72	6	162.1	−59.9	3.9	298.5	
28	Basalt	37°77, 33°75	7	181.0	−73.9	6.5	87.1	
29(1)	Basalt	37°79, 33°76	7	194.3	−47.0	9.5	41.2	
29(2)	Basalt	37°79, 33°76	7	8.3	44.4	3.9	244.5	*Gürsoy et al.* [1998]
30	Basalt	37°80, 33°77	7	7.3	67.0	11.8	28.2	
31	Basalt	37°85, 33°84	7	188.7	−49.4	6.8	80.4	
32	Basalt	37°82, 33°83	3	167.3	−41.7	16.7	55.6	

Table A1. (continued)

Site	Formation/Lithology/Region	Latitude(°)N, Longitude (°)E	N	D_s	I_s	α_{95}	k	Reference
33	Basalt	37°80, 33°78	6	352.0	75.9	6.0	125.7	
34	Basalt	37°82, 33°87	7	172.9	−58.8	4.4	181.9	
35	Basalt	37°83, 33°88	5	194.1	−60.4	4.9	249.4	
36	Basalt	37°81, 33°90	6	155.3	−65.3	7.8	74.2	
37	Basalt	37°80, 33°91	6	162.5	−42.1	6.0	126.5	
38	Basalt	37°77, 33°92	7	356.3	55.2	5.7	111.3	
41	Basalt	38°01, 34°07	8	341.8	50.1	3.6	244.2	
42	Basalt	38°03, 34°08	5	168.5	−54.3	9.9	60.1	
43	Basalt	38°03, 34°11	7	222.2	−74.7	11.6	28.0	
44	Basalt	38°05, 34°13	7	174.4	−41.5	6.3	93.9	
45	Basalt	38°04, 34°12	8	323.8	63.9	6.4	77.0	
3	Basalt	38°21, 37°36	6	134.8	−68.7	3.4	497.4	*Gürsoy et al.* [2011]
4	Basalt	38°21, 37°36	7	135.0	−70.1	3.8	303.5	
5	Basalt	38°20, 37°36	7	165.4	−33.8	5.1	142.8	
6	Basalt	38°21, 37°36	7	11.4	50.6	4.9	155.7	
7	Basalt	38°19, 37°37	7	179.7	−65.4	10.7	33.3	
8	Basalt	38°19, 37°37	6	160.8	−41.6	8.5	62.6	
11	Basalt	38°18, 37°37	6	347.8	64.9	7.6	78.8	
12	Basalt	38°16, 37°35	7	4.2	58.2	8.1	56.1	
14	Basalt	38°20, 37°47	8	170.4	−44.2	3.1	317.3	
15	Basalt	38°45, 38°16	7	337.2	34.3	4.7	147.2	
16	Basalt	38°46, 38°16	7	328.5	48.3	7.8	159.3	
17	Basalt	38°47, 38°16	5	353.7	46.0	7.0	133.4	
18	Basalt	38°47, 38°15	5	1.7	42.6	5.1	198.2	
21	Andesite	38°54, 38°15	6	163.1	−53.9	4.8	197.0	
22	Basalt	38°54, 38°15	7	158.8	−50.4	4.8	156.3	
23	Basalt	38°54, 38°16	8	129.8	−32.0	5.6	99.4	
24	Basalt	38°49, 38°14	6	359.4	45.6	10.1	45.5	
25	Basalt	38°52, 38°04	9	180.8	−51.5	7.8	44.4	
29	Basalt	38°56, 38°01	7	322.5	53.1	4.3	194.9	
32	Rhyolite	39°00, 38°03	7	344.3	66.0	4.5	200.5	
33	Andesite	39°00, 38°03	6	337.1	67.5	6.2	117.4	
34	Andesite	39°00, 38°03	8	322.6	55.4	9.1	37.7	
35	Andesite	39°00, 38°03	8	311.5	44.4	6.2	77.8	
36	Andesite	39°00, 38°03	7	310.7	65.8	7.8	60.0	
37	Basalt	39°01, 38°02	7	157.4	−46.7	4.4	192.4	*Gürsoy et al.* [2011]
38	Andesite	39°02, 38°00	6	332.0	50.1	4.1	264.6	
39	Andesite	39°02, 38°00	7	146.1	−28.2	11.4	28.9	
40	Andesite	39°02, 37°59	6	153.6	−42.2	3.9	302.6	
41	Andesite	39°01, 37°59	7	350.1	55.1	5.1	139.1	
42	Dacite	39°00, 37°59	7	345.6	62.4	5.2	137.6	
43	Dacite	39°00, 37°58	4	0.2	49.7	7.5	152.5	
46	Basalt	38°59, 37°56	5	357.6	43.0	5.7	183.7	
47	Andesite	39°02, 37°46	9	340.6	39.5	7.6	46.9	
48	Basalt	39°02, 37°47	7	344.7	59.8	2.9	440.9	
51	Andesite	39°02, 37°47	9	347.5	51.1	4.4	135.2	
53	Basalt	39°02, 37°47	7	330.9	45.0	4.1	220.8	
55	Andesite	39°01, 37°49	8	212.5	−66.7	8.8	40.3	
56	Basalt	39°02, 37°49	8	179.3	−27.6	6.6	70.9	
57	Basalt	39°00, 37°53	6	151.2	−74.0	9.3	53.0	
58	Basalt	39°01, 37°54	7	147.0	−25.0	8.3	53.8	
59	Basalt	39°01, 37°54	6	171.4	−61.4	4.6	214.0	
61	Basalt	39°02, 37°55	8	166.3	−47.8	7.8	51.4	
62	Basalt	39°02, 37°55	6	19.2	38.9	8.9	57.7	
64	Basalt	39°04, 37°56	7	327.0	48.9	6.5	86.1	
65	Basalt	39°07, 37°55	3	186.1	−40.5	5.8	451.6	
66	Basalt	39°08, 37°51	6	309.5	59.2	9.3	52.9	
67	Andesite	39°08, 37°50	6	345.7	37.3	6.2	119.1	
69	Basalt	39°06, 37°45	5	355.0	67.1	5.1	224.3	
72	Basalt	39°05, 37°47	6	169.8	−43.6	15.9	18.8	
73	Basalt	39°05, 37°48	7	127.3	−45.5	5.7	111.5	

Table A1. (continued)

Site	Formation/Lithology/Region	Latitude(°)N, Longitude (°)E	N	D_s	I_s	α_{95}	k	Reference
75	Basalt	39°06, 37°48	6	336.6	61.3	5.2	69.2	
76	Basalt	39°06, 37°49	7	331.6	55.6	6.3	93.3	
77	Basalt	39°05, 37°51	7	157.1	−43.2	5.5	120.4	
78	Andesite	39°07, 37°50	7	348.6	40.6	6.9	78.4	
79	Andesite	39°07, 37°50	6	144.7	−28.6	6.1	119.7	
83	Basalt	39°07, 38°17	5	334.0	55.5	6.2	151.2	
84	Basalt	39°06, 38°17	6	179.7	−62.9	7.9	72.3	
86	Basalt	39°15, 38°05	7	169.2	−58.7	9.6	40.2	
88	Basalt	39°16, 37°58	7	130.0	−67.3	5.3	132.0	
89	Basalt	39°16, 37°58	7	169.5	−81.8	3.7	272.0	
90	Basalt	39°16, 37°58	7	173.6	−61.3	4.2	212.1	
91	Basalt	39°16, 37°55	7	161.7	−58.6	7.4	68.0	
92	Basalt	39°16, 37°55	4	155.6	−67.3	8.4	121.8	
M12	Basalt	39°46, 36°47	6	153.7	−48.8	8.0	71.2	*Gürsoy et al.* [1997]
M13	Basalt	39°46, 36°47	8	145.0	−56.9	7.0	63.6	
M19	Basalt	39°37, 36°30	7	339.7	28.0	7.7	62.5	
M20	Basalt	39°37, 36°30	6	327.6	55.0	7.5	79.9	
M76	Basalt	39°18, 36°59	6	307.2	48.2	9.6	50.0	
M78	Basalt	39°18, 36°59	7	190.7	−12.8	18.7	11.4	
M101	Basalt	39°32, 36°22	6	126.2	−50.3	4.7	205.4	
M103	Basalt	39°32, 36°22	7	167.0	−47.5	3.5	297.5	
M104	Basalt	39°32, 36°22	6	26.0	53.8	3.9	298.3	*Gürsoy et al.* [1997]
M105	Andesite	39°74, 37°07	6	25.9	52.7	18.5	25.5	
M227	Basalt	39°69, 36°91	8	142.0	−34.2	6.3	112.8	
M228	Basalt	39°69, 36°91	5	168.3	−65.1	3.8	398.2	
S8	Volcanic	39°01, 37°42	5	348.0	34.0	6.3	146.0	*Platzman et al.* [1998]
S9(a)	Volcanic	39°16, 37°58	7	151.0	−56.0	3.2	367.0	
S9(b)	Volcanic	39°16, 37°58	5	143.0	−65.0	14.3	29.0	
S10	Volcanic	39°25, 36°12	6	131.0	−68.0	4.3	244.0	
S11	Volcanic	39°26, 36°18	7	150.0	−31.0	6.5	86.0	
UR	Evaporitic rocks	40°29, 34°40	7	178.5	−59.8	6.0	102.4	*Kaymakçı et al.* [2003]
KUC	Clastic rocks	40°28, 34°00	6	356.5	43.9	8.8	58.8	
B01	Red clastics	31°70, 39°50	7	329.2	39.8	8.6	50.3	*Lucifora et al.* [2013]
B02	Red clastics	31°70, 39°50	21	344.9	51.4	4.8	44.1	
B03	Red clastics	34°30, 40°30	13	19.9	60.9	10.1	17.9	
B04	Red clastics	34°30, 40°30	20	6.9	45.7	5.9	31.7	
SU01	Mudrocks	40°60, 33°50	8	201.7	−48.6	4.6	110.4	*Lucifora et al.* [2013]
SU02	Mudrocks	40°60, 33°50	9	191.2	−47.7	6.7	60.6	
TU01	Mudrocks	40°35, 34°10	23	25.6	52.8	7.0	19.9	
N6	Volcanic	38°38, 34°57	5	159.0	−40.0	5.8	176.0	*Platzman et al.* [1998]
1	İgnimbrite	38°62, 35°06	7	170.3	−52.1	2.8	480.5	*Piper et al.* [2002]
2	İgnimbrite	38°63, 35°10	6	167.8	−46.7	2.9	519.6	
3	İgnimbrite	38°65, 35°20	6	174.9	−48.6	1.2	2931	
5	İgnimbrite	38°60, 35°15	7	5.2	46.3	2.7	487.3	
6	İgnimbrite	38°63, 36°10	7	351.5	50.3	2.9	44.2	
7	İgnimbrite	38°84, 35°74	6	352.7	49.3	2.0	1114	
8	İgnimbrite	38°76, 35°63	10	359.8	47.4	3.5	196.2	
9	İgnimbrite	38°72, 35°26	9	5.5	41.9	5.3	96.4	
10	İgnimbrite	38°66, 36°12	9	354.7	52.0	2.5	429.1	
11	İgnimbrite	37°99, 34°00	9	163.8	−73.3	9.2	32.3	
12	İgnimbrite	38°56, 35°02	5	175.1	−42.4	2.0	1420	
13(1)	İgnimbrite	38°28, 34°33	7	165.4	−41.8	4.9	151.2	
13(2)	İgnimbrite	38°28, 34°33	7	177.0	−38.6	3.5	303.4	
14	İgnimbrite	38°39, 34°24	8	175.5	−43.4	6.5	74.3	
15	İgnimbrite	38°48, 34°96	7	161.3	−41.1	8.7	49.3	
17	İgnimbrite	38°34, 34°40	7	167.4	−44.5	7.5	65.1	
20	İgnimbrite	37°99, 34°00	6	186.5	−59.5	9.0	56.9	
22	İgnimbrite	38°36, 34°20	7	165.8	−45.5	3.1	388.4	
23	İgnimbrite	38°52, 34°82	6	160.0	−46.0	7.1	89.3	
24	İgnimbrite	38°51, 34°32	4	155.7	−43.6	7.7	143.2	
25	İgnimbrite	38°50, 34°29	7	159.6	−52.0	3.9	243.9	

Table A1. (continued)

Site	Formation/Lithology/Region	Latitude(°)N, Longitude (°)E	N	D_s	I_s	α_{95}	k	Reference
26	İgnimbrite	38°45, 34°89	6	162.1	−56.2	2.6	678.2	
27	İgnimbrite	38°70, 34°97	5	12.4	56.9	9.3	68.8	
28	İgnimbrite	38°61, 35°85	7	14.4	62.0	7.7	61.6	
31	İgnimbrite	38°63, 34°84	6	350.4	42.8	8.1	69.4	
33	İgnimbrite	38°63, 34°84	6	350.4	42.8	7.7	76.5	
KH-SH	Lava	40.3, 31.4	29	342.2	42.2	3.9	12.9	*Çinku et al.* [2010]
BEY	Lava	40.1, 31.5	92	214.2	−54.9	4.0	14.1	*Çinku et al.* [2010]
OR	Lava	40.4, 33.0	71	34.3	50.2	4.5	15.2	*Çinku et al.* [2010]
33	Sarkışla/Lava	37.0, 39.5	18	147.9	−55.0	10.9	11.0	*Gürsoy et al.* [1997]
35	Gürün/Lava	37.2, 38.8	7	157.0	−54.1	14.0	19.5	*Gürsoy et al.* [1997]
37	Gemerek/Sedimentary rocks	36.0, 39.2	35	111.9	−60.8	9.6	7.4	*Krijgsman et al.* [1996]
38	Gemerek/Sedimentary rocks	36.0, 39.2	41	307.9	32.2	6.7	11.9	*Krijgsman et al.* [1996]
39	İnkonak/Sediments	36.0, 39.2	30	129.8	−37.3	7.7	12.7	*Krijgsman et al.* [1996]
41	Yeniköy/Sediment	37.0, 39.4	49	126.3	−33.3	8.8	6.4	*Krijgsman et al.* [1996]
42	Yeniköy/Sediment	36.4, 39.1	32	329.6	47.7	7.2	13.5	*Krijgsman et al.* [1996]
43	Haramiköy/Sedimentary rocks	36.4, 39.1	37	190.1	−40.9	5.3	20.9	*Krijgsman et al.* [1996]
67	Karapınar/Lava	31.8, 38.5	5	156.9	−42.2	14.4	29.2	*Gürsoy et al.* [1998]
62	Karacadağ/Lava	33.6, 37.5	13	177.5	−57.6	7.0	36.0	*Gürsoy et al.* [1998]
58	Hasandağ/lava	33.7, 37.7	7	170.1	−57.6	10.9	31.6	*Gürsoy et al.* [1998]
29	Galatya/Lava	34.2, 38.0	15	196.8	−56.5	6.9	31.7	*Gürsoy et al.* [1999]
30	Çankırı/Sedimentary rocks	31.8, 40.6	3	185.8	−42.3	33.0	15.0	*Kaymakçı et al.* [2003]
32	Sivas/Lava	34.3, 40.3	5	148.3	−41.8	18.8	17.5	*Gürsoy et al.* [1997]
34	Kormac/Lava	36.2, 39.4	10	156.0	−47.6	19.0	7.4	*Gürsoy et al.* [1997]
45	Keseköy/Lava	36.9, 39.2	20	189.9	−47.4	5.8	32.8	*Krijgsman et al.* [1996]
51	Sille/İgnimbrit	32.0, 40.7	4	149.5	−51.8	11.3	67.1	*Tatar et al.* [2002]
52	Erenler/Sediment	32.4, 37.8	12	181.3	−46.4	8.6	26.4	*Tatar et al.* [2002]
55	Erenlerdağ/Sed.	32.1, 37.6	5	179.0	−50.8	13.4	33.6	*Tatar et al.* [2002]
59	Kapadokya/Lava	32.0, 37.5	10	174.0	−51.1	6.6	55.1	*Piper et al.* [2002]
60	Ermenek/Lava	34.8, 38.6	3	179.0	−53.0	8.4	216.4	*Kissel et al.* [1993]
61	Antakya/Lava	33.0, 36.7	13	168.0	−43.9	6.9	37.1	*Kissel et al.* [2003]
68	Nevsehir/Lava	36.2, 36.1	11	182.7	−52.3	10.2	21	*Tatar et al.* [2000]
69	Erciyes/Lava	34.7, 38.8	24	178.4	−53.0	5.6	28.9	*Tatar et al.* [2000]
74	Osmaniye/Lava	35.8, 38.9	8	191.3	−44.6	12.6	20.3	*Gürsoy et al.* [2003]
75	Karasu/Lava	36.0, 37.0	51	188.8	−54.7	4.0	25.8	*Tatar et al.* [2004]
76	Karasu/Lava	36.3, 36.8	7	189.5	−49.9	4.7	165.9	*Tatar et al.* [2004]
56	Ankara/Lava	36.5, 37.0	12	168.3	−51.7	12.1	13.8	*Piper et al.* [2010]
57	Polatlı/Lava	32.5, 39.8	3	198.9	−58.3	9.4	173.1	*Piper et al.* [2010]

7. Conclusions

Paleomagnetic directions in almost all sites, including Upper Jurassic to Miocene volcanic, sedimentary and ophiolitic rocks from the Niğde-Kırşehir Massif and the Taurides, and corroborated by previous results are considered to be of primary origin. This has been confirmed by fold tests associated with progressive unfolding [*McElhinny*, 1968; *McFadden*, 1990; *Watson and Enkin*, 1993]. Exception to the primary magnetization is observed in central Taurides from Upper Cretaceous limestones, where the end-member analysis confirmed a remagnetization.

Paleolatitudinal differences among the Pontides, the Taurides, and the Niğde-Kırşehir Massif decrease systematically from the Lower Jurassic to the Miocene. It supports collectively the geological data that the Kırşehir Massif was separated from the Tauride during the Late Triassic as a result of the opening of the southern branch of the NeoTethyan Ocean which rifted and drifted away from the African Plate. It remained as an independent entity till the Middle Eocene. However, the first interaction of this independent piece of continent began during the Late Cretaceous as a result of the demise of the surrounding branches of the Neotethyan Oceans which led the convergence between the Kırşehir Massif with the surrounding continents. This continued till the total obliteration of the oceanic and the remaining sea environments until the Miocene period.

The different senses of rotations in the central, SE Taurides, and the Niğde-Kırşehir Massif during the Late Cretaceous-Middle Eocene are interpreted as two-phase oroclinal bending after the emplacement of the ophiolitic slices, first in the SE Taurides and later in the central Taurides. In the Niğde-Kırşehir Massif, counterclockwise rotation progressively continued from Middle Eocene to the Middle Miocene, which is in concordance with the

coherent block rotation of its SE and SW areas. The Neotectonic deformation during the last 5 Myr affected the SE Taurides, while in the central Taurides and in the Niğde-Kırşehir Massif no significant rotation was detected in the middle Miocene. Furthermore, in places where the locations are close to fault zones, especially near the Tuz Gölü and Sarız faults, large rotations are established that are associated with the young (post-Miocene) tectonic activities of Anatolia.

Appendix A: Paleomagnetic Results From Previous Studies (For Abbreviations, See Table A1)

Previous paleomagnetic studies carried out in Central Anatolia, Taurides, and the Pontides are listed in Appendix A. The first column indicates the site, and the second column shows the formation/lithology/region. The declination (D_s) and inclination (I_s) values are given in stratigraphic coordinates, after tilt correction together with their site numbers (N) and statistical parameters. Each seperate study is denoted with the reference in the last line.

Acknowledgments

This study was financially supported by the Scientific and Technical Research Council of Turkey (TUBITAK) with project 111Y043. The authors also thank the Scientific Research Projects Coordination Unit of Istanbul University (Project UDP 37301) for their financial assistance. We are grateful to Erwin Appel for providing access to the paleomagnetic laboratory in the University of Tübingen. Previous paleomagnetic data to support this manuscript are listed in Appendix A. Douwe van Hinsbergen, Anthony Morris, Marco Maffione, and two anonymous reviewers are appreciated for their helpful comments.

References

Akıman, O., A. Erler, M. C. Göncüoglu, N. Gülec, A. Geven, K. Türeli, and Y. Kadioglu (1993), Geochemical characteristics of granitoids along the western margin of the Central Anatolian Crystalline Complex and their tectonic implications, *Geol. J.*, *28*, 371–382.

Akyürek, B., et al. (1984), Fundamental geological characteristics of Ankara-Elmadag-Kalecik area, Chamber of Geological Engineers of Turkey (TMMOB Jeoloji Mühendisleri Odasi) [in Turkish with English abstract], *J. Geol. Engineering*, *20*, 31–46.

Allerton, S., and F. J. Vine (1991), Spreading evolution of the Troodos ophiolite, Cyprus, *Geology*, *19*, 637–640.

Arıkan, Y. (1975), The geology and petroleum prospects of the Tuz Golu Basin, Ankara, Miner. Res. Explor. Inst. Turk. Bull. Foreign, Ankara, vol. 85, pp. 17–37.

Atabey, E., and E. Ayhan (1986), Niğde-Ulukışla-Çamardı-Çiftehan yöresinin jeolojisi, Rep. 8064, Miner. Res. Explor. Inst., Ankara, 69.

Beekman, P. H. (1966), The Pliocene and Quaternary volcanism in the Hasandağ-Melendizdağ region, *Miner. Res. Explor.Inst. Turkey*, *66*, 99–106.

Besse, J., and V. Courtillot (2002), Apparent and true polar wander and the geometry of the geomagnetic field over the last 200 Myr, *J. Geophys. Res.*, *107*(B11), 2300, doi:10.1029/2000JB000050.

Bilardello, D., and K. P. Kodama (2009a), Measuring remanence anisotropy of hematite in red beds: Anisotropy of high-field isothermal remanence magnetization (hf-AIR), *Geophys. J. Int.*, *178*(3), 1260–1272, doi:10.1111/j.1365-246X.2009.04231.x.

Bilardello, D., and P. K. Kodama (2009b), Magnetic fabric and inclination shallowing studies: Depositional and post-depositional processes in hematite and magnetite-bearing rocks, *Eos. Trans. AGU*, 90(52), Fall Meet. Suppl., Abstract GP43A-0841.

Bingöl, E., B. Akyürek, and B. Korkmazer (1973), The geology of the Biga Peninsula and some features of the Karakaya Formation [in Turkish with English abstract], in *Proceedings of the 50th Anniversary of the Turkish Republic Earth Science Congress*, pp. 70–77, Miner. Res. Explor. Inst., Ankara Publications.

Birgili, Ş., R. Yoldaş, and G. Ünalan (1975), Çankırı–Çorum havzasının jeolojisi ve petrol olanakları ön raporu. (Preliminary report of the geology and petroleum possibilities of the Çankırı–Çorum Basin.) [in Turkish], Türkiye Petrolleri Anonim Ortaklığı Rapor (TPAO Report), 1216.

Boztuğ, D., M. Tichomirowa, and K. Bombach (2007), 207Pb-206Pb single-zircon evaporation ages of some granitoid rocks reveal continent-oceanic island arc collision during the Cretaceous geodynamic evolution of the central Anatolian crust, Turkey, *J. Asian Earth Sci.*, *31*, 71–86.

Çataklı, A. S. (1983), Assemblage ophiolitique et roches associées de la partie occidentale du massif de Pozant-Karsant (Taurus cilicien, Turquie) Thèse d'Etat, Université de Nancy I.

Çelik, Ö. F., M. Delaloye, and G. Feraud (2006), Precise 40Ar-39Ar ages from the metamorphic sole rocks of the Tauride Belt Ophiolites, southern Turkey: Implications for the rapid cooling history, *Geol. Mag.*, *143*, 213–227.

Çemen, I., M. C. Göncüoglu, and K. Dirik (1999), Structural evolution of the Tuz Gölü basin in central Anatolia, Turkey, *J. Geol.*, *107*, 693–706.

Channell, J. E. T., O. Tüysüz, O. Bektaş, and A. M. C. Şengör (1996), Jurassic-Cretaceous paleomagmatısm and paleogeography of the Pontides (Turkey), *Tectonics*, *15*, 201–212.

Çinku, M. C. (2004), Paleomagnetic evidence of the Western Black Sea region [in Turkish], PhD thesis, Istanbul Univ. Institute of Science, Istanbul p. 222.

Çinku, M. C. (2011), Paleogeographic evidence on the Jurassic tectonic history of the Pontides: New paleomagnetic data from the Sakarya continent and Eastern Pontides, *Int. J. Earth. Sci.*, *100*(7), 1633–1645.

Çinku, M. C., and N. Orbay (2010), The origin of Neogene tectonic rotations in the Galatean volcanic massif, central Anatolia, *Int. J. Earth Sci.*, *99*(4), 413–426.

Çinku, M. C., T. Ustaömer, H. Ann, Z. M. Hisarli, F. Heller, and N. Orbay (2010), Southward migration of arc magmatism during latest Cretaceous associated with slab steepening, East Pontides, N Turkey: New paleomagnetic data from the Amasya region, PEPI, vol. 182, pp. 18–29.

Çinku, M. C., M. Z. Hisarlı, F. Heller, N. Orbay, and T. Ustaömer (2011), Middle Eocene paleomagnetic data from the eastern Sakarya Zone and the Central Pontides: Implications for the tectonic evolution of north central Anatolia, *Tectonics*, *30*, TC1008, doi:10.1029/2010TC002705.

Çinku, M. C., Z. M. Hisarli, M. N. Orbay, T. Ustaömer, H. Ann, S. Kravchenko, O. Rusakov, and N. Sayın (2013), Evidence of Early Cretaceous remagnetization in the Crimean Peninsula: A palaeomagnetic study from Mesozoic rocks in the Crimean and Western Pontides, conjugate margins of the Western Black Sea, *Geoph. J. Int.*, *195*(2), 821–843, doi:10.1093/gji/ggt260.

Çinku, M. C., M. Z. Hisarlı, A. M. Hirt, F. Heller, T. Ustaömer, N. Kaya, E. Öksüm, and N. Orbay (2015), Evidence of Late Cretaceous oroclinal bending in North-Central Anatolia: Paleomagnetic results from Mesozoic and Cenozoic rocks along the Izmir-Ankara-Erzincan Suture Zone Geological Society Special Issue; Palaeomagnetism in Fold and Thrust Belts: New Perspectives; Edt. Belen Oliva Urcia (accepted).

Clark, M. S., and A. H. F. Robertson (2005), Uppermost Cretaceous-Lower Tertiary Ulukışla Basin, south-central Turkey: Sedimentary evolution of part of a unified basin complex within an evolving Neotethyan suture zone, *Sediment. Geol.*, *71*, 15–51.

Deenen, M. H. L., C. G. Langereis, D. J. J. van Hinsbergen, and A. J. Biggin (2011), Geomagnetic secular variation and the statistics of palaeomagnetic directions, *Geophys. J. Int.*, *186*, 509–520.

Delibaş, O., and Y. Genç (2004), Origin and formation processes of iron, copper-molybdenum and lead mineralisations of Karacaali (Kırıkkale) Magmatic Complex, *Geol. Bull. Turkey*, *47*, 47–60.
Dellaloğlu, A. A., O. Tüysüz, O. H. Kaya, and B. Harput (1992), Kalecik (Ankara)-Eldivan-Yapraklı (Çankırı)-İskilip (Çorum) ve Devrez Çayı Arasındaki Alanın Jeolojisi ve Petrol Olanakları (Geology and Petroleum Potential of the Area Between Kalecik (Ankara)-Eldivan-Yapraklı (Çankırı)-İskilip (Çorum) and Devrez Çayı) Turkish Petroleum Corporation (TPAO) Report no. 3194 [in Turkish, unpublished].
Demirkol, C. (1981), Sultandağ kuzeybatısnıın jeolojisi ve Bey- şehir-Hoyran napı ile ilişkileri TÜBİTAK project no: TBAG-382.
Demirtaşlı, E., N. Turhan, A. Z. Bilgin, and M. Selim (1975), Bolkardağlarının Jeolojisi, in *Proceedings of the 50th Anniversary of the Turkish Republic Earth Science Congress*, pp. 42–47, Miner. Res. Explor. Inst., Ankara.
Dilek, Y., P. Thy, B. Hacker, and S. Grundvig (1999), Structure and petrology of Tauride ophiolites and mafic dyke intrusions (Turkey): Implications for the Neotethyan Ocean, *Geol. Soc. Am. Bull.*, *111*, 1192–1216.
Dirik, K. (2001), Neotectonic evolution of the northwestward arched segment of the Central Anatolian Fault Zone, Central Anatolia, Turkey, *Geod. Acta*, *14*, 147–158.
Dirik, K., and M. C. Göncüoglu (1996), Neotectonic characteristics of the Central Anatolia, *Int. Geol. Rev.*, *38/9*, 807–817.
Dönmez, M., A. E. Akçay, H. Kara, A. F. Yergök, and K. Esentürk (2008), *Türkiye jeoloji haritalari No.90 Kırşehir - İ30 Paftasi, 1:100 000*, Miner. Res. Explor. Inst., Ankara.
Enkin, R. J., and G. S. Watson (1996), Statistical analysis of paleomagnetic inclination data, *J. Geophys. Int.*, *126*, 495–504.
Evans, I., S. A. Hall, M. F. Carman, M. Senalp, and S. Coskun (1982), Paleomagnetic study of the Bilecik limestone (Jurassic), northwest Anatolia, *Earth Planet. Sci. Lett.*, *61*, 199–208.
Fisher, R. A. (1953), Dispersion on a sphere, *Proc. R. Soc. London*, *217*, 195–305.
Gallet, Y., J. Besse, L. Krystyn, H. Théveniaut, and J. Marcoux (1993), Magnetostratigraphy of the Kavur Tepe section (southwestern Turkey): A magnetic polarity time scale for the Norian, *Earth Planet. Sci. Lett.*, *117*(3–4), 443–456.
Gencalioglu-Kuscu, G., C. Atilla, R. A. F. Cas, and L. Kuscu (2007), Base surge deposits, eruption history, and depositional processes of a wet phreatomagmatic volcano in Central Anatolia (Cora Maar), *J. Volcanol. Geotherm. Res.*, *159*, 198–209.
Göğer, E., and K. Kıral (1969), Kızılören dolayının jeolojisi *Mineral Research and Exploration Institute of Turkey* Report No: 5204 (unpublished).
Gong, Z., M. J. Dekkers, D. Heslop, and T. A. T. Mullender (2009a), End member modeling of isothermal remanent magnetization (IRM) acquisition curves: A novel approach to diagnose remagnetization, *Geophys. J. Int.*, *178*, 693–701.
Gong, Z., D. J. J. van Hinsbergen, and M. J. Dekkers (2009b), Diachronous pervasive remagnetization in northern Iberian basins during Cretaceous rotation and extension, *Earth Planet. Sci. Lett.*, *284*, 292–301.
Görür, N., and O. Tüysüz (2001), Cretaceous to Miocene palaeogeographic evolution of Turkey: Implications for hydrocarbon potential, *J. Petrol. Geol.*, *24*, 119–146.
Görür, N., F. Y. Oktay, İ. Seymen, and A. M. C. Şengör (1984), Paleotectonic evolution of the Tuz Gölü basin complex, Central Anatolia: Sedimentary record of a Neo-Tethyan closure, in *The Geological Evolution of the Eastern Mediterranean*, *Geol. Soc. London Spec. Publ.*, vol. 17, edited by J. E. Dixon and A. H. F. Robertson, pp. 455–466, Geological Society, London.
Görür, N., O. Tüysüz, and A. M. C. Şengör (1998), Tectonic evolution of the Central Anatolian Basins, *Int. Geol. Rev.*, *40*, 831–850.
Gürsoy, H., J. D. A. Piper, O. Tatar, and H. Temiz (1997), A palaeomagnetic study of the Sivas Basin, Central Turkey: Crustal deformation during lateral escape of the Anatolian Block, *Tectonophysics*, *271*, 89–106.
Gürsoy, H., J. D. A. Piper, O. Tatar, and L. Mesci (1998), Paleomagnetic study of the Karaman and Karapinar volcanic complexes, central Turkey: Neotectonic rotation in the south-central sector of the Anatolian block, *Tectonophysics*, *299*, 191–211.
Gürsoy, H., J. A. Piper, and O. Tatar (1999), Palaeomagnetic study of the Galatean volcanic province, north-central Turkey: Neogene deformation at the northern border of the Anatolian Block, *Geol. J.*, *34*, 7–23.
Gürsoy, H., O. Tatar, J. D. A. Piper, A. Heimann, and L. Mesci (2003), Neotectonic deformation linking the East Anatolian and Karataş–Osmaniye intracontinental transform fault zones in the Gulf of İskenderun, southern Turkey, deduced from paleomagnetic study of the Ceyhan–Osmaniye volcanics, *Tectonics*, *22*(6), 1067, doi:10.1029/2003TC001524.
Gürsoy, H., O. Tatar, J. D. A. Piper, F. Koçbulut, Z. Akpınar, B. Huang, A. P. Roberts, and B. L. Mesci (2011), Paleomagnetic study of Kepezdağ and Yamadağ volcanic complexes, central Turkey: Neogene tectonic escape and block definition in the central-east Anatolides, *J. Geod.*, *51*, 308–326.
Hakyemez, Y., E. Elibol, M. Umut, B. Bakırhan, İ. Kara, H. Dağıstan, T. Metin, and N. Erdoğan (1992), The geology of Konya-Çumra-Akören and surrounding [in Turkish], Rep. 9449, p. 73, Miner. Res. Explor. Inst., Ankara.
Heslop, D., and M. Dillon (2007), Unmixing magnetic remanence curves without a priori knowledge, *Geophys. J. Int.*, *170*(2), 556–566.
Hisarlı, Z. M. (2011), New paleomagnetic constraints on the late Cretaceous and early Cenozoic tectonic history of the Eastern Pontides, *J. Geod.*, *52*, 114–128.
Hisarlı, Z. M., M. C. Çinku, and N. Orbay (2011), Paleomagnetic evidence of complex tectonic rotation pattern in the NW Anatolian region: Implications for the tectonic history since the Middle Eocene, *Tectonophysics*, *505*, 86–99.
Hurst, S. D., K. L. Verosub, and E. M. Moores (1992), Paleomagnetic constraints on the formation of the Solea Graben, Troodos Ophiolite, Cyprus, *Tectonophysics*, *208*, 431–445.
Innocenti, F., R. Mazzuoli, G. Pasquare, F. Radicati Di Brozoli, and L. Villari (1975), The Neogene calkalkaline volcanism of central Anatolia: Geochronological data of Kayseri-Nigde area, *Geol. Mag.*, *112*(4), 349–360.
Inwood, J., A. Morris, M. W. Anderson, and A. H. F. Robertson (2009), Neotethyan intraoceanic microplate rotation and variations in spreading axis orientation: Palaeomagnetic evidence from the Hatay ophiolite (southern Turkey), *Earth Planet. Sci. Lett.*, *280*, 105–117 (September 2008).
İşseven, T., and O. Tüysüz (2006), Palaeomagnetically defined rotations of fault-bounded continental blocks in the North Anatolian Shear Zone, North Central Anatolia, *J. Asian Earth Sci.*, *28*, 469–479.
Jackson, M., S. K. Banerjee, J. A. Marvin, R. Lu, and W. Gruber (1991), Detrital remanence inclination errors and anhysteretic remanence anisotropy: Quantitative model and experimental results, *Geophys. J. Int.*, *104*, 95–103.
Jaffey, N., and A. H. F. Robertson (2001), New sedimentological and structural data from the Ecemiş fault zone: Implications for its timing and offset and the Cenozoic tectonic escape of Anatolia, *J. Geo. Soc. London*, *158*, 367–378.
Juteau, T. (1980), Ophiolites of Turkey, *Ofioliti*, *2*, 199–237.
Kaymakçı, N., S. H. White, and P. M. Van Dijk (2000), Paleostress inversion in a multiphase deformed area: Kinematic and structural evolution of the Çankiri Basin (central Turkey), Part 1, in *Tectonics and Magmatism in Turkey and the Surrounding Area*, edited by E. Bozkurt, J. A. Winchester, and J. A. D. Piper, *Geol. Soc. London Spec. Publ.*, 173, 445–473.
Kaymakçı, N., C. E. Duermeijer, C. Langereis, S. H. White, and P. M. Van Dijk (2003), Palaeomagnetic evolution of the Çankırı Basin (central Anatolia, Turkey): Implications for oroclinal bending due to indentation, *Geol. Mag.*, *140*, 343–355.
Kirschvink, J. L. (1980), The least-squares line and plane and the analysis of palaeomagnetic data, *Geophys. J. R. Astron. Soc.*, *62*, 699–718.

Kissel, C., and A. Poisson (1986), Etude paleomagnetique preliminaire des formations neogene du bassin d'Antalya (Taurides occidentales-Turquie), *C.R. Acad. Sci. Paris Ser. II*, *302*(10), 711–716.
Kissel, C., and A. Poisson (1987), Etude paleomagnetique preliminaire des formations cenozoiques des Bey Dağları (Taurides occidentales, Turquie), *C.R. Acad. Sci. Paris Ser. II*, *304*(8), 343–348.
Kissel, C., O. Averbuch, D. Frizon de Lamotte, O. Monod, and S. Allerton (1993), Preliminary paleomagnetic evidence of a post-Eocene clockwise rotation of the Western Taurides thrust belt, east of the Isparta reentrant (Southern Turkey), *Earth Planet. Sci. Lett.*, *117*, 1–14.
Kissel, C., C. Laj, A. Poisson, and N. Görür (2003), Paleomagnetic Reconstruction of the Cenozoic Evolution of the Eastern Mediterranean, *Tectonophysics*, *362*, 199–217.
Koçyigit, A. (1991), An example of an accretionary fore –arc basin from northern Central Anatolia and its implications for the history of subduction of Neo –Tethys in Turkey, *Geol. Soc. Am. Bull.*, *103*, 22–36.
Koçyigit, A., S. Özkan, and F. B. Rojay (1988), Examples from the fore-arc basin remnants at the active margin of northern Neo –Tethys; Development and emplacement ages of the Anatolian nappe, Turkey, Ankara, *J Pure Appl Sci*, *21*, 183–210.
Kodama, K. P. (2009), Simplification of the anisotropy-based inclination correction technique for magnetite- and hematite bearing rocks: A case study for the Carboniferous Gleshaw and Mauch Chunk Formations, North America, *Geophys. J. Int.*, *176*, 467–477, doi:10.1111/j.1365-246X.2008.04013.x.
Krijgsman, W., M. Garcés, C. G. Langereis, R. Daams, J. van Dam, A. J. van der Meulen, J. Agustí, and L. Cabrera (1996), A new chronology for the middle to late Miocene continental record in Spain, *Earth Planet. Sci. Lett.*, *142*, 367–380.
Kruiver, P. P., M. J. Dekkers, and D. Heslop (2001), Quantification of magnetic coercivity components by the analysis of acquisition curves of isothermal remanent magnetisation, *Earth Planet. Sci. Lett.*, *189*, 269–276.
Lefebvre, C., M. J. M. Meijers, N. Kaymakçı, A. Peynircioğlu, C. G. Langereis, and D. J. J. Van Hinsbergen (2013), Reconstructing the geometry of central Anatolia during the late Cretaceous: Large-scale Cenozoic rotations and deformation between the Pontides and Taurides, *Earth Planet. Sci. Lett.*, *366*, 83–98.
Lowrie, W. (1990), Identification of ferromagnetic minerals in a rock by coercivity and unblocking temperature properties, *Geophys. Res. Lett.*, *17*, 159–162.
Lucifora, S., F. Cifelli, F. B. Rojay, and M. Mattei (2013), Paleomagnetic rotations in the Late Miocene sequence from the Çankırı Basin (Central Anatolia, Turkey): The role of strike–slip tectonics, *Turkey J. Earth Sci.*, *22*, 778–792.
McElhinny, M. W. (1964), Statistical significance of the fold test in palaeomagnetism, *Geophys. J. R. Astron. Soc.*, *8*, 338–340.
McElhinny, M. W. (1968), The northward drift of India - An examination of recent palaeomagnetic results, *Nature*, *217*, 342–344.
McFadden, P. L. (1990), The Fold Test as an Analytical tool, *Geophy. J. Inst.*, *135*, 329–338.
Meijers, M. J. M., N. Kaymakcı, D. J. J. Van Hinsbergen, C. G. Langereis, R. A. Stephenson, and J.-C. Hippolyte (2010), Late Cretaceous to Paleocene oroclinal bending in the Central Pontides (Turkey), *Tectonics*, *29*, TC4016, doi:10.1029/2009TC002620.
Meijers, M. J. M., D. J. J. Van Hinsbergen, C. G. Langereis, D. Altıner, M. J. Dekkers, N. Kaymakcı, and R. A. Stephenson (2011), Pervasive Paleogene remagnetization of the central Taurides fold and thrust belt (southern Turkey) and implications for rotations in the Isparta angle, *Geophys. J. Int.*, *184*, 1090–1112.
Morris, A. (2003), The late Cretaceous palaeolatitude of the Neotethyan spreading axis in the eastern Mediterranean region, *Tectonophysics*, *377*, 157–178.
Morris, A., and A. H. F. Robertson (1993), Miocene remagnetisation of carbonate platform and Antalya Complex units within the Isparta angle, SW Turkey, *Tectonophysics*, *220*, 243–266.
Morris, A., K. M. Creer, and A. H. F. Robertson (1990), Palaeomagnetic evidence for clockwise rotations related to dextral shear along the Southern Troodos Transform Fault, Cyprus, *Earth Planet. Sci. Lett.*, *99*, 250–262.
Morris, A., M. W. Anderson, and A. H. F. Robertson (1998), Multiple tectonic rotations and transform tectonism in an intraoceanic suture zone, SW Cyprus, *Tectonophysics*, *299*, 229–253.
Morris, A., M. W. Anderson, A. H. F. Robertson, and K. Al-Riyami (2002), Extreme tectonic rotations within an eastern Mediterranean ophiolite (Baer-Bassit, Syria), *Earth Planet. Sci. Lett.*, *202*, 247–261.
Nairn, S. (2010), Testing alternative models of continental collision in Central Turkey by a study of the sedimentology, provenance and tectonic setting of Late Cretaceous–Early Cenozoic syn-tectonic sedimentary basins, PhD thesis, 365 p., The Univ. of Edinburgh, U. K.
Nairn, S., A. H. F. Robertson, U. C. Ünlügenç, K. Taşlı, and N. İnan (2012), Tectonostratigraphic evolution of the Upper Cretaceous-Cenozoic central Anatolian basins: An integrated study of diachronous ocean basin closure and continental collision, *Geol. Soc. London Spec. Publ.*, doi:10.1144/SP372.9.
Norman, T. (1973a), Ankara Yahşıman bölgesinde Üst Kretase-Alt Tersiyer sedimentasyon, *Bull. Geol. Soc. Turkey*, *16*, 41–66.
Norman, T. (1973b), Ankara Yahşıman bölgesinin Eosen'den sonraki tektonik gelişmesi, *Bull. Geol. Soc. Turkey*, *16*, 67–81.
Norman, T. N. (1972), Ankara Yahşıhan bölgesinde Üst Kretase-Alt Tersiyer istifinin stratigrafisi, *Bull. Geol. Soc. Turkey*, *15*, 180–276.
Okay, A. I., and Ö. Şahintürk (1997), Geology of the eastern Pontides. Regional and petroleum geology of the Black Sea and surrounding regions (Editör: A. Robinson), *Am Assoc. Petrol. Geol. Mem.*, *68*, 291–311.
Okay, A. I., and O. Tüysüz (1999), Tethyan sutures of northern Turkey, in *The Mediterranean Basins, Tertiary Extension Within the Alpine Orogen*, *Spec. Publ.*, vol. 156, edited by B. Durand et al., pp. 475–515, Geological Society, London.
Okay, A. I., M. Satır, H. Maluski, M. Siyako, P. Monie, R. Metzger, and S. Akyüz (1996), Paleo- and Neo-Tethyan events in northwest Turkey: Geological and geochronological constraints, in *The Tectonics Evolution of Asia*, edited by A. Yin and M. Harrison, pp. 420–441, Cambridge Univ. Press, Cambridge, U. K.
Okay, A. I., M. Satır, and W. Siebel (2006), Pre-Alpide orogenic events in the Eastern Mediterranean region, in *European Lithosphere Dynamics*, *Memoirs*, vol. 32, edited by D. G. Gee and R. A. Stephenson, pp. 389–405, Geological Society, London.
Okay, A. I., G. Sunal, S. Sherlock, D. Altıner, O. Tüysüz, A. R. C. Kylander-Clark, and M. Aygül (2013), Early Cretaceous sedimentation and orogeny on the active margin of Eurasia: Southern Central Pontides, Turkey, *Tectonics*, *32*, 1247–1271, doi:10.1002/tect.20077.
Ömer, A. F., A. Morris, and M. W. Anderson (2013), First palaeomagnetic results from the Mersin ophiolite (Turkey), EGU General Assembly 2013, Vienna, Geophysical Research Abstracts, vol. 15, EGU2013-10793.
Özgül, N. (1976), Toroslann bazı temel jeoloji özellikleri, *Bull. Geol. Soc. Turkey*, *19–1*, 65–78.
Özgül, N. (1984), Stratigraphy and tectonic evolution of the central Taurides, in *Geology of the Taurus Belt*, edited by O. Tekeli and M. C. Göncüoğlu, pp. 77–90, Miner. Res. Explor. Inst., Ankara.
Özgül, N. (1997), Bozkır-Hadim-Taşkent (Orta Toros ların kuzey kesimi) dolayında yer alan Tektono stratigrafik birliklerin stratigrafisi, *Min. Res. Explor. Inst. Turkey Bull.*, *119*, 113–174.
Parlak, O. (1996), Geochemistry and geochronology of the Mersin ophiolite within the Eastern Mediterranean Tectonic Frame (southern Turkey), PhD thesis, Univ. de Genève, Switzerland.

Parlak, O., and M. Delaloye (1996), Geochemistry and timing of postmetamorphic dike emplacement in the Mersin ophiolite (Southern Turkey): New age constraints from 40Ar/39Ar geochronology, *Terra Nova*, *8*, 585–592.
Parlak, O., and M. Delaloye (1999), Precise 40Ar/39Ar ages from the metamorphic sole of the Mersin ophiolite (Southern Turkey), *Tectonophysics*, *301*, 145–158.
Parlak, O., V. Höck, and M. Delaloye (2000), Suprasubduction zone origin of the Pozant-Karsant ophiolite (southern Turkey) deduced from whole rock and mineral chemistry of the gabbroic cumulates, in *Tectonics and Magmatism in Turkey and the Surrounding Area*, edited by E. Bozkurt, J. A. Wınchester, and J. A. D. Pıper, *Geol. Soc. London Spec. Publ.*, 173, 219–234.
Parlak, O., V. Hock, and M. Delaloue (2002), The supra-subduction zone Pozanti–Karsanti ophiolite, southern Turkey: Evidence for high-pressure crystal fractionation of ultramafic cumulates, *Lithos*, *65*(1–2), 205–224.
Parlak, O., F. Karaoğlan, T. Rızaoğlu, U. Klotzli, F. Koller, and Z. Billor (2013), U–Pb and 40Ar–39Ar geochronology of the ophiolites and granitoids from the Tauride belt: Implications for the evolution of the Inner Tauride suture, *J. Geod.*, *65*, 22–37.
Pasquare, G. (1968), Geologie of the Senozoic volkanic area of central Anatolia. Atti della Acad No. *delince*; *menorie serie* VIII, IX s. 55–204 Roma.
Piper, J. D. A., J. M. Moore, O. Tatar, H. Gürsoy, and R. G. Park (1996), Paleomagnetic study of crustal deformation across an intracontinental transform: The north Anatolian fault zone in northern Turkey, paleomagnetism and tectonics of the Mediterranean Region, *Geol. Soc. Spec. Publ.*, *105*, 299–310.
Piper, J. D. A., O. Tatar, and H. Gürsoy (1997), Deformational behaviour of continental lithosphere deduced from block rotations across the North Anatolian fault zone in Turkey, *Earth Planet. Sci. Lett.*, *150*, 191–203.
Piper, J. D. A., H. Gürsoy, O. Tatar, T. Isseven, and A. Kocyiğit (2002), Paleomagnetic evidence for the Gondwanic origin of the Taurides and rotation of the Isparta angle, southern Turkey, *Geol. J.*, *37*, 317–336.
Piper, J. D. A., H. Gursoy, O. Tatar, M. E. Beck, A. Rao, F. Kocbulut, and B. L. Mesci (2010), Distributed neotectonic deformation in the Anatolides of Turkey: A palaeomagnetic analysis, *Tectonophysics*, *488*, 31–50.
Platzman, E. S., J. P. Platt, C. Tapirdamaz, M. Sanver, and C. C. Rundle (1994), Why there is no clockwise rotation along the North Anatolian Fault Zone?, *J. Geophys. Res.*, *99*, 21,705–21,715.
Platzman, E. S., C. Tapırdamaz, and M. Sanver (1998), Neogene anticlockwise rotation of central Anatolia (Turkey): Preliminary paleomagnetic and geochronological results, *Tectonophysics*, *299*, 175–189.
Pourteau, A., O. Candan, and R. Oberhansli (2010), High-pressure metasediments in central Turkey: Constraints on the Neotethyan closure history, *Tectonics*, *29*, TC5004, doi:10.1029/2009TC002650.
Rice, S. P., A. H. F. Robertson, and T. Ustaömer (2006), Late Cretaceous-Early Cenozoic tectonic evolution of the Eurasian active margin in the Central and Eastern Pontides, northern Turkey, *Geol. Soc., London Spec. Publ.*, *260*, 413–445.
Rice, S. P., A. H. F. Robertson, T. Ustaömer, N. Inan, and K. Taslı (2009), Late Cretaceous–Early Eocene tectonic development of the Tethyan suture zone in the Erzincan area, Eastern Pontides, Turkey, *Geol. Mag.*, *146*(4), 567–590.
Rigo de Righi, M., and A. Cortesini (1959), Regional studies of the Central Anatolian basin Progress Report (unpublished). *Turkish Gulf Oil Co.*, Report., No. 11.
Robertson, A. H., O. Parlak, and T. Ustaömer (2009), Melange genesis and ophiolite emplacement related to subduction of the northern margin of the Tauride-Anatolide continent, central and western Turkey, in *Collision and Collapse at the Africa-Arabia-Eurasia Subduction Zone*, edited by D. J. J. van Hinsbergen, M. A. Edwards, and R. Govers, pp. 9–66, Geological Society, London.
Robertson, A. H. F. (2002), Overview of the genesis and emplacement of Mesozoic ophiolites in the Eastern Mediterranean Tethyan Region, *Lithos*, *65*, 1–67.
Robertson, A. H. F., and J. E. Dixon (1984), Aspects of the geological evolution of the Eastern Mediterranean, in *The Geological Evolution Of The Eastern Mediterranean*, *Spec. Publ.*, vol. 17, edited by J. E. Dixon and A. H. F. Robertson, pp. 1–75, Geological Society, London.
Robertson, A. H. F., T. Ustaomer, E. A. Pickett, A. S. Collins, T. Andrew, and J. E. Dixon (2004), Testing models of Late Palaeozoic–Early Mesozoic orogeny in Western Turkey: Support for an evolving open-Tethys model, *J. Geol. Soc. London*, *161*, 501–511.
Sanver, M., and E. Ponat (1981), Kırşehir ve dolaylarina iliskin paleomagnetik bulgular. Kırşehir Masifinin rotasyonu, *İstanbul Yerbilimleri*, *2*, 2–8.
Sarıbudak, M. (1989), New results and a paleomagnetic overview of the Pontides in northern Turkey, *Geophys. J. Int.*, *99*, 521–531.
Şaroğlu, F., A. Boray, S. Özer, and İ. Kuşçu (1983), Orta Toroslar—Orta Anadolu'nun güneyinin neotektoniği ile ilgili görüşler, *Jeomorfoloji Bull.*, *11*, 35–44.
Schmidt, G. C. (1961), Stratigraphic nomenclature for the Adana region petroleum district VIII, *Petrol. Admin. Bull.*, *6*, 47–63.
Şengör, A. M. C. (1979), The North Anatolian transform fault: Its age, offset and tectonic significance, *J. Geol. Soc.*, *136*, 269–282.
Şengör, A. M. C., and Y. Yılmaz (1981), Tethyan evolution of Turkey: A plate tectonic approach, *Tectonophysics*, *75*, 181–241.
Şengör, A. M. C., Y. Yilmaz, and O. Süngürlü (1984), Tectonics of the Mediterranean Cimmerides: Nature and evolution of the western termination of Palaeo-Tethys, in *The Geological Evolution of the Eastern Mediterranean*, edited by J. E. Dixon and A. H. F. Robertson, *Geol. Soc. London, Spec. Publ.*, 17, 77–112.
Tan, X., and K. P. Kodama (2003), An analytical solution for correcting paleomagnetic inclination error, *Geophys. J. Int.*, *152*, 228–236.
Tan, X., K. P. Kodama, H. Chen, D. Fang, D. Sun, and Y. Li (2003), Paleomagnetism and magnetic anisotropy of Cretaceous red beds from the Tarim basin northwest China: Evidence for a rock magnetic cause of anomalously shallow paleomagnetic inclinations from central Asia, *J. Geophys. Res.*, *108*(B2), 2107, doi:10.1029/2001JB001608.
Tatar, O., J. D. A. Piper, R. G. Park, and H. Gürsoy (1995), Paleomagnetic study of block rotations in the Niksar overlap region of the North Anatolian Fault Zone, central Turkey, *Tectonophysics*, *244*, 251–266.
Tatar, O., J. D. A. Piper, H. Gürsoy, and H. Temiz (1996), Regional significance of neotectonic counterclockwise rotation in central Turkey, *Int. Geol. Rev.*, *38*, 692–700.
Tatar, O., J. D. A. Piper, and H. Gursoy (2000), Palaeomagnetic study of the Erciyes Sector of the Ecemis Fault Zone: Neotectonic deformation in the southeastern part of the Anatolian Block, in *Tectonics and Magmatism in Turkey and the Surrounding Area*, edited by E. Bozkurt, J. A. Winchester, and J. D. A. Piper, *Geol. Soc. London, Spec. Publ.*, 173, 423–440.
Tatar, O., H. Gürsoy, and J. D. A. Piper (2002), Differential neotectonic rotations in Anatolia and the Tauride arc: Palaeomagnetic investigation of the Erenlerdağı Complex and Isparta volcanic district, south-central Turkey, *J. Geol. Soc. London*, *159*, 281–294.
Tatar, O., J. D. A. Piper, H. Gürsoy, A. Heimann, and F. Koçbulut (2004), Neotectonic deformation in the transition zone between the Dead Sea Transform and the East Anatolian Fault Zone, Southern Turkey: A palaeomagnetic study of the Karasu Rift Volcanism, *Tectonophysics*, *385*, 17–43, doi:10.1016/j.tecto.2004.04.005.
Tekeli, O., A. Aksay, B. M. Urgun, and A. Işık (1983), Geology of the Aladağ Mountains, in *Proceedings of International Symposium*, edited by O. Tekeli and M. C. Göncüoğlu, pp. 143–158, Geology of the Taurus Belt, Ankara Turkey.
Torsvik, T. H., et al. (2012), Phanerozoic polar wander, palaeogeography and dynamics, *Earth Sci. Rev.*, *114*(3–4), 325–368, doi:10.1016/j.earscirev.2012.06.007.

Ünalan, G., V. Yüksel, T. Tekeli, O. Gonenç, Z. Seyirt, and S. Hüseyn (1976), Upper Cretaceous-Lower Tertiary stratigraphy and paleogeographic evolution of Haymana-Polatli region (SW Ankara) [in Turkish], *Turkish Geol. Soc. Bull.*, *1*, 9,159–176.

Ünlügenç, U. C., C. Demirkol, and Ü. Şafak (1993), Stratigraphical and sedimentological characteristics of the Karsantı Basin fill to the N-NE of the Adana Basin [in Turkish], in *Proceedings of the International Earth Science Congress on Aegean Regions (Izmir, 1990)*, edited by M. Y. Savaşçın and A. H. Eronat, vol. 1, pp. 353–370, Ankara.

Ustaömer, T., and A. H. Robertson (1997), Tectonic-sedimentary evolution of the north-Tethyan active margin in the central Pontides of northern Turkey, in *Regional and Petroleum Geology of the Black Sea Region*, *Memoir*, edited by A. G. Robinson, pp. 245–290, *Am Assoc. Petrol Geol.*, New York.

Vandamme, D. (1994), A new method to determine paleosecular variation, *Phys. Earth Planet. Int.*, *85*, 131–142.

Van Hinsbergen, D. J. J., M. J. Dekkers, and A. Koç (2010), Testing Miocene remagnetization of Bey Dağları: Timing and amount of Neogene rotations in SW Turkey, *Turkish J. Earth Sci.*, *19*, 123–156.

Watson, G. S. (1956), Analysis of dispersion on a sphere, *Geophys. J. Int.*, *7*, 153–15.

Watson, G. S., and R. J. Enkin (1993), The fold test in palaeomagnetism as a parameter estimation problem, *Geophys. Res. Lett.*, *20*, 2135–2137.

Weltje, G. J. (1997), End-member modeling of compositional data: Numerical statistical algorithms for solving the explicit mixing problem, *Math. Geol.*, *29*, 503–546.

Whitney, D. L., and Y. Dilek (1997), Core complex development in central Anatolia, Turkey, *Geology*, *25*, 1023–1026.

Whitney, D. L., and Y. Dilek (1998), Metamorphism during Alpine crustal thickening and extension in central Anatolia, Turkey: The Niğde Metamorphic Core Complex, *J.Petrol.*, *39*, 1385–1403.

Whitney, D. L., and M. A. Hamilton (2004), Timing of high-grade metamorphism in central Turkey and the assembly of Anatolia, *J. Geol. Soc London*, *161*, 823–828.

Yalınız, M. K., P. A. Floyd, and M. C. Göncüoğlu (1996), Supra-subduction zone ophiolites of Central Anatolia: Geochemical evidence from the Sarikaraman Ophiolite, Aksaray, Turkey, *Mineral. Mag.*, *60*, 697–710.

Yılmaz, A. (1994), An example of a post-collisional trough: Sivas Basin, Turkey, in *Proceeding, 10th Petroleum Congress of Turkey*, pp. 21–23, Turk. Assoc. of Pet. Geol. Publ., Ankara.

Yılmaz, Y. (1983), New evidence and model on the evolution of the southeast Anatolian orogen, *Geol. Soc. Am. Bull.*, *105*, 251–271.

Yılmaz, Y., S. C. Genc, E. Yigitbas, M. Bozcu, and K. Yılmaz (1995), Geological evolution of the Mesozoic continental margin of northwestern Anatolia, *Tectonophysics*, *243*, 155–171.

Yılmaz, Y., O. Tüysüz, E. Yiğitbaş, Ş. C. Genç, and A. M. C. Şengör (1997a), Geology and tectonic evolution of the Pontides, in *Regional and Petroleum Geology of the Black Sea and Surrounding Region*, *Memoir*, vol. 68, edited by A. G. Robinson, pp. 183–226, Am. Assoc. of Pet. Geol., Tulsa, Okla.

Yılmaz, Y., H. S. Serdar, C. Genc, E. Yiğitbaş, Ö. F. Gürer, A. Elmas, M. Yıldırım, M. Bozcu, and O. Gürpınar (1997b), The geology and evolution of the Tokat massif, South-Central Pontides, Turkey, *Int. Geol. Rev.*, *39*, 365–382.

Zijderveld, J. D. A. (1967), AC demagnetization of rocks: Analysis of results, in *Methods in Palaeomagnetism*, edited by D. W. Collinson, K. M. Creer, and S. K. Runcorn, pp. 254–286, Elsevier, Amsterdam.